

**Global patterns in halogen-induced
changes in vertically resolved
stratospheric ozone**

Dissertation
der Fakultät für Physik der
Ludwig-Maximilians-Universität München

vorgelegt von Birgit Haßler
aus Tübingen

München, 29. Juli 2009

1. Gutachter: Prof. Dr. Martin Dameris, LMU München
 2. Gutachter: Prof. Dr. Bernhard Mayer, LMU München
- Tag der mündlichen Prüfung: 23. Oktober 2009

Abstract

An accurate representation of the global distribution of stratospheric ozone and its temporal evolution is a prerequisite for making realistic predictions of the future composition of the atmosphere and the climate on Earth. Zonal mean ozone data sets are commonly used as boundary conditions for climate prediction models. However, it is widely known from total column ozone analyses that zonal asymmetries in the ozone distribution as well as in ozone trends exist. Vertically resolved analyses of longitudinal differences in ozone changes are scarce, mainly because the significance of those differences is still underestimated but also because of the lack of a suitable data set on which to perform such an analysis. This thesis presents a global evaluation of those differences in halogen-induced ozone changes undertaken to assess their occurrence and confirm their significance.

Since no vertically resolved ozone data set with sufficient temporal and spatial coverage for a global analysis was available, a new database was assembled using data from several satellite instruments and 136 ozone sounding stations globally. It consists of three grids, each with three dimensions (latitude, a vertical dimension and time), in which all measurements are stored in a binary format. All measurements were thoroughly quality checked before they were added to the database. Although ozone is the main focus of this thesis, additional trace gases, information about aerosols and temperature are stored in the database as well. Two sets of vertically resolved monthly mean ozone values from 1979 to 2006 were calculated: a zonal mean and a longitudinally resolved data set. Both are divided into 5° latitude bands, the longitudinally resolved data set additionally into 60° longitude bins. In spite of the inclusion of several data sources, spatial and temporal coverage of both data sets is not complete. Particularly in the longitudinally resolved data set, data gaps are so frequent that traditional methods of determining ozone changes cannot be applied. Therefore, a new approach was developed, a modification of the commonly used multiple, linear regression in which the explanatory variables are expanded in spherical harmonics to allow the description of spatial patterns in the fit coefficients, rather than calculating the fit coefficients of the explanatory variables for every grid point of the spatial grid separately. The expansion functions are fitted to the ozone values available for each atmospheric level, and the complete global pattern is thereby defined by the fitted functions.

This new approach was first tested on monthly, zonal mean ozone data. For that, the spherical harmonics of the basis functions in the regression model were only

expanded in latitude. The patterns of halogen-induced ozone changes obtained are similar to the results of similar analyses described in the literature. An interesting additional analysis is possible with a small modification of the method: the evolution of the vertically resolved, global stratospheric ozone during the last 10 years can be described. But, especially in the lowermost and lower stratosphere, problems related to the new method occur which are generated by the combined effects of missing data and small-scale ozone variability. The spherical harmonics are insufficiently constrained due to the data gaps and produce artifacts in the patterns of the fitting coefficients. Before the new approach was applied to the longitudinally resolved data set, which has significantly more missing data, sensitivity tests were performed to determine the optimal spherical harmonic expansion settings in consideration of the missing data. A complete set of longitudinally resolved monthly mean ozone values was necessary for the sensitivity tests. This test data set was obtained from a chemistry-climate model simulation with the same spatial and temporal characteristics as the observations. With comparisons between different regression approaches, using both complete and incomplete data sets, the final expansion settings were determined and regions with artifacts in the fit coefficients caused by data gaps are identified.

The new regression model was then applied to the longitudinally resolved, monthly mean ozone data set which was derived from the observations. Zonal asymmetries in halogen-induced ozone changes are primarily detected in polar regions and mid-latitudes in winter and spring when planetary wave activity and the influence of the polar vortices is strongest. Although the problems of the spherical harmonics regression already mentioned for the analyses of the zonal mean ozone data remain for the longitudinally resolved analysis, overall the longitudinally resolved results at selected pressure levels agree well with results from similar total column ozone analyses. It is therefore possible for the first time to obtain a global picture of vertically resolved, halogen-induced ozone changes.

Zusammenfassung

Die genaue Darstellung der globalen Verteilung von stratosphärischem Ozon und dessen zeitlicher Entwicklung ist eine Grundvoraussetzung für realistische Vorhersagen der zukünftigen Zusammensetzung der Atmosphäre und den Auswirkungen auf das Erdklima. Im Allgemeinen werden zonal gemittelte Ozondaten als Randbedingungen für Klimavorhersagen eingesetzt, obwohl durch Gesamtozonuntersuchungen bekannt ist, dass zonale Asymmetrien in der Ozonverteilung und in Ozontrends existieren. Vertikal aufgelöste Analysen längenabhängiger Unterschiede von Ozonveränderungen sind rar. Dies beruht hauptsächlich darauf, dass die Bedeutung dieser Unterschiede immer noch unterschätzt wird, aber auch darauf, dass ein geeigneter Datensatz fehlt, der eine solche Untersuchung erlauben würde. Mit der vorliegenden Arbeit werden diese Unterschiede in Ozonveränderungen, die durch Halogene in der Stratosphäre induziert sind, auf globaler Ebene untersucht, um ihr Vorkommen genauer abzuschätzen und ihre Bedeutung zu bestätigen.

Es existiert bisher kein vertikal aufgelöster Ozondatensatz, der eine für globale Analysen ausreichende zeitliche und räumliche Abdeckung aufweist. Daher wurde eine neue Datenbank aus Messungen verschiedener Satelliteninstrumente und von 136 Ozonsondierungsstationen aus der ganzen Welt zusammengestellt. Dieser Datensatz besteht aus drei Datengittern, die jeweils drei Dimensionen haben (Breitengrad, vertikale Dimension und Zeit), in denen alle Messungen im binären Format gespeichert werden. Alle Messungen wurden sorgfältig qualitätsgeprüft, bevor sie zur Datenbank hinzugefügt wurden. Obwohl das Hauptaugenmerk dieser Arbeit auf Ozon liegt, wurden Messungen weiterer Spurengase, Aerosole und der Temperatur der Datenbank ebenfalls hinzugefügt. Es wurden zwei Datensätze vertikal aufgelöster Ozonmonatsmittel für den Zeitraum von 1979 bis 2006 berechnet: Einer besteht aus zonalen Mitteln und einer enthält längenaufgelöste Daten. Beide sind in 5° -Breitenbänder aufgeteilt, der längenaufgelöste Datensatz zusätzlich in 60° -Längenabschnitte. Trotz der Berücksichtigung verschiedener Datenquellen ist die zeitliche und räumliche Abdeckung beider Datensätze lückenhaft. Besonders im längenaufgelösten Datensatz sind die Datenlücken so zahlreich, dass herkömmliche Methoden zur Bestimmung von Ozonänderungen nicht angewandt werden können. Deshalb wurde eine neue Methode entwickelt, eine Abänderung der üblicherweise benutzten multiplen, linearen Regression, in der die beschreibenden Größen (Basisfunktionen) mit Kugelflächenfunktionen aufgeweitet werden. Dies ermöglicht eine Beschreibung räumlicher Muster in den Anpassungskoeffizienten anstatt der separaten Bestimmung dieser Koeffizienten für jeden Gitterpunkt des räumlichen Gitters. Diese Aufweitungsfunktionen werden

an die vorhandenen Ozonwerte jeder einzelnen atmosphärischen Schicht angepasst, womit das vollständige globale Muster der Koeffizienten der Basisfunktionen bestimmbar ist.

Diese neue Methode wurde zuerst mit zonalen Mitteln monatlicher Ozonwerte getestet. Dafür wurden die Kugelflächenfunktionen der Basisfunktionen im Regressionsmodell nur für die geographische Breite expandiert. Die erhaltenen Muster halogen-induzierter Ozonveränderungen sind vergleichbar mit Ergebnissen ähnlicher Analysen, die in der Literatur beschrieben sind. Eine interessante zusätzliche Analyse ist mit einer kleinen Abänderung der Methode möglich: Es kann damit die Entwicklung von vertikal aufgelöstem, globalem stratosphärischem Ozon während der letzten zehn Jahre beschrieben werden. Vor allem in der untersten und unteren Stratosphäre treten jedoch Probleme beim Anwenden der neuen Methode auf. Diese werden durch eine Kombination der Effekte von Datenlücken und kleinräumiger Ozonvariabilität hervorgerufen. Die Kugelflächenfunktionen sind durch die Datenlücken nur unzureichend definiert und erzeugen deshalb Artefakte in den Mustern der Anpassungskoeffizienten. Bevor die neue Methode auf den längenaufgelösten Datensatz angewandt wurde, der deutlich mehr Fehlwerte besitzt als der Datensatz des zonal gemittelten Ozons, wurden Sensitivitätstests durchgeführt. Damit wurden die optimale Expansionseinstellungen für die Kugelflächenfunktionen unter Berücksichtigung der Fehlwerte bestimmt. Dafür war ein vollständiger, längenaufgelöster Datensatz von Ozonmonatsmittelwerten notwendig. Dieser Testdatensatz stammt von einer Simulation mit einem Chemie-Klima-Modell und hat dieselben zeitlichen und räumlichen Eigenschaften wie der Datensatz der Beobachtungen. Mit Vergleichen zwischen verschiedenen Regressionsansätzen, wofür ein kompletter und ein lückenhafter Datensatz herangezogen wurden, konnten die endgültigen Expansionseinstellungen bestimmt werden. Außerdem wurden Regionen mit Artefakten in den Anpassungskoeffizienten, die durch Datenlücken hervorgerufen werden, ausgewiesen.

Das neue Regressionsmodell wurde auf den längenaufgelösten, monatlich gemittelten Ozondatensatz angewandt, der aus den Beobachtungen berechnet wurde. Zonale Asymmetrien in halogen-induzierten Ozonveränderungen sind hauptsächlich in den Polargebieten und den Mittelbreiten im Winter und Frühling vorhanden, wenn die Aktivität der planetaren Wellen und der Einfluss der Polarwirbel am stärksten ist. Die bereits für die Auswertung des zonal gemittelten Ozondatensatzes erwähnten Probleme der Regression mit eingebauten Kugelflächenfunktionen bestehen auch für die Auswertung des längenaufgelösten Ozondatensatzes. Dennoch stimmen die Ergebnisse der längenaufgelösten Auswertung für ausgewählte Druckstufen gut mit Ergebnissen ähnlicher Auswertungen mit Gesamt Ozon überein. Es ist deshalb zum ersten Mal möglich, ein globales Bild von vertikal aufgelösten, halogen-induzierten Ozonveränderungen zu erhalten.

Contents

1	Introduction	1
1.1	Current state of knowledge	2
1.2	The Earth's atmosphere	6
1.3	Dynamics of the atmosphere	8
1.3.1	General circulation	8
1.3.2	Polar vortices	11
1.3.3	Quasi-biennial oscillation in the tropics	13
1.3.4	Stratosphere-troposphere exchange	14
1.4	Stratospheric ozone chemistry	14
1.4.1	Principle ozone production and destruction reactions	14
1.4.2	Catalytic cycles	15
1.4.3	Heterogeneous chemistry	16
1.5	Thesis Outline	19
2	Observational data basis	21
2.1	Database structure	22
2.2	Data sources	24
2.2.1	SAGE I and II	24
2.2.2	HALOE	26
2.2.3	POAM II and III	27

2.2.4	LIMS	28
2.2.5	Ozonesonde data	29
2.3	Calculation of the monthly mean data	33
2.4	Database temporal, latitudinal and longitudinal coverage	34
2.5	Summary	39
3	Regression	41
3.1	Background, history and use of regression models	42
3.2	Spherical harmonics	46
3.2.1	Physical background	46
3.2.2	Implementation in a regression model	49
3.3	Regression model	52
3.3.1	Regression model	52
3.3.2	Explanatory variables	53
3.3.3	Uncertainties on the regression coefficients	59
3.3.4	Autocorrelation	60
3.4	Summary	62
4	Analysis of zonal mean data	65
4.1	Vertically resolved zonal mean ozone changes	66
4.2	Did ozone from 1997 to 2007 change as expected?	72
4.2.1	CUSUM methodology and modification	73
4.2.2	Results	75
4.3	Summary	78
5	Sensitivity tests for regression results	79
5.1	Chemistry-climate model data set	79

5.1.1	The E39C-A model	79
5.1.2	The REF SCN2d simulation	80
5.1.3	Model grid adjustment	81
5.2	Methodology	82
5.3	Sensitivity to the use of spherical harmonics in a regression (sensitivity test 1)	84
5.4	Sensitivity to data gaps (sensitivity test 2)	89
5.5	Sensitivity to spherical harmonics and data gaps (sensitivity test 3)	92
5.6	Summary	98
6	Analysis of longitudinally resolved data	99
6.1	Preliminary remarks	99
6.2	Halogen-induced changes in the northern polar regions in spring	102
6.3	Halogen-induced changes in the southern polar regions in spring	108
6.4	Halogen-induced changes in southern mid-latitudes in spring	115
6.5	Halogen-induced changes in northern mid-latitudes in winter	119
6.6	Halogen-induced changes in the tropics in northern summer	126
6.7	Summary	128
7	Conclusion and Outlook	131
7.1	Conclusion	132
7.2	Outlook	134
A	Acronyms and Abbreviations	137

List of Figures

1.1	Vertical structure of the atmosphere in the mid-latitudes.	7
1.2	General circulation of the atmosphere.	9
1.3	Schematic of stratospheric transport.	11
1.4	Antarctic polar vortex.	13
2.1	Schematic of database structure.	22
2.2	Percentage ozonesonde ozone errors.	32
2.3	Temporal coverage of the database.	35
2.4	Percentage of available monthly means from 1979 to 2006.	36
2.5	Longitudinal deviation from ozone zonal means between 40°N and 45°N.	38
3.1	Schematic overview of the three different types of spherical harmonics.	50
3.2	Latitudinally and vertically resolved EESC concentrations.	55
4.1	Latitude-pressure illustration of halogen-induced ozone changes.	67
4.2	Latitude-time illustration of halogen-induced ozone changes.	70
4.3	Schematic of the CUSUM method.	74
4.4	Schematic of CUSUM significance test.	75
4.5	β value plot for all latitudes and pressure levels.	76

5.1	Schematic diagram of the selection criteria for comparable values.	83
5.2	EESC coefficients evaluated for March for sensitivity test 1. . . .	86
5.3	EESC coefficients evaluated for September for sensitivity test 1. .	87
5.4	Fraction of significant and comparable data for sensitivity test 1. .	88
5.5	EESC coefficients evaluated for March for sensitivity test 2. . . .	90
5.6	EESC coefficients evaluated for September for sensitivity test 2. .	91
5.7	Fraction of significant and comparable data for sensitivity test 2. .	93
5.8	EESC coefficients evaluated for March for sensitivity test 3. . . .	94
5.9	EESC coefficients evaluated for September for sensitivity test 3. .	95
5.10	Fraction of significant and comparable data for sensitivity test 3. .	97
6.1	Vertically resolved comparability values.	101
6.2	Zonal asymmetries in ozone changes in March for selected pressure levels.	104
6.3	Vertically resolved ozone changes in March for selected longitude bins.	106
6.4	Zonal asymmetries in ozone changes in October for selected pressure levels.	110
6.5	Vertically resolved ozone changes in October for selected longitude bins.	112
6.6	Vertically and longitudinally resolved ozone changes in October for selected latitude regions.	114
6.7	Total column ozone over Southern Hemisphere mid-latitudes. . . .	116
6.8	Ozone changes in Southern Hemisphere mid-latitudes in October.	117
6.9	Zonal asymmetries in ozone changes in January for selected pressure levels (part 1).	120
6.10	Zonal asymmetries in ozone changes in January for selected pressure levels (part 2).	121

6.11 Vertically and longitudinally resolved ozone changes in the northern high latitudes in January.	123
6.12 Zonal asymmetries in ozone changes in August for selected pressure levels.	127

List of Tables

2.1	Meta data for satellite-based measurements of the BDBP.	25
4.1	Minimum EESC coefficients in the tropics and southern high latitudes.	71

Chapter 1

Introduction

Stratospheric ozone is important for all life on Earth because it absorbs incoming ultra-violet (UV) radiation. Without its presence harmful solar UV radiation would make life on the Earth's surface impossible. Ozone depletion to date has already affected humans and terrestrial and aquatic ecosystems (*Solomon, 2008*). Since the Antarctic ozone hole was discovered in 1985 (*Farman et al., 1985*), halogen-induced ozone depletion and resulting changes in atmospheric ozone distribution have been the focus of intensive research. Recent studies suggest that changes in stratospheric ozone not only influence the amount of incoming harmful UV radiation but also constitute a negative radiative forcing of climate (*World Meteorological Organization, 2007, Chapter 5*). The magnitude of this forcing depends on the season and on the vertical ozone distribution (*Forster and Shine, 1997*). Since ozone profiles can differ considerably for different regions of the Earth, the spatial ozone distribution has to be represented accurately for a realistic climate change estimation. While radiative transfer models for process studies, UV or radiative transfer calculations are very detailed and complex (for example *Mayer and Kylling, 2005*), the coupled Atmosphere-Ocean General Climate Models (AOGCMs) used by the Intergovernmental Panel on Climate Change (IPCC) to project future climate change cannot consider so many details due to the limitations of computing time and the lack of suitable boundary condition data sets. The latter is the reason why zonal asymmetries in stratospheric ozone were not included in the recent projection of climate change by the IPCC, although there is evidence that there are mechanisms causing longitudinal differences in halogen-induced ozone changes and that these differences contribute to the observed changes in surface climate in the Arctic (*Gillett et al., 2009*) and Antarctic regions (*Crook et al., 2008; Gillett et al., 2009*). For a reliable estimate

of the future global climate, for example for the next IPCC report, the implementation of a stratosphere, with all its aspects, in climate prediction models will be indispensable (*Baldwin et al.*, 2007).

In this thesis, global patterns in halogen-induced changes in vertically resolved stratospheric ozone are closely examined. Zonal asymmetries in the stratospheric ozone distribution are well known, as well as are zonal asymmetries in total column ozone. However, global analyses of changes in ozone profiles were impossible because the available data sets, up to now, do not allow the application of conventional statistical methods with high resolution globally due to insufficient temporal and spatial coverage. Longitudinal differences in ozone changes at the same latitude are small compared to the latitudinal variance and their origin is only partly understood. Nevertheless, failing to consider them in climate change analyses for future climate predictions unnecessarily enhances the uncertainties. To this end, a new database was assembled and statistical analyses methods were adapted to allow, for the first time, global estimates of halogen-induced changes of ozone profiles, resolved in both latitude and longitude.

1.1 Current state of knowledge

Most analyses of halogen-induced ozone changes - stratospheric as well as total column - are applied to zonal mean data (see for example *World Meteorological Organization*, 2007, Chapter 6) for two related reasons: (1) data sets with a sufficient longitudinal resolution to allow such analyses are scarce, and (2) zonal mean analyses are thought to be sufficient for most applications and that longitudinal structures in trends can be disregarded. Deviations from the zonal mean, though, shed light on dynamical developments since they cannot be explained by chemical processes alone (*World Meteorological Organization*, 2003, Chapter 4). With the many years of satellite measurements now available, the total column ozone data set is now long and dense enough to make longitudinally resolved trend analyses possible.

The earliest studies of longitudinal differences in ozone trends were published in the early to mid 1990s. *Niu et al.* (1992) used the nearly global total column ozone measurements from the Total Ozone Mapping Spectrometer (TOMS) (70°S-70°N) to estimate ozone trends as a function of latitude, longitude and month. They found zonal asymmetries in the northern and southern high-latitude trends with the strongest trend in the Antarctic region. However, no mechanisms

which could cause those longitudinal differences were explored. *Stolarski et al.* (1992) analyzed the same data set, and confirmed the trend findings with selected ground-based measurements. Awareness of the importance of longitudinal structures in ozone trends grew within the community during subsequent years and longitudinal differences in trends were explicitly mentioned in *World Meteorological Organization* (1999, Chapter 4). Global TOMS total column ozone data were also analyzed by *Steinbrecht et al.* (2003) in a study which aimed to quantify natural and anthropogenically induced ozone variability in different seasons. Again, in this study, no explanation for the zonal asymmetries in ozone trends were given. *Fioletov et al.* (2002) analyzed not only global TOMS total column ozone data but also five additional data sets built from ground-based or satellite measurements as well as assimilated data, and compared derived total column ozone trends. The annual and seasonal analyses show the highest longitudinal variability in the northern and southern high latitudes. While in the northern high latitudes the displacement of the polar vortex most likely causes the zonal asymmetric trends, the reason for the variability in the southern high latitudes might rather be attributed to the non-circular shape of the vortex.

More regionally confined total column ozone trends were reported by *Hood and Zaff* (1995). They showed that the zonally asymmetric trends in the mid-latitudes in northern winter are caused by changes in stationary planetary-scale waves. Furthermore, they suggested that the climate variability of the troposphere, where the waves often originate, plays a major role in inducing those changes. The importance of the consideration of longitudinally resolved trends was emphasized by *World Meteorological Organization* (1999, Chapter 4) where the studies from *Stolarski et al.* (1992) and *Hood and Zaff* (1995) were described in detail. In the following years, the mechanism suggested by *Hood and Zaff* (1995) was further investigated with a linear quasi-geostrophic transport model (*Peters and Entzian*, 1999). *Efstathiou et al.* (2003) linked the total column ozone behavior of stations from selected Northern Hemispheric geographical regions to mid-latitude wave activity. *Peters et al.* (2008) recently analyzed four decades of Northern Hemispheric winter total column ozone data and quantified the relationship between zonally asymmetric ozone changes and geopotential perturbations. In late winter, a different process introduces longitudinal differences in the northern mid-latitude ozone fields: the breakup of the Arctic polar vortex. *Knudsen and Andersen* (2001) suggested that spring ozone trends in the northern mid-latitudes are only partially caused by changes in circulation, which are caused by wave breaking, but also by transport of ozone-depleted air from the vortex. However, *Nikulin and Karpechko* (2005) found out that the export of ozone-poor air is important in late

winter and early spring when the vortex breaks up. In early spring, stationary wave breaking remains the major originator of zonally asymmetric ozone trends. *Andersen and Knudsen (2006)* identified the preferred location of the Arctic vortex remnants and quantified that effect on the total column ozone trends. In recent years, Southern Hemispheric longitudinally resolved total column ozone trends were also studied. *Malanca et al. (2005)* focus on the mid-latitudes of the Southern Hemisphere where longitudinal structures also appear in total column ozone trends (see for example *Niu et al., 1992*, and *Fioletov et al., 2002*). The zonally asymmetric patterns in this region migrate eastward during the analyzed decades (1980-2000) which is linked to the interannual variability of stationary planetary waves and differing changes in the wave amplitudes. *Grytsai et al. (2007)* showed that it was not the amplitude but the phases of quasi-stationary waves 1 and 2 in the southern mid-latitudes that changed during the last 25 years. However, they focused not on mid-latitude zonal asymmetries, but on Antarctic total column ozone disturbances in spring. These are, according to *Grytsai et al. (2007)*, not only caused by the ozone depletion in the polar vortex region but also by the longitudinal position of the ozone maximum in the mid- and sub-polar regions due to the dynamical accumulation of ozone in the collar region of the polar vortex.

The data basis for analyses concerning longitudinal differences in spatially high-resolved ozone profile data sets is even today not sufficient to allow vertically resolved, global estimations of long-term ozone changes. Therefore only a limited number of studies are available which address those issues and only for confined latitude areas. The fact that many of those studies were published only recently shows the growing awareness of the community that neglecting the zonal asymmetries in ozone trends could conceal important atmospheric mechanisms, although the regional differences in European and Canadian trends in ozone profiles was already pointed out in *World Meteorological Organization (1999, Chapter 4)*. So far, vertically resolved ozone changes have been mainly analyzed for the tropical tropopause region, the northern mid-latitude lower stratosphere region and the Antarctic lower stratosphere region. Analyses concerning the tropical tropopause region describe zonal wave 1 pattern in ozone which can be seen in profiles of the Stratospheric Aerosol and Gas Experiment II (SAGE II) (*Wang et al., 2002, 2006b*), in profiles from the relatively newly established tropical ozone sounding stations (*Thompson et al., 2003a*), and in satellite and ozonesonde combined data sets (*Randel et al., 2007*). The wave 1 signal is a result of tropospheric downwelling and it is enhanced by ozone transported from biomass burning locations, nitric oxide (NO) produced by lightning (*Thompson et al., 2003a*), as well as

ozone increases via large-scale transport (*Randel et al.*, 2007). Zonal differences in ozone trends, however, are discussed only for the other two regions mentioned. The northern mid-latitude, lower stratosphere was the focus of the analysis by *Kirchner and Peters* (2003). They used a general circulation model (GCM) to address the question of feedback mechanisms between the zonally asymmetric ozone field and atmospheric circulation. They showed that planetary waves influence the ozone distribution of the upper troposphere and lower stratosphere, and that the altered ozone “triggered a systematic alteration of the circulation over the North Atlantic-European region” (*Kirchner and Peters*, 2003). The vertically resolved ozone data fields for their study were a combination of satellite measurements and ozone soundings. *Gabriel et al.* (2007) used ECMWF reanalysis (ERA-40) of ozone data for their determination of the effect of zonally asymmetric ozone on stratospheric temperature and planetary wave propagation. Their results suggest that the amplitude of wave 1 has increased from the late 1950s to the beginning of the 21st century and that the preferred travel regions of stratospheric and lower mesospheric waves shifted upward and eastward. Furthermore, the zonally asymmetric ozone induced a wave 1 like pattern in stratospheric temperature which increases with height. *Gabriel et al.* (2007) pointed out that the use of the ERA-40 reanalyses might introduce some uncertainties in the results but that no better three-dimensional data set was available at that time. *Gillett et al.* (2009) confirmed the stratospheric temperature pattern found by *Gabriel et al.* (2007), based on the analysis of chemistry-climate model output. A recent study by *Crook et al.* (2008) addressed the zonal differences in ozone profiles in the Antarctic region. They used a high-vertical resolution, ocean-atmosphere model to compare the effects of prescribed zonal mean ozone fields to three dimensional (3-D) ozone distributions. The 3-D ozone data set was obtained from ERA-40 reanalyses. The effect of prescribing zonal mean ozone data fields results in an underestimation of stratospheric and upper tropospheric cooling during late Southern Hemispheric spring comparable to the cooling caused by ozone depletion itself over the last three decades. This cooling is responsible for Southern Hemisphere temperature and geopotential height trends. These findings highlight the importance of zonally resolved ozone data fields for transient model simulations. *Gillett et al.* (2009) confirmed the findings of *Crook et al.* (2008).

Before the new approach to obtain global vertically resolved, halogen-induced ozone changes is introduced and explained, it is important to recall the most important dynamical and chemical characteristics of the atmospheric region which is the main focus of this study: the stratosphere. Features of adjacent atmospheric layers are also described where they contribute to an understanding of

the stratospheric ozone distribution.

1.2 The Earth's atmosphere

There are several possibilities for describing the vertical structure of the atmosphere: by temperature, by composition, and by the degree of ionization. Most commonly, the various vertical atmospheric layers are defined according to changes in temperature with altitude (e.g. *Brasseur and Solomon*, 1986; *Andrews*, 2000). Figure 1.1 illustrates the vertical structure of the atmosphere, with examples shown for a mid-latitude summer and winter profile, defined by changes in temperature lapse rate. The layer extending from the ground to about 8-18 km is called the **troposphere** and is characterized by decreasing temperatures with increasing height (on average 6.5 K/km). The vertical extent of the troposphere depends on latitude, with a maximum thickness of about 18 km in the tropics and a minimum thickness of about 8 km in the polar regions. Most weather phenomena, such as cloud formation and precipitation, are confined to the troposphere. Vertical mixing of air is easily possible due to the static stability characteristics of the troposphere. Static stability is defined as the stability of the atmosphere in hydrostatic equilibrium with respect to vertical displacements. In regions where the temperature decreases with increasing altitude, as in the troposphere, the atmosphere is unstable and vertical mixing is facilitated. About 80% of the atmosphere's mass is contained in the troposphere, most of it being nitrogen (78%) and oxygen (21%) with some trace gases. The boundary between the troposphere and the adjacent layer is called the **tropopause**. Here the temperature stops decreasing with height, the static stability increases and vertical air motion is impeded.

Above the tropopause is the **stratosphere** which extends up to about 50 km. The temperature in this layer increases with height which further increases the static stability and therefore greatly impedes vertical air movement. About 19.9% of the total mass of the atmosphere is found in the stratosphere. Probably the most noteworthy feature of the stratosphere is that it contains the majority of the atmosphere's ozone molecules. The ability of ozone to absorb solar UV radiation leads to the heating of the stratosphere (*Reid*, 2000) which causes temperature to increase with altitude in this atmospheric layer. Because it absorbs incoming solar UV, the ozone layer is very important for life on Earth. Ozone concentrations vary with altitude and location. However, ozone is mostly found between 10 to 50 km, in the so called 'ozone layer'. The maximum concentration of the ozone is

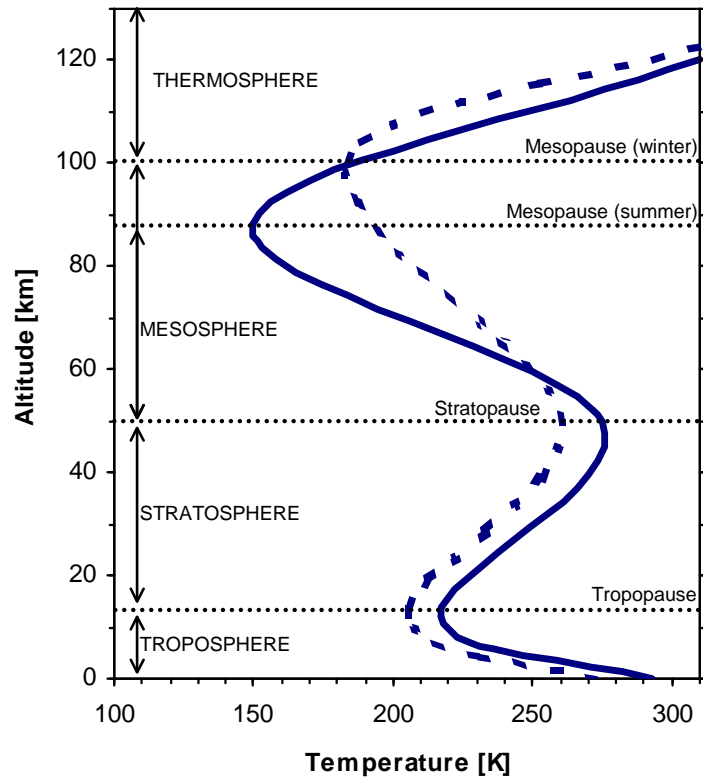


Figure 1.1: Vertical structure of the atmosphere in the mid-latitudes, classified by temperature. The dashed line denotes the winter profile, the solid line the summer profile.

located at around 25 km, on a global average. At the top of the stratosphere, at around 50 km, the temperature of the stratosphere reaches a maximum of about 270 K (-3°C). The region of this stratospheric temperature maximum is called the **stratopause** and separates the stratosphere from the layer above, called the **mesosphere**.

The mesosphere extends up to 88 km in summer and up to 100 km in winter and is characterized by continuously decreasing temperature. This is due to the low concentration of ozone molecules which could absorb UV radiation and therefore heat their surroundings (*Ahrens, 1994*). At the top of the mesosphere, at the **mesopause**, the lowest average temperature of the atmosphere is reached. This temperature is lower in summer than in winter, however, the magnitude of the temperature difference is strongly dependent on latitude: while it is practically non-existent for the tropical mesopause, it can range from around 120 K ($\sim -150^{\circ}\text{C}$) to around 180 K ($\sim -90^{\circ}\text{C}$) in polar regions. Figure 1.1 shows the differences in the mesopause height and temperature for the mid-latitudes (described for example by *Yu and She, 1995*). The different seasonal mesopause charac-

teristics are due to lower gravity wave activity in summer with less transported energy and momentum and thus less heating. The adjacent layer, which extends from the mesopause to about 500 km, is called the **thermosphere**, where the temperature increases rapidly again. Oxygen molecules absorb high-energy solar radiation and get ionized. This generates temperatures that can reach a maximum greater than ≈ 1450 K at the upper boundary of the thermosphere. This is where the **exosphere** begins. In this region, at the edge of interplanetary space, the air density is so low that it can almost be referred to as vacuum, the few atoms and molecules left often shoot off into space, ultimately escaping Earth's gravitational pull (*Ahrens, 1994*).

1.3 Dynamics of the atmosphere

1.3.1 General circulation

The expression **general circulation** of the atmosphere is usually taken to mean all motions that contribute to atmospheric flow on a global scale. That motion is fundamentally driven by two main processes: the differential heating of the Earth, which is caused by differences in the intensity of solar radiation received at different locations on the Earth's surface, and the Earth's rotation. The differential heating causes temperature gradients from the equator to the poles which result in air pressure differences. The second process, the Earth's rotation, carries along everything connected to the Earth's surface, including the atmosphere. The dominant force balance in the atmosphere is the interaction between those two forces.

The difference in solar heating between tropics and polar regions causes thermal convection: heated air at the equator rises and flows poleward, it cools and sinks, and flows back to the equator. At the same time the poleward flowing air is deflected to the east by the Coriolis force and the equatorward flowing air close to the Earth's surface is deflected to the west. These surface winds are known as the 'trade winds' (see Figure 1.2) and the resulting circulation is called the **Hadley cell** (*Holton, 2004*). In the 18th century, at the beginning of atmospheric circulation research, it was assumed that the descending branch of the Hadley cell would be located in the polar regions. Today it is well-known that due to baroclinic instability this one-cell model is not true, but that the global circulation is formed by three cells: the Hadley cell, the Ferrel cell and the Polar cell (see

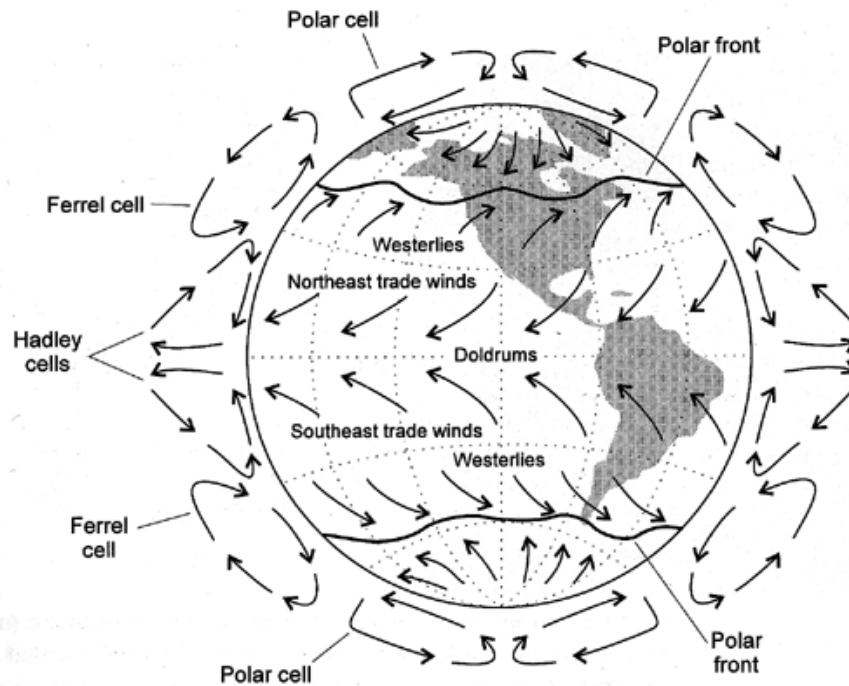


Figure 1.2: Schematics of the general circulation of the atmosphere with wind and surface pressure distribution (Source: <http://hercules.gcsu.edu/~sdatta/home/teaching/>).

Figure 1.2). These cells and the resulting winds are confined to the troposphere.

Differential heating of polar and equatorial regions occurs also in the stratosphere. However, observed temperatures in the winter hemisphere do not agree with the radiative values predicted solely by differential heating (*Holton et al.*, 1995): temperatures at the poles are higher whereas temperatures in the tropics are lower than for radiative equilibrium. In the summer hemisphere stratospheric temperatures do not deviate from radiative equilibrium. Only with hemispheric transport, with rising air in the tropics, poleward transport and descending air in the middle and polar latitudes, can these differences be explained: where air moves upward, adiabatic cooling lowers the temperature in this region below its radiative equilibrium value and where air moves downward, adiabatic warming raises the temperature above its radiative equilibrium value. Temperatures at high-latitudes are, therefore, in winter warmer than expected from differential heating and at low latitudes colder than expected. The resultant transport system was first suggested by *Brewer* (1949) and *Dobson* (1956) and is now known as the **Brewer-Dobson circulation** in honor of their work. The radiative imbalance effect alone cannot explain the existence of the Brewer-Dobson circulation.

Only with an additional external forcing can the flow of air parcels be accounted for. Today it is well-understood that breaking and dissipation of planetary-scale **Rossby waves** originating from the troposphere (*Haynes et al.*, 1991) are the primary cause for this main stratospheric transport system.

Rossby waves belong to the class of atmospheric waves which are observed on a horizontal scale of many thousands of kilometers and periods of several days. Therefore, they are also referred to as planetary waves (*Andrews*, 2000). Their restoring mechanism, the mechanism which drives the waves, is the latitudinal gradient of potential vorticity which is caused by the variation in the Coriolis effect with latitude (*Andrews et al.*, 1987). The zonal phase propagation of Rossby waves is always westward with respect to the background flow (*Andrews*, 2000). Rossby waves are called **stationary** if they have a wave pattern that is fixed with respect to the Earth and are forced either by large-scale topography or continent-ocean heating contrasts (*Holton*, 2004). Since significant topography is missing in the Southern Hemisphere and there is less land-ocean contrasts, stationary Rossby waves are less frequent there than in the Northern Hemisphere. This results in an air-flow in the Southern Hemisphere stratosphere which is less zonally asymmetric than in the Northern Hemisphere. In the summer hemisphere this mean flow is westward, whereas in the winter hemisphere it is eastward. Vertical propagation of stationary Rossby waves, and ultimately breaking and dissipation, is only possible with an eastward background flow (*Charney and Drazin*, 1961; *Andrews*, 2000) which is why Rossby waves contribute significantly to the circulation of the winter hemisphere and not to the circulation of the summer hemisphere.

Figure 1.3 shows a schematic overview of the stratospheric transport mechanisms as outlined so far. Air rises in the tropics from the troposphere to the stratosphere. This motion is responsible for transporting chemical constituents, such as halogen compounds, from the troposphere to the stratosphere and, therefore, making them available for stratospheric chemistry (see Section 1.4). From the tropics the air is transported in the stratosphere to the polar regions. Poleward of about 30° the transport is also downward. In the extratropical stratosphere it is powered by the breaking and dissipation of Rossby waves. This region is therefore called the **surf zone**, or the **extratropical ‘pump’** region. Since wave breaking does not occur in the summer hemisphere, the Brewer-Dobson circulation is much stronger in winter and early spring. In addition, since wave activity is stronger in the Northern Hemisphere, the Brewer-Dobson circulation is stronger there than in the Southern Hemisphere. There are two main transport ‘barriers’, one separating

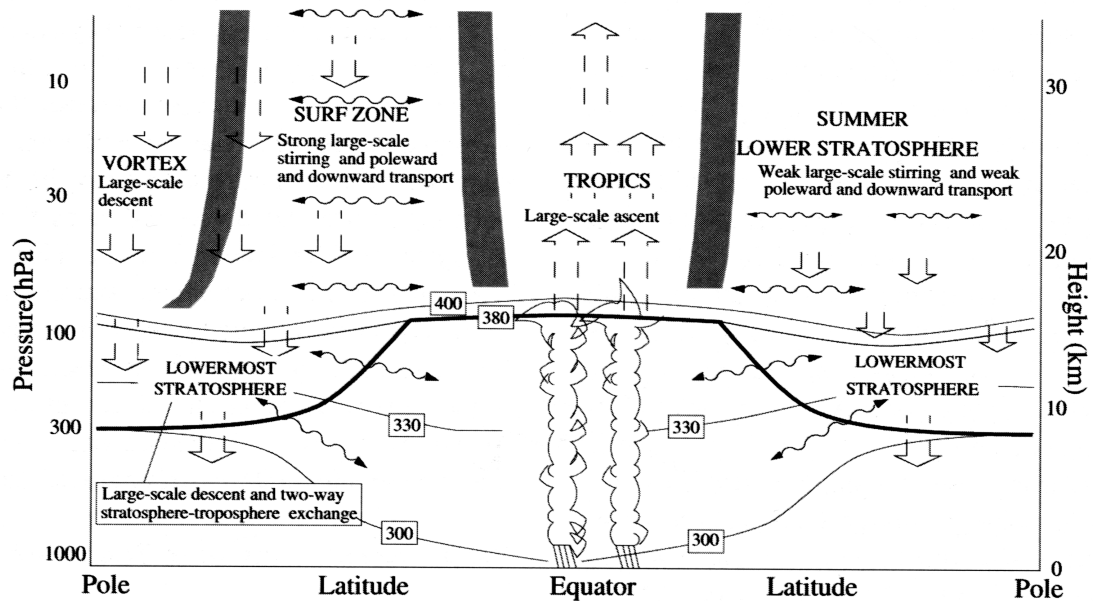


Figure 1.3: Schematic of the lower stratospheric transport characteristics (adopted from *World Meteorological Organization*, 1999, Chapter 7). Broad arrows denote the rising of air in the tropics and associated sinking in the mid-latitudes and polar regions. Wavy arrows indicate stirring along isentropic surfaces. The thick black line represents the tropopause. Thin black lines denote isentropic surfaces. Gray regions represent transport 'barriers'.

the tropics from mid-latitudes (also known as the 'tropical pipe'; *Plumb*, 1996) and the more prominent one in the polar regions, at the edge of the polar vortex (*Juckes and McIntyre*, 1987).

1.3.2 Polar vortices

In both hemispheres the polar stratospheric regions are bordered by the polar night jet which is induced by temperature contrasts between cold polar air masses and adjacent warmer air masses from the mid-latitudes. The region poleward of this jet stream is called **polar vortex**. During winter and early spring when temperature differences are highest, the polar night jet is fastest and the polar vortex is strongest. Polar vortices occur in both hemispheres and, while they are strongest, reduce air mass transport across their edges (Figure 1.4). These edges are normally located close to the latitude separating day and night during polar winter (*Reid*, 2000). Solar radiative heating stops over the polar regions in winter, whereas emission of thermal radiation continues (*Dessler*, 2000). This results in cooling of the polar stratosphere. As mentioned above, due to higher wave

activity in winter in the Northern Hemisphere, the Brewer-Dobson circulation is stronger there than in the Southern Hemisphere. Therefore, there is more air descending in the Northern Hemisphere which results in more adiabatic warming and therefore the temperature gradient between air inside and outside the vortex is not as steep as in the Southern Hemisphere (*Shepherd, 2008*). Consequently, the Antarctic polar vortex is stronger than the Arctic polar vortex. Additionally, the hemispheric differences in wave activity also explain the differences in the vortices' stability. The dissipation of planetary waves can cause a deceleration of the polar night jet. Since those waves show a distinct longitudinal pattern, the dissipation can cause a displacement of the vortex (*Haynes, 2005*). If the wave forcing is strong enough, it is possible that the polar vortex is not only displaced but breaks up which is then accompanied by a strong warming of the stratosphere inside the polar region (*Brasseur and Solomon, 1986*). This reverses the meridional temperature gradient and can even create a reverse of the polar night jet (*Holton, 2004*). This phenomenon is called a **sudden stratospheric warming** and was not observed in the Southern Hemisphere until 2002 when the Antarctic vortex was split due to wave activity (*Hoppel et al., 2003*). The usual break-up of the polar vortices is caused by the returning sun in spring. Polar temperatures increase due to solar radiative heating and with the thermal-wind balance the velocity of the polar night jet decreases.

The stratospheric ozone distribution is strongly linked to the Brewer-Dobson circulation and the winter hemisphere polar vortex. Ozone is transported in winter from the region of highest production rate in the tropical, upper stratosphere to the extra-tropics and high latitudes. Mixing by waves flattens the resulting ozone gradients. The primary effect of dynamics, however, is via temperature and transport of chemical species that provide catalysts for stratospheric ozone chemistry (*Shepherd, 2008*). In regions below ~ 30 km, and during polar night where the lifetime of ozone is comparable to transport time scales, transport and dynamics become quite important for the ozone distribution. For example, wave activity causes the differences in the stability of the Arctic and Antarctic vortex. Those differences result in different vortex temperatures which has dramatic implications for polar ozone chemistry: in the Antarctic vortex temperatures are low enough to allow the formation of polar stratospheric clouds (PSCs, see Section 1.4.3), which play a major role in ozone depletion, in greater quantities than in the Arctic. In late spring, the polar vortex breaks up and ozone-poor air from the vortex is rapidly mixed with ozone-rich air from the mid-latitudes, resulting in a relatively uniform, latitudinal ozone distribution during the summer months (*Shepherd, 2008*).

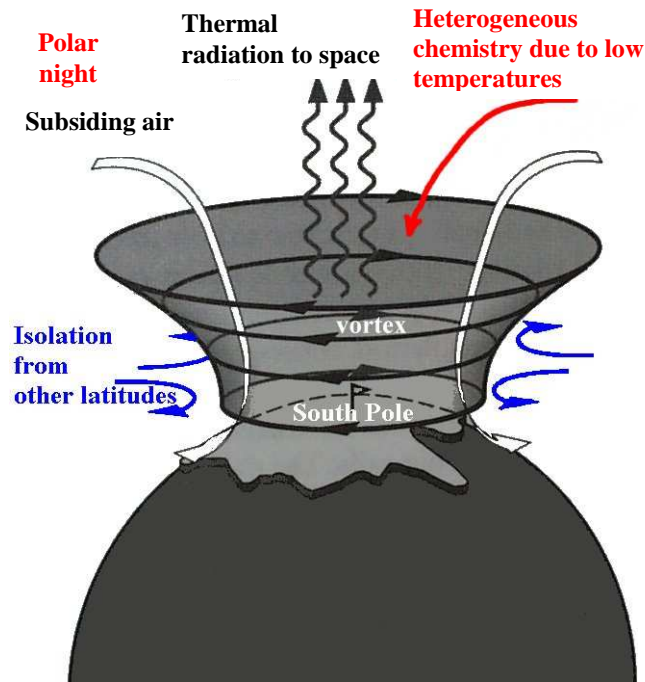


Figure 1.4: Schematic of the Antarctic polar vortex during polar darkness and prevailing processes (modified from <http://www.ldeo.columbia.edu>).

1.3.3 Quasi-biennial oscillation in the tropics

Wave forcing also plays an important role in the formation of the quasi-biennial oscillation (QBO) in the tropical stratosphere. The QBO is a quasi-periodic oscillation between easterly and westerly equatorial zonal winds with a mean period of about 28 months. The wind reversal begins at the top of the stratosphere and propagates downward until the winds have changed all the way down to the tropical tropopause. The QBO is driven by a combination of gravity, Rossby-gravity and Kelvin waves which are initiated in the tropical troposphere. They propagate upward to the stratosphere where they dissipate and deposit their easterly or westerly zonal momentum where the wind speed coincides with the phase speed of the waves (*Baldwin et al.*, 2001). Due to the additional momentum those regions accelerate resulting in the downward propagation of the wind reversal. Although the QBO is in the tropics, it affects the extra-tropical stratospheric circulation as far as the polar regions by modulating eddy diffusive transport in the extra-tropical regions.

A detailed description of the effects of the QBO on ozone is given in Section 3.3.2.4.

1.3.4 Stratosphere-troposphere exchange

As stated in *World Meteorological Organization* (2007, Chapter 5) ‘a complete description of atmospheric dynamics requires an understanding of both’ the stratosphere and troposphere. Although air movement, and therefore transport through the tropopause, is in most regions of the globe hindered by the vertical temperature gradient, there are mechanisms by which an exchange between troposphere and stratosphere is possible. One of the main mechanisms of the effect of the troposphere on the stratosphere is the air mass transport in the upward branch of the Brewer-Dobson circulation in the tropics by overshooting convection. The air is then moved within the stratosphere to the extra-tropics where it descends. Stratospheric air masses can enter the troposphere, for example, where isentropic surfaces (surfaces of constant potential temperature) intersect with the tropopause. This happens in the mid- and high latitudes in the so called lowermost stratosphere (see Figure 1.3). Along those surfaces, irreversible transport from the stratosphere to the troposphere can take place (*Holton et al.*, 1995). Furthermore, an exchange of stratospheric and tropospheric air can be caused by tropopause folds.

An effect of the troposphere on the stratosphere which is not related to air mass exchange is induced by changes in propagation characteristics of tropospheric waves. Due to those changes, the stratospheric circulation characteristics might change, and could feed back to the troposphere by downward propagation of stratospheric zonal mean anomalies (e.g. *Baldwin and Dunkerton*, 1999).

1.4 Stratospheric ozone chemistry

1.4.1 Principle ozone production and destruction reactions

In the stratosphere the principle chemical reaction that leads to ozone production is the photolysis of molecular oxygen by UV solar radiation with wavelengths less than 250 nm:

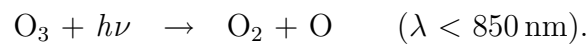


where $h\nu$ represents the energy of a photon (with h being Planck’s Constant and ν being the frequency) and λ is the wavelength. The oxygen atoms combine

rapidly with molecular oxygen in the presence of a third reactant molecule, M (usually N₂, *Staehelin et al.*, 2001), needed to balance energy and momentum in the reaction, to produce ozone:



However, sunlight with wavelength < 850 nm also dissociates ozone molecules by the equation:



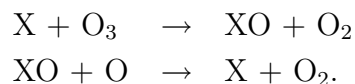
Since the oxygen atoms have very short lifetimes, they either quickly combine with O₂ form ozone again, or react with an ozone atom to form two oxygen molecules again:



This cycle of ozone production and destruction was proposed in 1930 by Sidney Chapman and is called the **Chapman Cycle**. If not perturbed, it produces and destroys ozone in the stratosphere in equal amounts (*Reid*, 2000), such that an equilibrium of O, O₂, O₃ and O₄ is maintained.

1.4.2 Catalytic cycles

Calculating the ozone content of the stratosphere according to the Chapman Cycle, however, overestimates the ozone maximum by a factor of two compared to observations. One of the main reasons for this is the neglect of other ozone-destroying reactions, the **catalytic cycles** (*Andrews*, 2000). The two main reactions in a catalytic destruction cycle are:



The net effect of a catalytic cycle therefore is:



which has the same effect as the ozone destruction path suggested by Chapman. X in the above equations is a catalyst atom, molecule or radical which takes part in a reaction but is not itself consumed by it. One single catalyst molecule can therefore destroy many ozone molecules before it breaks the catalytic cycle by reacting with some other atom or molecule. The most common species for X belong to the families of odd-nitrogen (NO_x), odd-hydrogen (HO_x), odd-chlorine (Cl_x) (*Reid*, 2000), and odd-bromine (Br_x) (*McConnell and Jin*, 2008), and are NO, OH, H, Cl and Br. Catalytic cycles are most important in the stratosphere at mid-latitudes (*McConnell and Jin*, 2008), although their importance varies at different atmospheric levels: in the lower stratosphere (15-25 km) all four catalytic families can contribute to ozone destruction, whereas at higher altitudes (25-40 km) the destruction is dominated by the odd-nitrogen family (*Dessler*, 2000; *Reid*, 2000). Although the total chlorine amount in the stratosphere is about 160 times larger than total bromine, bromine plays an important role in ozone depletion since it is much more effective than chlorine on a per-atom basis (*World Meteorological Organization*, 2007, Chapter 4). All reactions discussed above happen between gases only, therefore they are all classified as gas-phase chemistry.

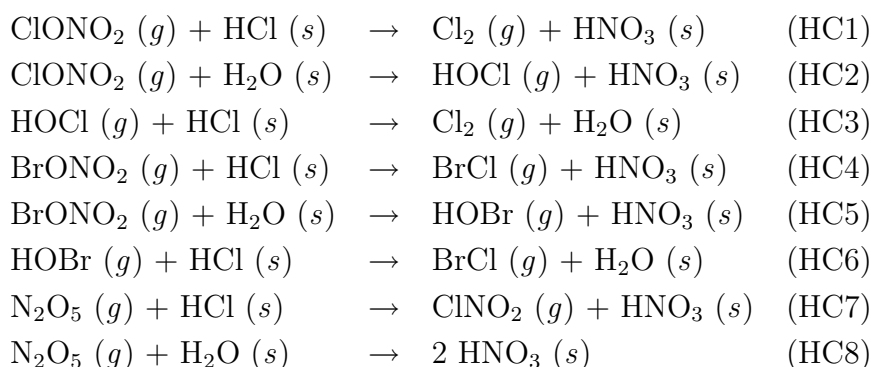
1.4.3 Heterogeneous chemistry

Gas-phase chemistry alone contributes to ozone depletion only in the upper stratosphere (*Staehelin et al.*, 2001). At lower stratospheric levels, and especially at high latitudes, reactions of gases with liquid or solid particles play an important role, the so-called heterogeneous reactions. The main processes of those reactions are adsorption (accumulation of atoms or molecules on the surface) and absorption (atoms or molecules are taken up by the volume) of the gaseous molecules by the condensed particles. Chemical reactions then follow, forming different products. Heterogeneous reactions are extremely important for understanding the stratospheric ozone budget/balance, since they free chlorine and bromine from reservoir species (long-lived compounds which are relatively inert) into reactive forms.

There are two common species of particles on which heterogeneous chemistry can occur: stratospheric sulfate aerosols and PSCs. The **stratospheric sulfate aerosols** are typically composed of sulfuric acid (H_2SO_4) and water (*McConnell and Jin*, 2008), at least at the mid-latitudes where temperatures are warm enough to maintain the particles in a liquid state. The sulfuric acid originates from tropospheric carbonyl sulfide (COS) and sulfur dioxide (SO_2) which was carried

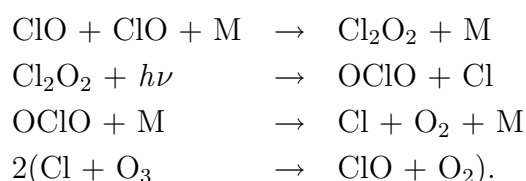
along two main pathways into the stratosphere: either by lifting along the tropical branch of the Brewer-Dobson circulation or by the direct injection of SO₂ from large volcanic eruptions. **Polar stratospheric clouds** form under very cold conditions which are found only within the polar vortex regions during winter and early spring, from the tropopause up to ~25 km (*Dessler, 2000*). PSCs are fundamental to an understanding of polar stratospheric ozone depletion: on their surface unreactive chlorine reservoir species (like hydrochloric acid, HCl, and chlorine nitrate, ClONO₂) can be converted into reactive chlorine radicals. They are a condensation product of water vapor, sulfate aerosols and nitric acid. The exact formation temperature depends on pressure and on the abundance of trace gases necessary to the formation. Two classes of PSCs can be differentiated: Type I and Type II. Type I PSCs form at temperatures around 195 K and are composed of nitric acid trihydrate (NAT) which consists of frozen nitric acid and water, as well as supercooled ternary solutions (STS) which combine water, sulfuric acid and nitric acid (*McConnell and Jin, 2008*). Type I PSCs are further divided into Type Ia and Type Ib. The PSCs of the former type consist of crystalline particles whereas the particles of the latter type are liquid. Type II PSCs form only at temperatures below 188 K and consist of frozen water particles. With typical radii of 5-20 μm they are considerably larger than PSCs of Type I (0.5-1 μm; *Dessler, 2000*).

Key heterogeneous reactions, either on sulfate aerosols or PSCs, as given by *Solomon (1999)* and *McConnell and Jin (2008)*, are:

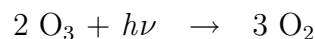


Letters in brackets denote if the reaction participant is gaseous (*g*) or solid (*s*). Reaction HC5 and HC8 are not very dependent on temperature (*Dessler, 2000*) unlike the other reactions. For the latter, reaction rates increase drastically for low temperatures, therefore they are most important for understanding the polar ozone budget. HC5 and HC8 are additionally important for heterogeneous reactions at mid-latitudes (on sulfate aerosols).

Molecules such as hydrogen chloride (HCl) and chlorine nitrate (ClONO₂) are reservoir species since they are relatively unreactive in their gaseous form. The conversion of those reservoirs on PSCs into Cl_x (for example by reaction HCl and HC3) is called **chlorine activation** (*Dessler, 2000*). Since PSCs are composed of HNO₃ and H₂O these species are removed from the stratosphere when sufficiently large PSCs undergo sedimentation. These processes are known as **denitrification** and **dehydration**, respectively. The photochemically labile chlorine molecules (Cl₂ as well as HOCl) are short-lived and can be rapidly photolyzed when the sun comes back to high latitudes in spring. The Cl₂ molecules are split in two chlorine atoms which can participate in the odd-chlorine catalytic cycle which is described in Section 1.4.2 to destroy ozone. The photolysis of HOCl releases ClO which then can destroy ozone through the following reactions:



The net reaction then is:



A reaction set similar to the above mentioned ClO-ClO reaction exists for the reaction of BrO with ClO. Ozone loss due to the BrO-ClO reactions is about half of the loss caused by the ClO-ClO reactions, although BrO concentrations in the stratosphere are much smaller than ClO concentrations.

It is obvious from the reactions described above that Cl₂O₂ (also called the **ClO dimer**, *Molina and Molina, 1987*) plays a major role in high-latitude ozone depletion as soon as the sun comes back to the polar regions. However, with the returning sun the deactivation of chlorine also starts and, therefore, the depletion of ozone decreases: Temperatures within the polar vortex steadily increase again with the return of the sun which leads to suppressed formation of PSCs and, therefore, to less chlorine activation. HNO₃ molecules still in the stratosphere are destroyed by photolysis producing NO₂ which will react with ClO to reform the reservoir species ClONO₂ (*Dessler, 2000*). However, with the denitrification due to PSC sedimentation a possible pathway of chlorine deactivation is shut off and more ozone can be destroyed before Cl_x can be deactivated. In such denitrified air, chlorine is, therefore, preferentially deactivated by reactions with CH₄ and HCHO to reform the reservoir species HCl (*McConnell and Jin, 2008*).

In theory, these mechanisms are effective in the polar regions of both hemispheres. Nevertheless, ozone depletion over the Arctic is less severe than over the Antarctic. This is due to the less stable and warmer Arctic vortex (see Section 1.3.2) which reduces the frequency of temperatures low enough to form PSCs and, therefore, results in less chlorine activation (*Dessler, 2000*). Furthermore, in the Arctic, denitrification is reduced as a result of fewer PSCs and, therefore, deactivation of Cl_x is faster and the time period during which ozone can be destroyed is shorter.

For a detailed description of the most common and important chemical reactions involved in stratospheric ozone depletion see *Solomon (1999)*, *Dessler (2000)* and *McConnell and Jin (2008)*.

1.5 Thesis Outline

The research reported in this thesis is presented in five parts in Chapters 2 to 6. The main focus is the identification and investigation of longitudinally resolved, halogen-induced changes in ozone profiles and the associated additional work on creating a suitable data base and globally applicable analyses methods.

In **Chapter 2** the observational data base necessary for the study is described. Since no existing three-dimensional ozone data set can provide the required spatial and temporal coverage in a sufficiently high vertical resolution, a new database had to be assembled. Vertically resolved monthly mean zonal means of ozone, as well as longitudinally resolved monthly means, were calculated from this new database from 1979 to 2006. But even with the use of the new database data gaps exist in both calculated data sets. A traditional approach to determine halogen-induced ozone changes, the use of a linear regression model, was not applicable globally. Therefore a new approach was developed: a regression model was modified so that the regression fit coefficients can be expanded in the horizontal using spherical harmonics. That way fit coefficients for missing data can be determined by evaluating the expansion equations which were fitted to the available data. The physical background of this new approach and a description of its implementation in a regression model are given in **Chapter 3**.

In **Chapter 4** a first application of the new regression approach is described. It was tested on the vertically resolved, monthly mean zonal mean ozone data since there are fewer data gaps compared to the longitudinally resolved data set. Additionally, results can be compared more easily since studies based on zonal mean ozone data are more abundant facilitating a first evaluation of the new

method. With the planned expansions of the spherical harmonics in longitude, it was necessary to perform sensitivity tests to estimate the ability of the spherical-harmonics-based regression to capture more complex global patterns and deal with more missing data. In **Chapter 5**, the results of three different sensitivity tests performed are reported. These tests were based on chemistry-climate model simulations since a complete data set, with temporal and spatial characteristics identical to the observations, was needed to evaluate the influence of data gaps. Results of the sensitivity tests assist in the interpretation of the longitudinally resolved regression outcome which is presented in **Chapter 6**. Five examples of longitudinally dependent halogen-induced changes on ozone are described in detail and their results are compared to available total column ozone studies.

In **Chapter 7** the analyses carried out for this thesis are summarized and overall conclusions of the results of the main chapters are presented. In addition, possible extensions to the different new approaches are presented and possible future applications are outlined.

Chapter 2

Observational data basis

Most vertically resolved analyses of ozone changes are based on zonal mean data since the data density is seldom sufficient to allow longitudinally resolved analyses. There are two commonly used vertical ozone profile databases currently available for diagnosing trends in ozone as a function of latitude and altitude (*Fortuin and Kelder, 1998; Randel and Wu, 2007*). Both report monthly mean zonal mean data only, with no longitudinal resolution. To be able to analyze longitudinally resolved ozone profiles a new database had to be assembled where the stored data had to have a high vertical resolution, good temporal and spatial coverage and an uncertainty estimate on each measurement. This database is called the BDBP (binary database of profiles) and is described in detail in *Hassler et al. (2008)*. Many source gas profiles were added to the BDBP but only ozone is relevant for the planned analyses. Therefore, the following sections include descriptions of the BDBP structure, data sources and coverage of the latest available version 1.1.0.5, but confined to ozone only.

The analyses described later in this thesis are based on monthly mean values, a temporal unit which is commonly used for analyses of long-term changes and variability in ozone. Since individual measurements are stored in the BDBP, it was possible to assemble the monthly means according to the desired spatial resolution, zonal mean or longitudinally resolved grid. The method applied to calculate the monthly means is described in the last section of this chapter.

the database. For each grid, the data are stored in 90 files, each of which span 2° in geographic latitude or, for Grid III, 2° of equivalent latitude, for convenience.

For the work presented here only data from Grid II were analyzed since its vertical dimension is also used in a chemistry-climate model data set which is used for sensitivity tests and is described later in this thesis. Grid II is therefore the only grid described in more detail. It has 70 pressure levels spaced approximately 1 km apart given by:

$$p_n = p_0 e^{-n/7}, n = 1..70, \quad (2.1)$$

where $p_0=1013.25$ hPa.

The pressure levels are exactly 1 km apart when the scale height (RT/g) is 7 km ($R=286.9$ N m kg $^{-1}$ K $^{-1}$, $g=9.8$ m s $^{-1}$).

Each measurement comprises a value, an error in percent, and a data descriptor (e.g. ‘Ozone_LowRes’). The length of each measurement set varies according to the number of measurements available. In this way, the grids are kept compact since no null values need to be stored. If the source data are in the form of vertical profiles, values are interpolated onto the pre-defined vertical levels with the result that the profile is no longer kept as a single entity within the grid. Each measurement set has its own unique time stamp and therefore the measurement sets at a given pressure level and latitude bin need not be equally spaced in time (see Figure 2.1).

The primary target variable of the BDBP so far is ozone and the data sources used have been selected to optimize the spatial and temporal coverage for this variable. Where other coincident measurements (e.g. NO $_2$ or H $_2$ O) are available from the data sources, these have been added to the grids. Two different types of ozone are provided, namely high resolution ozone (data descriptor: Ozone_HighRes) and low resolution ozone (data descriptor: Ozone_LowRes). Both types of ozone are given in number density (10^{18} molecules/m 3). The high resolution ozone comes from ozonesondes only. The low resolution ozone comprises satellite-based measurements and are also derived from the ozonesonde profiles after a 1500 m FWHM Gaussian filter has been applied. The width of the Gaussian filter was selected based on comparisons between smoothed ozonesonde profiles and SAGE II profiles. By providing both high and low resolution ozone data from the ozonesondes, comparisons between ozonesondes and satellite-based measurements are facilitated. The analyses presented here are based on the low resolution ozone values only.

2.2 Data sources

Criteria for the selection of source data for this version of the BDBP were:

1. Only profile data are considered and profiles with high vertical resolution (i.e. better than ~ 1.5 km) are preferred. Two data source groups fulfilling these criteria are solar occultation satellite-based instruments and ozonesondes. Lidar and aircraft profile measurements would also have been suitable but have not yet been included in the BDBP since coincident temperature or pressure data were required to permit the data to be included in Grids II and III and these were not always available. Furthermore, these data sources would not have added significant quantities of data to the BDBP.
2. The measurement errors should preferably be small.
3. Source data spanning longer periods were given higher priority.
4. Measurements covering a data sparse time period or region of the globe were given high priority. For those measurements even a lower vertical resolution than ~ 1.5 km was acceptable.

These criteria led to the use of HALOE, SAGE I, SAGE II, POAM II, POAM III, LIMS and ozonesondes as data sources for this version of the BDBP. The specifics concerning the addition of each of these data sources are given in Subsections 2.2.1 to 2.2.5, and information about data coverage and resolution is given in Table 2.1.

2.2.1 SAGE I and II

2.2.1.1 SAGE I and II instrument and data information

Both Stratospheric Aerosol and Gas Experiment (SAGE) instruments were built and launched by the National Aeronautics and Space Administration (NASA) (see for example *McCormick et al.*, 1989; *Cunnold et al.*, 1989; *Nazaryan and McCormick*, 2005; *Liu et al.*, 2006). A newly revised Version 6.1 of the SAGE I data was provided by L.W. Thomason (NASA; personal communication). The SAGE I measurements start in February 1979 and stop in November 1981 spanning 79°S to 79°N .

Version 6.2 SAGE II data were used (*Wang et al.*, 2006a, http://eosweb.larc.nasa.gov/project/sage2/table_sage2.html) which started in October 1984 and ended in August 2005. The spatial coverage spans 80°S to 80°N (see Tab. 2.1), although coverage can be sparse at higher latitudes in winter (*Wang et al.*, 2002).

Table 2.1: Coverage, vertical resolution, period spanned and source of the data for the satellite-based measurements included in Version 1.1.0.5 of the BDBP.

Instrument	Latitudinal coverage	Altitude range	Period spanned	Data Source
HALOE	80°S - 80°N	10-90 km	10/1991 - 11/2005	NASA
LIMS	64°S - 84°N	15-64 km	10/1978 - 05/1979	NASA
POAM II	88°S - 63°S 55°N - 71°N	15-50 km	10/1993 - 11/1996	NRL
POAM III	88°S - 62°S 54°N - 71°N	5-60 km	04/1998 - 11/2005	NRL
SAGE I	79°S - 79°N	10-70 km	02/1979 - 11/1981	NASA ^a
SAGE II	80°S - 80°N	5-60 km	10/1984 - 08/2005	NASA

^aL.W.Thomason, personal communication

Measurement errors for SAGE I and SAGE II, included in the BDBP, are given in the source data files and are calculated by accounting for all known sources of uncertainty in the measurement. For both SAGE I and II the temperature and pressure values included in the data files were not retrieved parameters, but were provided by the National Meteorological Center (NMC). Nevertheless they were used to determine the levels at which the data were inserted into Grid II and Grid III, and were also included as measurements within each measurement set.

Since both SAGE I and SAGE II measure trace gas profiles with the solar occultation method, an additional identifier specifying whether the measurement was made at sunrise or sunset was included in each SAGE measurement set.

2.2.1.2 Altitude correction for SAGE I data

There is a known altitude error in SAGE I observations (*Veiga et al.*, 1995). *Wang et al.* (1996) discuss and analyze this error in detail. For version 1.0.0.0 of the BDBP this fact had to be dealt with separately (*Hassler et al.*, 2008) since the data files provided did not include a correction for the altitude error. However, the newest revision of the SAGE I data which is used for the BDBP from version 1.1.0.2 onwards already includes corrections for the known problems and errors of the data (L.W. Thomason, NASA, personal communication).

2.2.1.3 Screening of SAGE I data

There are few publications that describe how best to screen SAGE I data to remove outliers. Therefore, in this analysis, data quality controls, similar to those performed for the SAGE II data (described below), were applied to remove outliers from the O₃ and NO₂ data. Particularly below 15 km, measurements of O₃ and NO₂ can be affected by aerosols. Therefore, measurements of O₃ and NO₂ were removed if the aerosol extinction at 1000 nm was higher than 0.001/km (L.W. Thomason, NASA, personal communication). Nevertheless, the utility of the SAGE I data below 15 km is limited to qualitative rather than quantitative analyses (e.g. looking for geographical regions of enhanced upper tropospheric ozone). These data are retained in the BDBP with their high error values to allow later screening.

2.2.1.4 Screening of SAGE II data

Rind et al. (2005) showed that O₃, NO₂ and H₂O measurements from SAGE II are affected by interference from aerosols and clouds. Since the original SAGE II data are only available in an unscreened version (although they are provided with quality flags for unreliable data) additional treatment of the data was necessary to ensure the highest possible quality. The screening was performed following the suggestions of *Wang et al.* (1996) and *Rind et al.* (2005) and is described in detail in *Hassler et al.* (2008).

2.2.2 HALOE

The Halogen Occultation Experiment (HALOE) was launched in September 1991 as a NASA project. Measurements are available from October 1991 until November 2005 in the latest Version 19. HALOE uses solar occultation to simultaneously measure, amongst others, vertical profiles of O₃, HCl, HF, CH₄, H₂O, NO and NO₂ which are added to the BDBP. Temperature and pressure profiles above 35 km are retrieved from measurements whereas below 35 km fields from the National Center for Environmental Prediction (NCEP) are used (*SPARC/IOC/GAW*, 1998). These pressures and temperatures were used to determine the levels at which the data were inserted into Grid II and Grid III, and were also included as measurements within each measurement set. The altitude range of the measurements extends from ~15 km to 60-130 km, depending on the species. Although

the vertical resolution of the profiles is ~ 1.6 km, the data were included in the BDBP since these measurements provide good global coverage and have been used in numerous previous studies (*McKenna et al.*, 2002; *Steil et al.*, 2003; *Remsberg and Deaver*, 2005). For every measurement a measurement error is also provided in the source data files and these are added to the BDBP. A sunrise/sunset identifier is also included in each measurement set. HALOE data are already screened for cirrus cloud contamination, described in *Hervig and McHugh* (1999), and therefore no additional screening of the data was done. A detailed analysis of the HALOE ozone data quality (Version 18) is presented in *Bhatt et al.* (1999). For a more detailed HALOE data description see *Russell III et al.* (1993).

2.2.3 POAM II and III

The Polar Ozone and Aerosol Measurement II (POAM II) instrument was developed by the Naval Research Laboratory (NRL) to measure the vertical distribution of atmospheric O_3 , H_2O , NO_2 , aerosol extinction, and temperature. It covers a spectral range from approximately 350 to 1060 nm in nine channels. The latest available version is Version 6 which covers the period October 1993 to November 1996. Measurements were made between 55° and $71^\circ N$ and between 63° and $88^\circ S$ with a vertical resolution of ~ 1 km. The profiles of the different measured species cover an altitude range from 10 km to 50 km (see Table 2.1). For a more detailed description of the POAM II instrument and the retrievals see *Glaccum et al.* (1996) and *Lumpe et al.* (1997), respectively.

POAM III was launched after the satellite on which POAM II was located failed. It started measurements in April 1998 and ended in November 2005. Version 4 is the latest available dataset for POAM III. In this version, quality flags for the profiles of O_3 , H_2O and NO_2 were included to allow screening of lower quality measurements resulting from sunspot activity and aerosol artifacts (*Lumpe et al.*, 2006). Beside these additions, POAM III data sets contain the same species as POAM II, with the measuring channels for the aerosol extinctions slightly shifted. The vertical resolution is also ~ 1 km (*Randall et al.*, 2003), and the measurements were made in almost identical latitude bands (from 54° - $71^\circ N$ and 62° - $88^\circ S$). The altitude range is slightly bigger for POAM III than for POAM II. For a more detailed description of the POAM III instrument and its retrieval algorithms see *Lucke et al.* (1999) and *Lumpe et al.* (2002), respectively.

Since temperature and pressure are not directly measured with the POAM instruments, both variables are taken from reanalyses, either from the UK Met Office

(UKMO) or NCEP and are included in the database. For sorting POAM II and POAM III in Grid II (latitude/pressure) and Grid III (equivalent latitude/potential temperature), the pressure and temperature values from NCEP were used. A sunrise/sunset identifier is also included in each measurement set. Error values are available for both POAM II and POAM III from the original data files and could therefore be added to the database.

2.2.4 LIMS

The Limb Infrared Monitor of the Stratosphere (LIMS) experiment was launched on NIMBUS 7 and was operational from October 1978 through May 1979. It used infrared limb scanning radiometry to simultaneously measure vertical profiles of temperature, O₃, H₂O, HNO₃ and NO₂. In 2002 a reprocessed version (Version 6) of the LIMS data became available (<http://daac.gsfc.nasa.gov/>). It incorporates updated spectroscopic parameters, better estimation of instrument and spacecraft motion effects in the radiances, improved pressure registration of radiance profiles, and retrievals for all scans (*Remsberg et al.*, 2007). Data profiles cover a pressure range from 100 hPa to 0.1 hPa with a vertical resolution of ~ 3.7 km, and a latitude range from 84°N - 64°S (*Gille and Russell III*, 1984). Values for data precision and accuracy are included in the original data files and therefore error values could be added to the database. Since both sunrise and sunset profiles are available from LIMS, an appropriate identifier was included in each measurement set. More details about the instrument description can be found in *Gille and Russell III* (1984), and the validation of the ozone measurements is described in detail in *Remsberg et al.* (2007).

The LIMS data are the only satellite-derived profiles in the BDBP which are not obtained by the solar-occultation method. Although the profiles have a lower vertical resolution than originally presupposed for data sources in the BDBP, the few months of LIMS data were added since they cover a time period where only SAGE I provides data otherwise. Since the very early data of a time period are especially important for analyses of ozone changes, the low vertical resolution of the LIMS data was accepted. With the reprocessed Version 6 the quality of the data improved significantly (*Remsberg et al.*, 2007) so that no further screening was necessary.

2.2.5 Ozonesonde data

2.2.5.1 Ozonesonde data selection

Ozonesondes are balloon-borne instruments that measure in-situ ozone with a wet-chemical method. Ambient air is pumped through an electrolytic cell containing a buffered potassium iodide solution where ozone oxidises the iodide into iodine. The resultant current within the cell is directly proportional to the ozone concentration in the cell. There are several different ozonesonde types in use globally, with the most common being the electrochemical concentration cell (ECC) (*Komhyr, 1969*), the Brewer-Mast (BM) bubbler (*Brewer and Milford, 1960*) and the carbon-iodine (CI) sonde (*Komhyr, 1965*). All ozonesondes are flown together with a radiosonde to measure pressure, temperature and relative humidity.

Many studies analysing the suitability of ozonesonde measurements for long-term ozone trend detection have been published (*Tiao et al., 1986; Bodeker et al., 1998; Logan et al., 1999*). Although the quality of the ozonesonde data depends on the sonde preparation (*Smit et al., 2007*), the experience of the measuring team and some sources of error particular to each instrument, the measurement uncertainties are generally small and can be quantified. The ozonesonde measurements are also still the only data included in version 1.1.0.5 of the BDBP that provide coverage in the troposphere. The ozonesonde data were subjected to thorough quality checks (described below) before being added to the BDBP.

Seven different sources for ozonesonde data were used for the database, mostly databases publicly available in the Internet from WOUDC, NOAA, NDACC and SHADOZ*. A more detailed description of the data sources is given in *Hassler et al. (2008)*. In total, profiles from 136 stations were added to the BDBP spanning 82°N to 90°S (see Appendix in *Hassler et al., 2008*). As long as the sonde type was detailed in the original data file, that sounding was rated as a potential candidate to be added to the database after passing several quality checks which are described below. Soundings from the following sonde types were accepted: Brewer-Mast, Brewer-GDR (*Ronnebeck and Sonntag, 1976*), ECC, Carbon-Iodine, Indian (*Shreedharan, 1968*) and Regener. Where the altitude or time after launch was not available in the original data file, or when the values were unrealistic (e.g. a time after launch of 3 hours for the first data level), these were (re)calculated from the pressure and temperature measurements assuming a mean ascent rate of 6 m/s.

*Abbreviations are explained in Appendix A

Normalization factors (NFs) are calculated by dividing a total column ozone value derived from the ozonesonde ozone profile by an independent total column ozone measurement available either from a coincident ground-based (Dobson or Brewer spectrophotometer) or satellite-based column ozone measurement. For the ozonesonde flights added to the BDBP, new NFs were calculated as follows. First the ozone column from the surface to the top of the ozonesonde flight was calculated using trapezoidal integration. Then the missing ozone between the top of the flight and the top of the atmosphere was added using the climatology of *McPeters et al.* (2007). Added together these provide the total column ozone estimate from the ozonesonde flight. The independent total column ozone value was extracted from the combined total column ozone database from the National Institute of Water and Atmospheric Research (NIWA) (*Müller et al.*, 2008) according to the date, time, and location of the ozonesonde flight. Because this combined total column ozone database is available only from November 1978 onwards, new NFs could not be calculated for flights prior to that date. For flights not reaching 30 hPa the uncertainty on the partial column above the top of the flight is large and a reliable new NF could not be calculated. Therefore, flights not reaching 30 hPa were rejected. Both the original NFs listed in the data files (if available), and the new NFs, are considered for quality checks. If both NFs are available, the original NF must be between 0.9 and 1.1 and the new NF must be between 0.8 and 1.2. If only one NF is available then only the check appropriate for that NF is performed. Ozonesondes profiles from stations equatorward of the polar circles (66° latitude) were not added to the BDBP if neither NF was available. Exceptions were made for profiles from stations poleward of the polar circles. Since during polar night independent total column ozone measurements are rarely available, it was not possible, in most cases, to calculate NFs. Nevertheless, those profiles were added to the BDBP if they met the 30 hPa criterium.

Each ozonesonde measurement set includes the original NF, or the new NF if the original is not available (except for the profiles which were taken during polar night), so that users of the ozonesonde data in the BDBP can choose whether or not to apply the NF to the ozone measurements. While the NF is stored in the BDBP it was not applied to the ozonesonde data. If NFs were applied to the ozone soundings in the original data files they were de-applied before the ozone measurements were added to the BDBP.

Since the measurements in the BDBP are stored at specific altitude/pressure/theta levels, the values for those levels extracted from the ozonesonde profiles must be

interpolated. For an interpolated value to be added to the database at least one measurement must be within 200 m of the respective level.

The period for which data are available differs from station to station. Flights started in the early 1960s at a few stations distributed globally. At many stations flights were done just for a few years, while other stations have measurements only during some months or during campaigns, and some stations have a continuous time series of ozone profiles up until the present. In the late 1990s, new ozonesonde stations were chosen to cover regions poorly represented at that time, specifically in the tropics and southern hemisphere (*Thompson et al.*, 2003b). Combining all seven ozonesonde data sources, flights from the early 1960s to 2006 were added to the BDBP as long as profiles were available and of suitable quality.

2.2.5.2 Ozonesonde data errors

The ozonesonde data files obtained through the sources briefly mentioned above for the most part do not include the measurement errors associated with each measurement, neither for ozone, temperature, relative humidity nor pressure. To estimate the error on the ozone measurement, information about sonde type, quality, and measurement errors were obtained from *Smit and Kley* (1996) unless otherwise specified (see below). According to their suggested classification of sonde type and altitude range, different ozone error values were applied (see Figure 2.2). In addition:

- ECC ozonesondes: error values were taken from *Komhyr et al.* (1985). For Lauder the error profiles for ECC ozonesondes of the 4A and 5A series described by *Bodeker et al.* (1998) were applied.
- Regener ozonesondes: those sondes were not tested in the analysis of *Smit and Kley* (1996), but it is known that the errors of those sondes tend to be quite high (*World Meteorological Organization*, 1989), so relatively high error values, commensurate with other ozonesonde types with high errors, were assumed.

Error values for temperature, pressure and relative humidity for the soundings were chosen according to literature and radiosonde specifications. For more detail on those errors see *Hassler et al.* (2008).

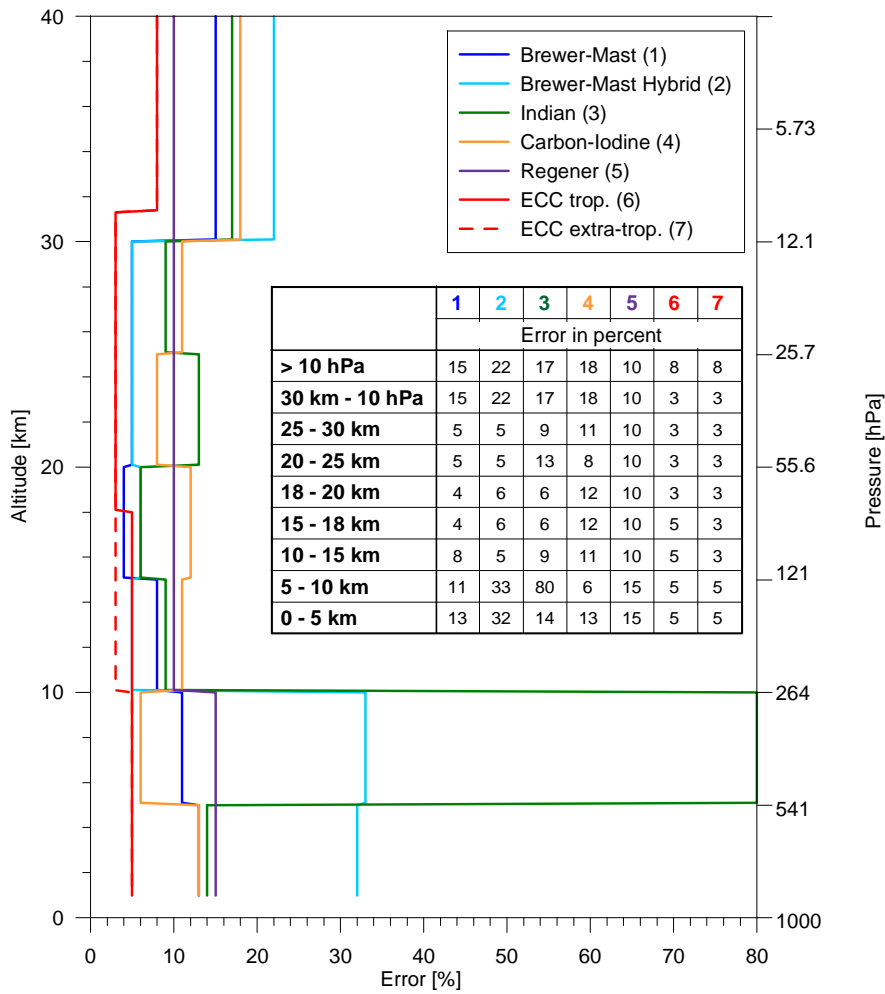


Figure 2.2: Ozone errors [%] for six different ozonesonde types and different altitude/pressure regions as included in the BDBP. Values are obtained from *Smit and Kley (1996)*, or *Komhyr et al. (1985)*.

2.2.5.3 Quality check

Several checks were made to screen and remove poor quality data from the ozonesonde data files, viz. (with respect to the ozone measurements):

- Individual ozone records are rejected when negative ozone partial pressures, 0.0 mPa ozone partial pressures within 60° of the equator, or ozone partial pressure ≥ 25 mPa at altitudes above 30 hPa are measured.
- Entire ozone profiles are rejected when unrealistically low ozone values over the whole profile (profile mean < 2 mPa and profile maximum < 4 mPa) are found or when more than 33% of all ozone values in the profile are 0.0 mPa.
- When two identical records at the same pressure/altitude level (not defined as ascending and descending values) are found, one is rejected.

2.3 Calculation of the monthly mean data

For the regression analyses presented in this thesis monthly mean data were required. As described in *Hassler et al.* (2009, accepted), monthly mean ozone number density time series, on the latitude/pressure grid described in Section 2.1, were calculated from all available data sources in the BDBP. For the analysis described in Chapter 4, zonal mean monthly means were necessary whereas individual time series for different longitude bins had to be calculated for the analysis described in Chapter 6. The monthly mean calculation was in both cases the same, with the exception that a longitudinal bias correction for unequal sampling of measurements was applied for the calculation of the zonal mean time series. The whole globe was gridded into 36 latitude bands of 5° width. For the longitudinally resolved analysis those latitude bands were further divided into six longitude bins of 60° each.

The version of the BDBP which was the basis for the monthly mean calculations (Version 1.1.0.5) does not consider the issues of possible inhomogeneities between the different data sources. While comprehensive screening was applied, systematic offsets and drifts between the data sources are likely (*McPeters et al.*, 1999; *Randall et al.*, 2003; *Nazaryan et al.*, 2005). However, only when combining the different data sources is the temporal and spatial coverage sufficient to allow longitudinally resolved analyses. Removing the offsets and drifts between the data sources has not yet been implemented and is a topic for future extensions of analyses presented here. Therefore, a method to partially address this issue was developed for calculating the monthly means from the available data sources in the BDBP.

All data for a given month in a given latitude band or longitude bin were counted, and a monthly mean was only calculated if a minimum of six values per month was available. The only exception to that rule is if only ozonesonde measurements were available in that particular month, the monthly mean was calculated even with only one available ozone value. This reduced requirement is based on the fact that most sounding stations launch an ozonesonde only once a week, some even less often, and that some stations cover geographical regions where no other measurements are available. Any information in those regions about ozone development, even based on only one value, increases the chance of a realistic global estimation of ozone changes.

The available data points are then sorted in order of magnitude. Since for every value an error is also stored in the BDBP (see Section 2.1), it is possible to take

the uncertainty on the measurements into account in calculating the monthly mean value. The errors (σ) are transformed into weights (w) according to the following formula:

$$w_i = \frac{1}{\sigma_i^2}. \quad (2.2)$$

After this transformation the weights were normalized so that all weights add up to 1. The weights between 0 and 0.25 (lowest quartile), and between 0.75 and 1 (highest quartile) were then set to 0. In doing so it is possible to select only the ‘conservative’ middle values of all available data points (no very high or very low values) for the calculation of the monthly mean.

Error values on profiles derived from satellite measurements generally increase with decreasing altitude. Although those errors would result in a very small weight for the monthly mean calculation, some satellite measurements were not considered at all below a minimum pressure level to ensure the quality and representativeness of the calculated mean: SAGE II data were only incorporated in monthly means higher than ~ 250 hPa, whereas SAGE I and LIMS data were only considered for pressures lower than ~ 77 hPa.

Monthly means for each latitude/longitude bin and each pressure level were calculated as (*Paradine and Rivett, 1964*):

$$\bar{x} = \frac{\sum w_i x_i}{\sum w_i}, \quad (2.3)$$

where x_i is the i -th value, and w_i is the weight for the i -th value.

Although multiple data sources were used to calculate the monthly mean ozone values, there were periods and locations where there were insufficient data to calculate a valid monthly mean. In the next section, the temporal and spatial coverage of both zonal mean and longitudinally resolved data sets, will be discussed in more detail.

2.4 Database temporal, latitudinal and longitudinal coverage

By combining measurements from several satellite-based instruments and from ozonesondes, it is possible to achieve high temporal and spatial coverage in the BDBP. Table 2.1 summarizes the temporal coverage of the satellites and these, together with the ozonesondes, are shown graphically in Figure 2.3. Note that

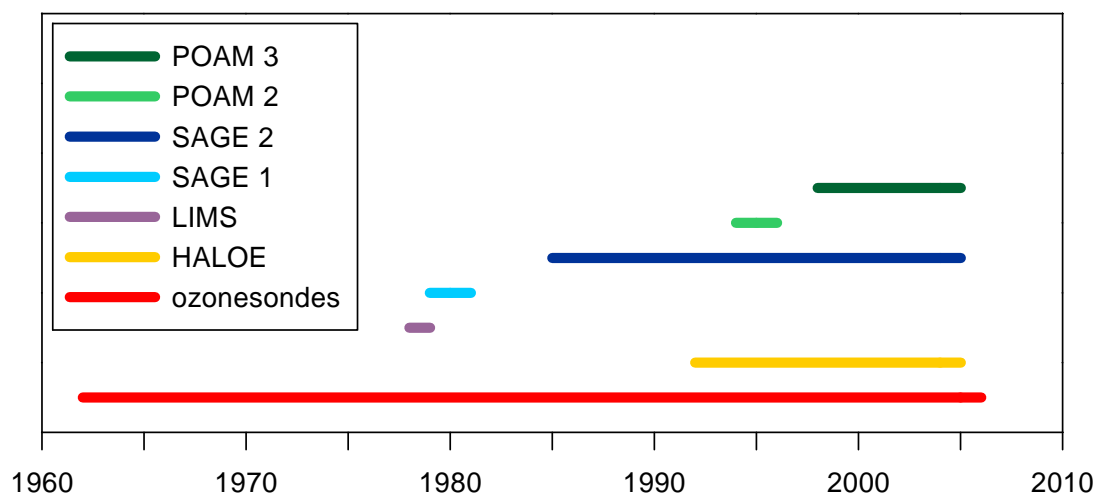


Figure 2.3: Temporal coverage of the database. The red line represents the time period which is covered by ozonesonde data, the yellow line represents the coverage by HALOE etc.

although the ozonesonde data cover a long time period, the spatial coverage can be poor due to the number and location of the ozonesonde stations. In version 1.1.0.5 of the BDBP, for 2006, only ozonesonde data are available, and so the spatial coverage for 2006 is poorer than for the preceding years.

After calculating the monthly means, the percentage of all available values for a given latitude band and pressure level was calculated. The results are shown in Figure 2.4. The upper part of the figure shows the available monthly means for the longitudinally resolved data set, whereas the lower part shows the results for the zonal mean data set. A value of 100% is reached if there are no missing values in the whole time series for a given latitude band (zonal means) or all six longitude bins per latitude band (longitudinally resolved).

It is obvious that the coverage, or data availability, for both data sets is not the same for all latitudes and pressure levels. There are hemispheric differences in coverage, with a higher measurement density, especially at pressures higher than ~ 5 hPa, in the Northern hemisphere. That is caused by a larger number of ozone sounding stations in the Northern hemisphere (see Appendix in *Hassler et al.*, 2008), especially in the mid-latitudes. Without considering the ozonesondes for the monthly mean calculations, the available measurements in the lower stratosphere and particularly in the troposphere would be significantly lower. An optimal coverage of 100% is reached for the latitude band 50°N - 55°N in the zonal mean data set (Figure 2.4 (b)), for pressures higher than 13 hPa. Only a few monthly means are missing for the same pressure range for the latitude band

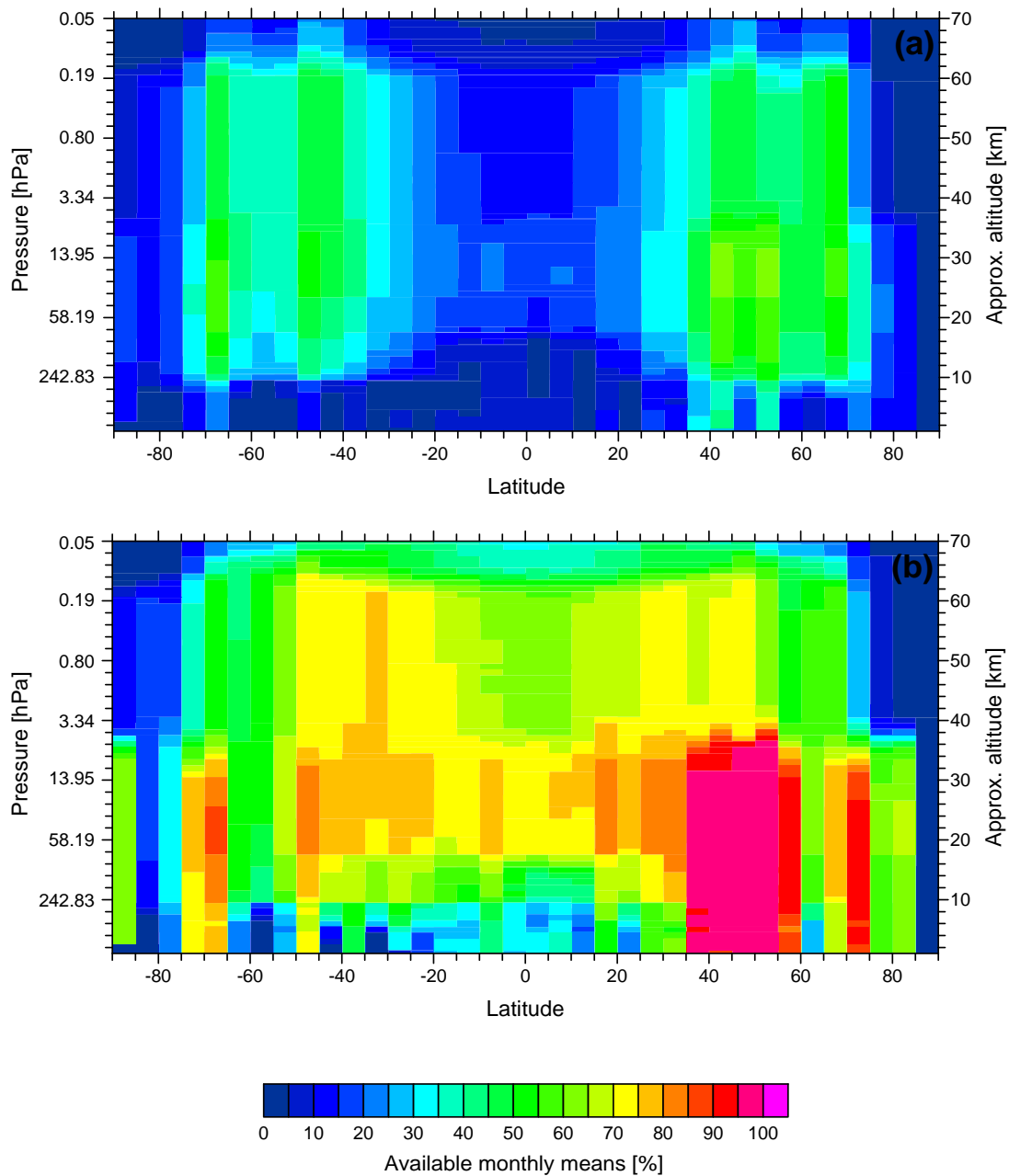


Figure 2.4: Percentage of available monthly mean values in the period 1979 to 2006 as a function of pressure levels and latitude. a) longitudinally resolved data set, b) zonal mean data set.

45°N-50°N. Especially in the high latitudes and the tropics, the number of available monthly means is lower, in an extreme case with no monthly mean values at all poleward of 85°N. This lack of data is either caused by no coverage of any of the instruments contributing to the BDBP (e.g. North Pole region) or a low spatial and temporal measurement density (e.g. the tropics).

Increasing the number of grid cells in longitude (from one in the case of zonal means to six for the longitudinally resolved data set) results in a decrease in data coverage, as can be seen in Figure 2.4 (a). The reduced availability indicates that the spatial distribution of the measurements within one latitude band is not even but with some regions where the measurement density is high (e.g. Europe) and regions where no measurements at all are available (e.g. over oceans). This given measurement distribution emphasizes the importance of a longitudinal bias correction when calculating zonal mean monthly means as mentioned in Section 2.3. Considering the reduction in data coverage for the longitudinally resolved data set, it becomes clear that a partition of all measurements within one latitude band into more than six longitude bins is not advisable. Even with only six longitude bins per latitude band, substantial temporal and spatial data gaps are obvious (Figure 2.4 (a)).

Figure 2.5 shows an example of vertically and temporally resolved percentage deviations from zonal mean monthly mean ozone for the latitude band 40°N to 45°N for all six longitude bins. Zonal means and deviations were calculated for every month separately. Blue colors in the graphs represent negative deviations, red colors represent positive deviations. White areas indicate missing monthly means for the respective longitude bin. The gray dashed line at ~ 35 km is displayed to help attributing the deviations to the respective pressure/altitude regions. While the distribution of monthly means calculated from satellite data is very similar for all six longitude bins, the addition of the ozonesondes significantly increases coverage in the troposphere and lower stratosphere of the longitude bins to which the sounding stations are assigned. Overall, percentage deviation is largest for all six longitude bins in the region around the tropopause. Ozone variability is highest there, with many small scale fluctuations, which increases the deviations from the zonal mean. The strongest negative deviations occur between 120°W and 60°W, whereas the strongest positive deviations are present exactly 180° shifted, between 120°E and 180°E. Further distinct longitudinal differences can be seen above ~ 40 km. Deviations are significantly smaller there, but they are mostly positive between 120°E and 120°W, whereas negative deviations prevail in the longitude bins around the 0° meridian. While this figure does not necessarily

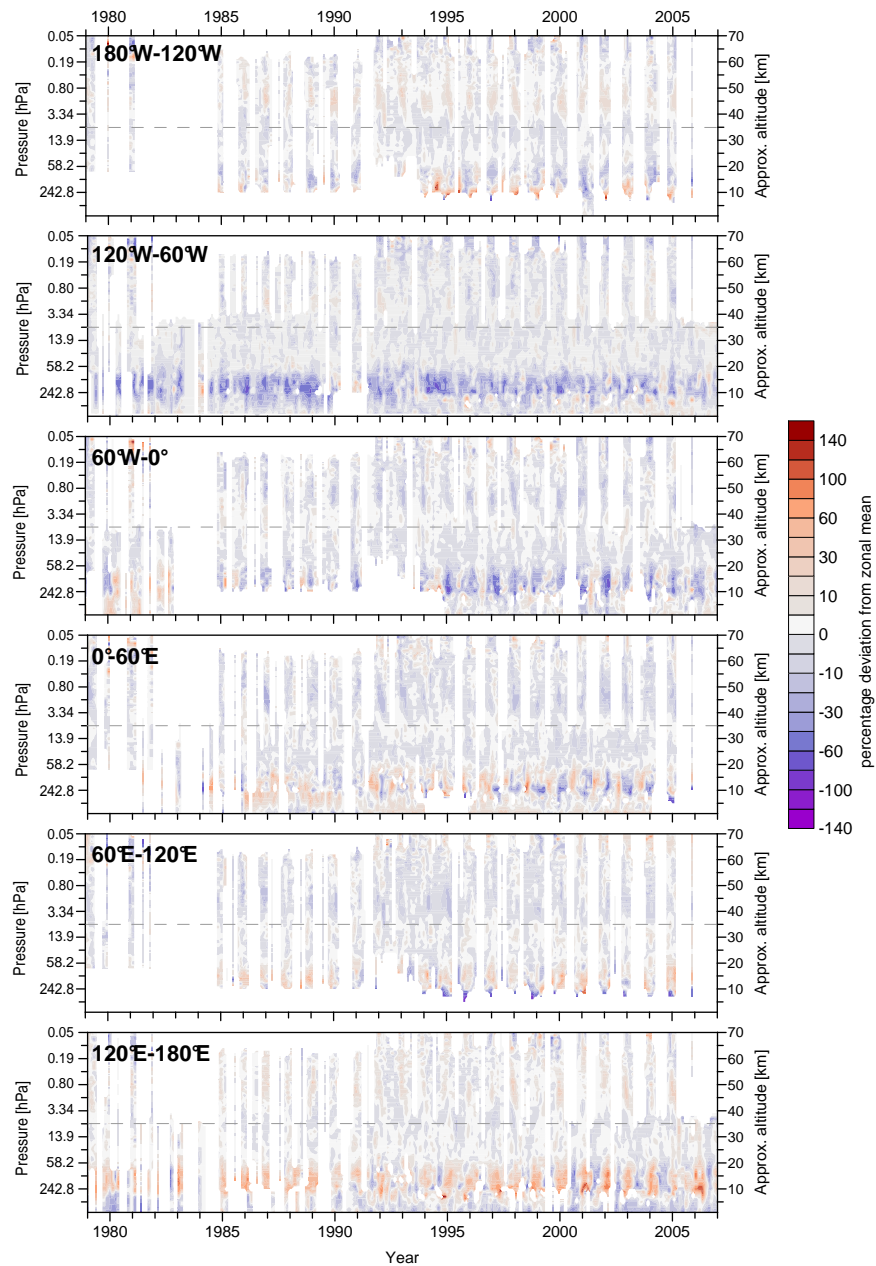


Figure 2.5: Percentage deviation from zonal mean monthly mean ozone between 40°N and 45°N from 1979 to 2006 for all six longitude bins. Red colors indicate more ozone than the zonal mean for the respective month, blue colors indicate less ozone. White areas represent regions where no data were available. The gray dashed line represents the approximate altitude of 35 km.

demonstrate longitudinal differences in ozone changes, it helps getting a better understanding of the characteristics of the longitudinally resolved data set.

2.5 Summary

A new database of vertically high resolved ozone profiles was assembled from several satellite instruments and ozonesondes. All measurements were thoroughly quality checked and then added to three predefined database grids. Longitudinally resolved and zonal mean monthly means were calculated from the grid based on pressure levels for 5° latitude bands. Data coverage is for most latitude bands acceptable in the zonal mean data set. However, even with a partition of each latitude band into only six longitude bins, data coverage is significantly reduced for the longitudinally resolved data set. Therefore, a traditional approach of estimating ozone changes (multiple linear regression) could not be applied successfully. A new method had to be developed which would be applicable in spite of the data gaps. This new method is described in detail in the following chapter, as well as general information about linear regression methods and the most commonly used explanatory variables.

Chapter 3

Regression

Linear regression analysis is the most appropriate method to determine trends in atmospheric data sets. Especially for the detection of ozone changes, in the column and within profiles, a wide variety of regression analyses are used. The approaches differ in the preparation of the time series to be analyzed, in the selection of the regression basis functions (explanatory variables), in the preparation of the basis functions, and consideration of the fundamentals of statistical regression.

In the following section the development of regression models as trend estimators in ozone research is briefly described to provide an overview of the regression techniques previously used. The standard regression technique used is normally applied to individual ozone time series. Since the aim of the analyses planned for this study are to provide global results of halogen-induced ozone changes for several pressure levels, either the conventional time series regression would have to be applied for each pressure level and for each latitude and longitude separately, or a new approach where one global fit for each pressure level is employed would need to be developed. This latter, global, approach was chosen as the method for determining ozone changes in this study, since numerous occurrences of data gaps inhibited the global application of a standard regression. The mathematical basis for the new analyses is the use of spherical harmonics to represent the spatial variability of global ozone distribution. These are described in detail in Section 3.2. The newly developed regression model, in which the spherical harmonics are incorporated, is explained in detail in Section 3.3, together with a discussion of the explanatory variables used and a consideration of uncertainties in the regression coefficients.

It is well known that time series data of atmospheric constituents can be serially correlated. To account for that, auto-regressive descriptors of the serial auto-correlation are employed. However, the standard auto-regressive models consider only serial auto-correlation and not spatial auto-correlation since such models are applied only to discrete time series. Since the global data set which is used in this study is not only a function of time, but also a function of latitude and longitude, the correlation between data is not only temporal but also spatial. Therefore, the usual treatment of auto-correlation in the data has to be adjusted before it can be used in the global regression analysis. The temporal and spatial autocorrelation treatments are described at the end of Section 3.3.

3.1 Background, history and use of regression models

To describe a linear relationship between two variables, a the simple linear regression method is applied where an independent variable, x , also called the predictor or explanatory variable, is linked with a dependent variable, y , also called the predictand (see Equation 3.1; *Wilks*, 2006).

$$y = a + bx \tag{3.1}$$

This method tries to express the relationship between predictor variable and predictand as linear dependance of y on x . The summand a and the coefficient b of that linear dependance are determined so that y is the best possible representation of x . In many cases, however, more than one variable is required to optimally predict the dependent variable (*von Storch and Zwiers*, 2002). In such cases a multiple linear regression method is applied where the dependent variable, y , is a function of several combined independent variables x_n :

$$y = a_0 + a_1x_1 + a_2x_2 + \dots + a_nx_n . \tag{3.2}$$

Those independent variables are chosen **a-priori**, according to their known influence on y . Each of the n explanatory variables has its own coefficient a_n , called a regression parameter, with a_0 being the regression constant (*Wilks*, 2006). The combination of the explanatory variables is linear, thus the regression model is linear in its parameters. However, the explanatory variables themselves can be non-linear functions in time (*von Storch and Zwiers*, 2002).

Although total column ozone measurements started early in the 20th century, attempts to analyze ozone time series with regression methods began several

decades later after *Molina and Rowland (1974)* and *Cicerone et al. (1974)* had published their work on catalytic ozone destruction cycles in the stratosphere due to man-made chlorofluoromethanes which belong to the chlorofluorocarbons. *Hill et al. (1977)* analyzed total column ozone data from 9 stations located in different regions of the world to find the first signs of a non-natural global ozone change. They used a linear ramp-function (also known as a hockey stick) with a level baseline until 1970 and a linear trend thereafter. Since then regression analyses found their way into the scientific community, mostly for analyses of total column ozone (from ground-based measurements and satellites) since the temporal quality of the available vertically resolved ozone data was still quite poor (*Harris et al., 1997*). Early analyses did not account for seasonal variation in the ozone trends (e.g. *Reinsel, 1981*; *St. John et al., 1981*; *Oehlert, 1986*; *Reinsel et al., 1987*) although it was suspected that substantial differences in the seasonal variation of ozone existed. In the late 1980s *Rowland et al. (1988)* analyzed several Dobson time series for the first time with respect to seasonal dependances and could prove that ozone destruction indeed had a seasonal component. With increasing availability of satellite measurements, global trend analyses became more common and new details about ozone trends were discovered, for example longitudinal variations in total column ozone trends (*Stolarski et al., 1992*; *Niu et al., 1992*), or the latitude dependance of seasonal trends (*Bojkov et al., 1990*). An overview of the most commonly used regression models (seasonal, uniform, regional or latitudinal) in the late 1980s for total column ozone is given in *World Meteorological Organization (1989)*. However, limitations of regression models as tools for discovering trends revealed themselves as well: trends are very sensitive to the length of the analyzed time series (*Hollandsworth et al., 1995*), and to data quality and stability (*Harris et al., 1997*). These factors remain key obstacles for trend analyses. In recent years little has changed with the regression method itself, but more with the choice of explanatory variables (*Wohlmann et al., 2007*; *Mäder et al., 2007*), or the extent of the analysis (*Steinbrecht et al., 2003*).

Before the mid 1990s, the vertical distribution of ozone and vertically resolved trends were not given much attention (*Logan, 1994*). The temporal density of measurements from ozonesondes was not high enough to allow many trend studies, with the exception of a few sounding stations world-wide. Although ozonesonde data are not without difficulties (*Tiao et al., 1986*) they provided for a long time the only available data for trend analyses in the lower stratosphere and upper troposphere (*Logan, 1994*). Quantifying vertical ozone trends provides insight into possible mechanisms as well as inferring possible impacts on climate (*Harris et al., 1997*). The first comprehensive ozonesonde trend analyses were

done by *Logan (1994)* and *Miller et al. (1995)*. Later, more extensive studies were published based on vertical high resolution global satellite ozone measurements (*Wang et al., 1996; Cunnold et al., 2000; Nazaryan et al., 2007*). Nevertheless, spatial coverage of ozone profile measurements is still insufficient to allow global vertically resolved trend analyses with the traditional methods.

Linear regression analyses of long-term changes and variability in ozone have their pitfalls and a number of publications have highlighted these. *Tiao et al. (1986)* pointed out that the length of the analyzed data series affects the statistical significance of derived trends. *Weatherhead et al. (1998, 2000)* stated that there were three factors on which the ability of trend detection depends: (i) the size of the trend to be detected, (ii) the noise in the data, and (iii) the autocorrelation of the noise in the data. Over the past decade scientists have analyzed ozone data for any sign of a slow down in ozone depletion or even ozone recovery. As *Reinsel et al. (2002)* and *Reinsel et al. (2005)* pointed out, for such analyses it is essential to be able to determine the errors on the regression coefficients precisely in order to detect small changes in trends. Although many studies deal with important information about the application of regression methods, a fundamental guide on how to use regression models for ozone trend detection, with a precise description of factors to consider, is still missing.

The choice of explanatory variables (or basis functions) is the beginning point for regression analyses, and depends strongly on the purpose of the regression. A core combination of basis functions used to determine long-term changes and variability in ozone has converged on a set which can now be thought of as the standard (*Harris et al., 1997; World Meteorological Organization, 2007, Chapter 3*): a seasonal cycle, a number of geophysical influences, for example the QBO, the solar cycle (or solar flux) and volcanic aerosols. Either a linear term or a time series of equivalent effective stratospheric chlorine (EESC; for more detail on EESC see *World Meteorological Organization, 2007, Chapter 6; Newman et al., 2007*) is then used to explain the ozone trends, the ozone change caused by the release of chlorofluorocarbons (CFCs) into the atmosphere. For studies where the goal is to assess the effects of CFCs on ozone, the basis functions detailed above are sufficient to capture the main influences. If the goal of the regression is to explain the ozone variability in the best possible way or address the influence of atmospheric dynamics on ozone variability, additional basis functions such as teleconnection patterns (*Appenzeller et al., 2000; Brönnimann et al., 2000; Steinbrecht et al., 2001*), tropopause height (*Steinbrecht et al., 1998*) or lower stratospheric temperature (*Steinbrecht et al., 2003*) are used. However, not all dynamical basis

functions are without problems. In some cases it is possible that the temporal development of the dynamical basis function is dependent on ozone concentrations (e.g. stratospheric temperature) in which case the cause and effect cannot be separated properly and the effect of the basis function on ozone distribution is not unambiguously assignable.

Initially, accounting for seasonal dependancies in ozone trends was done by only analyzing data from selected months or seasons (e.g. *Rowland et al.*, 1988), but more accurate ways of considering seasonal variation were introduced in recent years. Those are based on harmonic analyses where temporal variations are expressed as a sum of a series of *sin* and *cos* functions (*Wilks*, 2006), also known as Fourier series. So instead of applying the regression monthwise (or seasonalwise), the whole-year ozone data are used in the regression in which the basis functions account for seasonality. The month-to-month changes are then accounted for by the included Fourier pairs. The stronger the expected seasonal dependance of the basis function the higher the number of expansions in Fourier pairs. An expanded offset term included in the regression then represents the seasonal cycle (used for example in *Bodeker et al.*, 1998).

A first attempt to estimate the halogen-induced ozone changes for the zonal mean data described in Section 2.3 with an approach similar to the above described methods was made for the following project: the development of a vertically resolved, monthly mean ozone database from 1850 to 2100 for constraining global climate model simulations (i.e. AOGCMs). Since climate model simulations for the IPCC 4th assessment report differed in their treatment of ozone radiative forcing (*Miller et al.*, 2006) the need of a homogeneous global and vertically resolved ozone data set for future climate model simulations is more urgent then ever. To keep this database as close to reality as possible only the future and very early years of the time period to cover should be derived from coupled chemistry-climate models, but the core from 1979 to 2006 should be based on observations. Naturally, the observational core had to be complete. To fill in the data gaps which the monthly mean data set derived from the BDBP contain a regression constrained interpolation was applied, as described in *Hassler et al.* (2009, accepted). Therefor the variability in monthly mean ozone was addressed to several known geophysical sources by a traditional linear regression. The regression was fitted first to latitude regions and pressure levels where fewest data were missing. If more than 20% of the data were not available values were ‘borrowed’ from neighbouring pressure levels and latitude regions to ensure that sufficient data were available for the regression model fit. Borrowed values were corrected for

latitudinal and vertical gradients, and they were only used to reliably constrain the regression model, not to actually fill the data gaps. The latter was done by linear interpolation between the regression residuals and adding the obtained interpolated residuals back to the regression results. For more details on this project and the described regression constrained interpolation see *Hassler et al.* (2009, accepted).

While it was possible to fill the data gaps of the zonal mean monthly mean data set by regression constrained interpolation, applying a similar approach to the longitudinally resolved data set was impossible since significantly more data are missing and sampling biases are more pronounced. The completed vertically resolved zonal mean ozone data set shows overall realistic ozone distributions, however, there are problems with overestimated gradients and propagating errors due to the borrowing process. Trying to fill even more missing data with this method would enhance those problems drastically. A different approach had to be found where data gaps would not matter so much. Similar to harmonics describing temporal dependencies in data sets (see earlier in this section), harmonics could also describe spatial connections and could be fitted even with some data gaps. The physical fundamentals of those harmonics and their implementation in a regression model are described in the following sections.

3.2 Spherical harmonics

3.2.1 Physical background

Laplace's equation is a linear second-order differential equation. This common and important equation (Eq. 3.3) can describe many problems of theoretical physics, e.g. electromagnetic phenomena, hydrodynamics, heat flow and gravitation (*Arfken*, 1970), and is expressed in its most general form with the squared del operator ∇ which is applied on a function f .

$$\nabla^2 f = 0 \tag{3.3}$$

Depending on the problem to be solved, Laplace's equation can be expressed in different coordinate systems:

Laplace's equation in Cartesian Coordinates (3-dim)

$$\nabla^2 f = \frac{\partial^2 f}{\partial x^2} + \frac{\partial^2 f}{\partial y^2} + \frac{\partial^2 f}{\partial z^2} = 0 \tag{3.4}$$

Laplace's equation in Spherical Coordinates (r , θ and φ ; 3-dim)

$$\nabla^2 f = \underbrace{\frac{1}{r^2} \frac{\partial}{\partial r} \left(r^2 \frac{\partial f}{\partial r} \right)}_{\text{radial part}} + \underbrace{\frac{1}{r^2 \sin \theta} \frac{\partial}{\partial \theta} \left(\sin \theta \frac{\partial f}{\partial \theta} \right) + \frac{1}{r^2 \sin^2 \theta} \frac{\partial^2 f}{\partial \varphi^2}}_{\text{angular part}} = 0 \quad (3.5)$$

The function f can be imagined as a product of functions each containing only a single variable (Byerly, 2007):

$$f(r, \theta, \varphi) = R(r)\Theta(\theta)\Phi(\varphi) . \quad (3.6)$$

The **spherical harmonics** are then an orthogonal set of solutions to Laplace's equation of three dimensions defined in spherical coordinates. If only the angular portion is considered the resulting functions are called **surface spherical harmonics**, whereas the solution considering the radial part of Laplace's equation as well is called **solid spherical harmonics**. Since only surface spherical harmonics are of interest for the presented work the term 'spherical harmonics' refers hereafter to surface spherical harmonics.

The most common way to get particular solutions of partial differential equations is by the method of separation of variables. For that, the function $f(r, \theta, \varphi)$ in Equation 3.5 is replaced by the right hand side of Equation 3.6. That gives:

$$\underbrace{\frac{1}{R(r)} \frac{\partial}{\partial r} \left(r \frac{\partial R(r)}{\partial r} \right)}_{\text{only dependent on } r} + \underbrace{\frac{1}{\sin \theta} \frac{1}{\Theta(\theta)} \frac{\partial}{\partial \theta} \left(\sin \theta \frac{\partial \Theta(\theta)}{\partial \theta} \right) + \frac{1}{\sin^2 \theta} \frac{1}{\Phi(\varphi)} \frac{\partial^2 \Phi(\varphi)}{\partial \varphi^2}}_{\text{dependent on } \theta \text{ and } \varphi} = 0 . \quad (3.7)$$

Since the two parts labeled in Equation 3.7 have the variables separated (only r in the first part of the equation, θ and φ in the second part), those two parts are independent from each other. That means both parts must be equal to a constant which in this case was chosen to be the integer $l(l+1)$. Equation 3.7 then resolves into two differential equations of which the one containing the angular portion of Laplace's equation (defined with $\Theta(\theta)$ and $\Phi(\varphi)$) is

$$\frac{\Phi(\varphi)}{\sin \theta} \frac{d}{d\theta} \left(\sin \theta \frac{d\Theta}{d\theta} \right) + \frac{\Theta(\theta)}{\sin^2 \theta} \frac{d^2 \Phi}{d\varphi^2} + l(l+1)\Theta(\theta)\Phi(\varphi) = 0 . \quad (3.8)$$

The method of separation of variables is applied a second time with the constant chosen this time as the integer m^2 . This results in the following two equations:

$$\frac{1}{\Phi(\varphi)} \frac{d^2 \Phi(\varphi)}{d\varphi^2} = -m^2 , \quad (3.9)$$

$$l(l+1)\sin^2(\theta) + \frac{\sin\theta}{\Theta(\theta)} \frac{d}{d\theta} \left[\sin\theta \frac{d\Theta}{d\theta} \right] = m^2, \quad (3.10)$$

for some m and l . Equation 3.9 is the separated azimuthal equation (only dependent on φ), and is the well known equation of a harmonic oscillator. Equation 3.10 depends only on the polar angle (θ) and leads to the **associated Legendre functions** (Arfken, 1970). The combination of both differential equations gives the angular solution of Laplace's equation. It includes the products of trigonometric functions and the associated Legendre functions:

$$Y_l^m = N e^{im\varphi} P_l^m(\cos\theta). \quad (3.11)$$

Y_l^m is called a spherical harmonic function of degree l and order m . N is a normalization constant, $e^{im\varphi}$ describes the trigonometric functions of the product (function of the longitude angle φ), and $P_l^m(\cos\theta)$ the associated Legendre function (function of θ). In choosing the boundary conditions as periodic in φ and regular at both the north and south poles, it is ensured that the degree l and the order m are integers that satisfy $l \geq 0$ and $|m| \leq l$.

Associated Legendre functions can be expressed as shown in Equation 3.12 where $P_l(\cos\theta)$ are the so called **Legendre functions**. Evaluated examples of both groups of functions (for $0 \leq l \leq 3$ and $0 \leq m \leq 3$) are listed below. For $m = 0$ the associated Legendre function $P_l^m(\cos\theta)$ is identical with the Legendre function $P_l(\cos\theta)$.

$$P_l^m(\cos\theta) = (-1)^m (\sin\theta)^m \frac{d^m}{d(\cos\theta)^m} (P_l(\cos\theta)) \quad (3.12)$$

$$\begin{aligned} P_0^0(\cos\theta) &= 1 & P_3^0(\cos\theta) &= \frac{1}{2}(5\cos^3\theta - 3\cos\theta) \\ P_1^0(\cos\theta) &= \cos\theta & P_3^1(\cos\theta) &= -\frac{3}{2}(5\cos^2\theta - 1)\sin\theta \\ P_1^1(\cos\theta) &= -\sin\theta & P_3^2(\cos\theta) &= 15\cos\theta\sin^2\theta \\ & & P_3^3(\cos\theta) &= -15\sin^3\theta \\ P_2^0(\cos\theta) &= \frac{1}{2}(3\cos^2\theta - 1) \\ P_2^1(\cos\theta) &= -3\cos\theta\sin\theta \\ P_2^2(\cos\theta) &= 3\sin^2\theta \end{aligned}$$

The spherical harmonics form a complete set of orthonormal functions. Any square-integrable function can therefore be evaluated over the surface of a sphere,

by expansion with a linear combination of those harmonics (*Butkov*, 1968):

$$f(\theta, \varphi) = \sum_{l=0}^{\infty} \sum_{m=-l}^l f_l^m Y_l^m(\theta, \varphi). \quad (3.13)$$

Since many applications of spherical harmonics only require real-value spherical functions, it is more convenient to express them as real-valued spherical harmonics:

$$Y_l^m = \begin{cases} Y_l^0 & \text{if } m = 0 \\ \frac{1}{\sqrt{2}}(Y_l^m + (-1)^m Y_l^{-m}) = \sqrt{2}N_{(l,m)}P_l^m(\cos \theta) \cos m\varphi & \text{if } m > 0 \\ \frac{1}{i\sqrt{2}}(Y_l^{-m} - (-1)^m Y_l^m) = \sqrt{2}N_{(l,m)}P_l^{-m}(\cos \theta) \sin m\varphi & \text{if } m < 0 \end{cases} \quad (3.14)$$

Three different types of spherical harmonics are distinguished (see Figure 3.1):

1. If $m = 0$ the spherical harmonics only consist of the associated Legendre functions and hence do not depend on longitude. They are circular symmetric and are referred to as **zonal**.
2. If $l = |m|$ the resulting spherical harmonics are called **sectoral**.
3. For all other combinations of l and m the spherical harmonics divide the unit sphere in several blocks of latitude and longitude. They are then called **tesseral**.

Spherical harmonics are not only an important tool in the field of theoretical physics but also in chemistry for the computation of atomic electron configuration, representation of gravitational fields, and in recent years indispensable in real time computer graphic applications.

For a more detailed overview of the physical background of spherical harmonics and associated Legendre functions see *Margenau and Murphy* (1956), *Pipes* (1958), *Butkov* (1968), *Arfken* (1970) and *Byerly* (2007).

3.2.2 Implementation in a regression model

The global distribution of any variable, e.g. a trace gas on some pressure level, or total column ozone, can be described in terms of expansions of spherical harmonics. The choice of l and m in the equations outlined in Section 3.2.1 determines the resolution at which the global distribution is resolved. Since the purpose

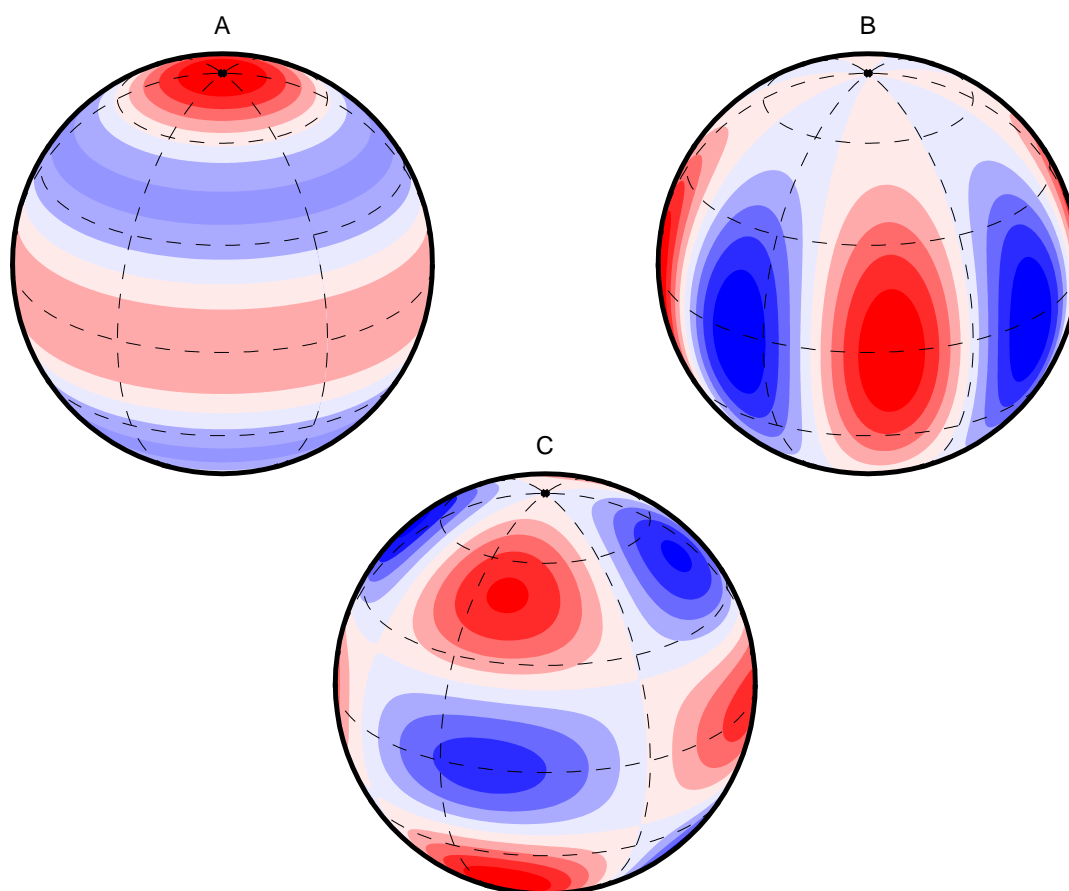


Figure 3.1: Schematic overview of the three different types of spherical harmonics. A) zonal spherical harmonics, $l = 4$ and $m = 0$, B) sectoral spherical harmonics, $l = 4$ and $m = 4$, C) tesseral spherical harmonics, $l = 4$ and $m = 2$.

of this study is to investigate the global pattern of halogen-induced changes in ozone, the use of spherical harmonic expansions was obvious: Ozone time series would not have to be analyzed individually for each pressure, latitude and longitude bin, but could be fitted with a single fit of a regression model for each pressure level.

There are two major advantages of this approach compared to using a traditional regression applied individually at each latitude and longitude:

1. Application of spherical harmonics acknowledges the spatial correlation in halogen-induced ozone changes between neighboring latitude/longitude bins. In the real world, ozone concentrations at some atmospheric layer are related to concentrations at nearby locations via transport; they ‘know’ about each other.

2. For the traditional one-dimensional regression approach (treating each latitude/longitude bin separately) missing data can be problematic for the fitting of the basis functions. With the spherical harmonics approach, missing data are more easily accommodated since the spherical harmonics fit to the available data.

The implementation of the spherical harmonics in a regression model follows the one-dimensional expansion of basis functions in Fourier terms to account for seasonality in the fit coefficients (described in more detail in Section 3.3). Each coefficient of the Fourier expansions is then further expanded in the selected number of spherical harmonics which are a function of latitude and longitude. The values at a given pressure or altitude level that are passed to the regression model, must include the associated latitude and longitude in addition to the ozone, its error value, and its time stamp.

Degree (l) and order (m) of the spherical harmonics have to be defined in advance. For both analyses, with zonal mean monthly mean ozone values and with longitudinally resolved monthly mean ozone values, the order m was the same for all basis functions. For the zonal mean analysis, no expansion in longitude was necessary, i.e. $m = 0$. Where longitudinally resolved data were analyzed, m was set to 2 for all basis functions to allow patterns similar to wave one and wave two structures to be resolved. The exact number of expansions in latitude was determined using sensitivity tests which are described in detail in Chapter 5.

3.3 Regression model

3.3.1 Regression model

The newly developed regression model where spherical harmonics are used to account for spatial patterns in the regression coefficients:

$$\begin{aligned}
O_3(t, s) = & a_1(t, s) \times \text{Offset} + & (N = 4) \\
& a_{2a}(t, s) \times \text{EESC}(t, \Gamma) + & (N = 4) \\
& a_{2b}(t, s) \times \text{Linear}(t) + & (N = 4) \\
& a_3(t, s) \times \text{QBO}_{50hPa}(t) + & (N = 2) \\
& a_4(t, s) \times \text{QBO}_{50hPa}(t) \text{ orthog.} + & (N = 2) \quad (3.15) \\
& a_5(t, s) \times \text{Solar}(t) + & (N = 0) \\
& a_6(t, s) \times \text{Pinatubo}(t, \theta) + & (N = 1) \\
& a_7(t, s) \times \text{ENSO}(t) + & (N = 0) \\
& R(t, s)
\end{aligned}$$

where t is the decimal year (for the monthly means the middle of the month is used as the time stamp, so January 1979 is converted to $1979 + 1/12 \times 1/2 = 1979.0417$) and s is the geographical dependence (for zonal mean analyses s represents only the dependence on latitude, for the longitudinally resolved analyses s represents the dependence on latitude as well as longitude). $O_3(t, s)$ is the measured ozone. The regression model is applied to every pressure level separately. Γ indicates the age-of-air dependence of EESC which is described in more detail below, as well as the chosen basis functions. Although the main purpose of the regression was to obtain an estimate of halogen-induced ozone changes it is important to include the additional basis functions in the regression to reduce the error on the estimates of the changes. By taking out ozone variability caused by other sources the signal induced by halogens is more distinct and a more precise fit is possible.

The coefficients $a_1(t, s)$ to $a_7(t, s)$ are expanded in Fourier terms to account for seasonal variability as follows:

$$a_i(t, s) = a_{i0}(s) + \sum_{k=1}^N \left[a_{i(2k-1)}(s) \sin(2\pi k(t - 0.5)/12) + a_{i(2k)}(s) \cos(2\pi k(t - 0.5)/12) \right] \quad (3.16)$$

where N was chosen individually for each basis function to account for high seasonal structure in the fit coefficient where necessary. The selected number of Fourier pairs (N) for each basis function are shown in Equation 3.15. Each

coefficient of the Fourier expansion is further expanded in spherical harmonics to account for the dependancy of the fit coefficients on latitude and longitude, as described above.

In an ideal case the basis functions used in a regression model should be orthogonal to each other. Using measured atmospheric parameters as basis functions this assumption is almost always violated. It is possible, for example, that two basis functions have a similar temporal pattern for the whole time period analyzed, or for parts of it. The ozone variability which fits to this pattern cannot be unambiguously assigned to either one of the two and the retrieved coefficients for each may contain an unphysical quantity as a result. To avoid this problem it would be necessary to orthogonalize all basis functions as suggested by *Bodeker et al.* (1998). However, due to the orthogonalization the characteristics of the basis functions, and therefore their direct connection to atmospheric processes change. So the standard practice in regression analyses is to only remove the means of the basis functions. The basis functions for these analyses are additionally detrended, which means orthogonalized to a linear trend term. This is done to remove any signal similar to the linear part of the EESC time series. It might result in some loss of ozone changes which should have been addressed to the detrended basis functions (for example if climate change influences those basis functions in such a way that a change in ozone occurs). However, without the detrending of the basis functions different to EESC a trusted estimation of halogen-induced ozone changes is not possible. Removing the mean of the basis functions and detrending them is the so called preprocessing of the basis functions. In the following sections all basis functions of the used regression model (see Eq. 3.15) are described in detail, including information about undertaken preprocessing.

3.3.2 Explanatory variables

3.3.2.1 Offset

The offset term in Equation 3.15 is independent of the time t . It is used to remove the mean and, when expanded in a Fourier expansion, the seasonal cycle from the ozone data. With an expansion in 4 Fourier pairs the seasonality in ozone at 12, 6, 4 and 3 month periodicity can be explained. No preprocessing of the offset term was necessary.

3.3.2.2 EESC

In earlier studies, the long-term ozone change was expected to be linear in response to the approximately linear increase in ozone-depleting substances (ODS). But the change in ODSs after the mid 1990s is no longer linear with time (*World Meteorological Organization*, 2007, Chapter 3), therefore other proxies for anthropogenically caused ozone depletion are necessary, either by fitting different linear functions (piecewise linear trend concept) or by using basis functions which are proportional to the stratospheric content of ODSs (for more detail see *World Meteorological Organization*, 2007, Chapter 6). One of the latter is the EESC function, an index reflecting the amount of active (which means ozone-depleting) chlorine and bromine in the stratosphere.

Concentrations of chemical constituents in the atmosphere are not only dependent on chemical reaction rates but also on transport. Areas of production and areas of destruction are located in different regions of the atmosphere which are sometimes connected via transport. Source gases which contribute to ozone depletion enter the stratosphere from the troposphere in the tropics but only start depleting ozone after exposure to UV radiation for some time (see Section 1.3.1 and Section 1.3.2). Therefore, a time series like EESC, if it is chosen as a basis function for regression analyses, should be dependent on latitude and altitude to account for the atmospheric transport, the different residence times and photochemical conditions. *Newman et al.* (2007) introduced a new formulation of EESC that includes transport time dependencies based on the concept of age-of-air (Γ). This concept summarizes the average transport time of an air parcel from the troposphere to the stratosphere (*Waugh and Hall*, 2002). Travel times of all air parcels combined result in an ‘age spectrum’ that can be used as an descriptor of transport.

For the regression model described here, the EESC basis function was determined for each latitude and pressure level separately. The age-of-air for the different locations were defined from Figure 7 of *Waugh and Hall* (2002), with the contour lines extrapolated to 90°S and 90°N, as well as from 10 km to 70 km. This age-of-air value was then used to define an EESC time series according to *Newman et al.* (2007), representing the active chlorine and bromine at a specified latitude and altitude. Below 10 km the concepts of age-of-air and EESC are not applicable. Therefore, the EESC basis function was never used in regressions of tropospheric ozone.

Figure 3.2 shows the EESC concentrations for the time period 1970 to 2020 as a

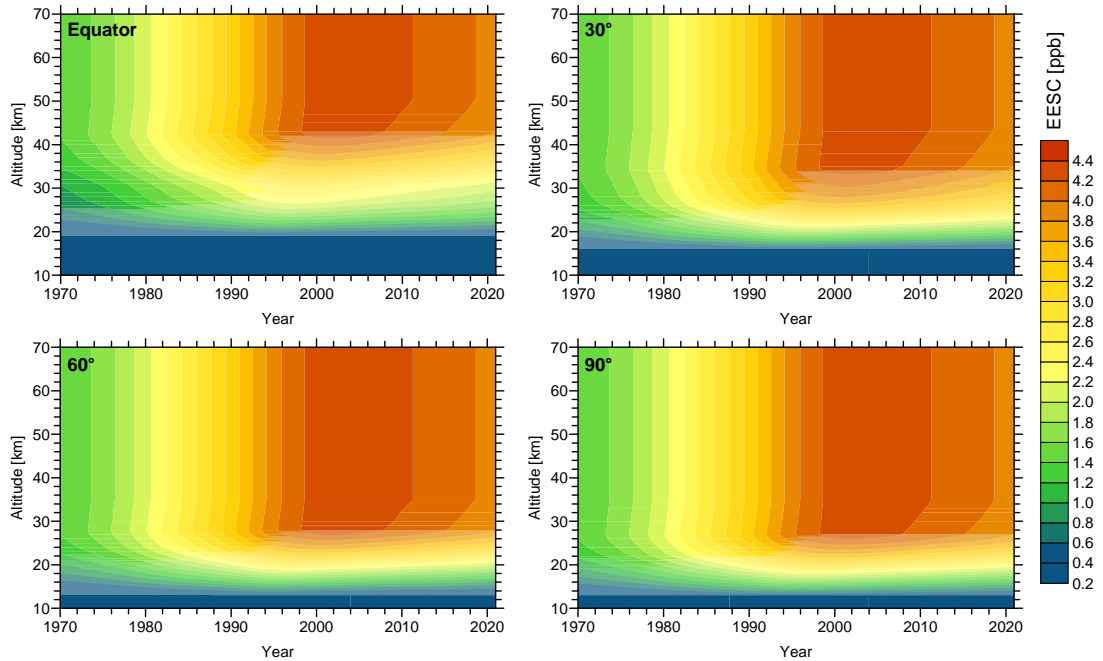


Figure 3.2: EESC concentrations from 1970 to 2020 as a function of altitude (10 km to 70 km) at the equator, 30°, 60° and 90° (valid for both hemispheres).

function of altitude for four different latitude regions, considering the age-of-air concept. The age-of-air distribution is assumed to be symmetric for the two hemispheres (*Waugh and Hall, 2002*). It can be seen that the peak values of EESC reach lower altitudes while moving from the equator to high latitudes and that the peak values are shifted in time.

The effect of EESC on ozone is known to have a distinct seasonal cycle. Therefore, the EESC term in the regression was expanded in 4 Fourier pairs. The mean of the EESC time series over the period of ozone data was removed as part of the preprocessing.

3.3.2.3 Linear trend

Since EESC is defined for the stratosphere, it is therefore not applicable as basis function for the troposphere. Nevertheless, changes in tropospheric chemistry and small scale transport systems can make an impact on tropospheric ozone concentrations. To take those possible effects into account a linear trend term was included in the regression when it was run for tropospheric pressure levels. Since the EESC basis function was then excluded, linear trend and EESC were never used as basis functions at the same time.

Preprocessing and Fourier expansions are identical to those of the EESC basis function. However, since the focus of this study is on stratospheric ozone changes, the linear trend basis function is described only for the sake of completeness.

3.3.2.4 QBO

The equatorial zonal wind oscillates quasi-periodically between easterlies and westerlies in the tropical lower and middle stratosphere with a mean period between 28 and 29 months. This is known as the quasi-biennial oscillation. Both wind regimes propagate downward from the mid-stratosphere to the tropical tropopause where they dissipate. The QBO dominates the variability of the equatorial stratosphere by affecting stratospheric circulation and mixing atmospheric constituents (*Baldwin et al.*, 2001), but it also affects the variability of the extra-tropical stratosphere. Time series of the QBO are normally given as the equatorial zonal wind component and are available for several pressure levels. Because of its known influence on ozone (*Tung and Yang*, 1994; *Baldwin et al.*, 2001) the QBO is one of the commonly used basis functions for ozone regression analyses. Many studies have shown the influence of the QBO on total ozone and the vertical ozone distribution, not just in the tropical region but also at middle and high latitudes (*SPARC/IOC/GAW*, 1998; *World Meteorological Organization*, 1999, Chapter 4; *Stahelin et al.*, 2001). Since the QBO is a phenomenon which originates in the tropics and has a changing signature with increasing latitude and altitude (*Baldwin et al.*, 2001), a successful implementation in a global, vertically resolved regression model has to account for time lags in latitudinal and vertical directions compared to the original tropical signal. There are three generally applied methods to achieve this:

1. The QBO time series at one level is used as a basis function. To account for time lags, the regression is recalculated with the QBO time series shifted by a defined time in a positive direction (forward in time) (*Bodeker et al.*, 1998). For the regression with the best fit of the QBO, the sum of the regression residuals becomes smallest.
2. Two QBO time series at different pressure levels are selected which are quasi orthogonal to each other. They are not sinusoidal and show variability within their cycles, so absolute orthogonality is not strictly possible. Nevertheless, in combining those two time series any phase shift can be obtained (*Steinbrecht et al.*, 2003). *Randel and Wu* (1996) used not only a

combination of two different QBO time series but a linear combination of the QBO time series at most available pressure levels.

3. Instead of using measured QBO values at two different levels, only one QBO time series is selected and lagged against itself until the product of the two time series over the period of the regression is closest to 0. The lagged time series is then, by construction, orthogonal to the original. This method was chosen to account for QBO time lags in this study, with the original QBO time series measured at 50 hPa.

The monthly QBO data were made available by the Freie Universität Berlin through their website (<http://www.geo.fu-berlin.de/met/ag/strat/produkte/qbo/index.html>). To account for up to semi-annual dependancies both QBO basis function coefficients were expanded in 2 Fourier terms. The mean value and a possible trend were removed before the orthogonal time series was created.

3.3.2.5 Solar cycle

The term ‘solar cycle’ refers to the solar activity cycle which has a period of about 11 years. It is most clearly manifested in the number of sunspots (*Stahelin et al.*, 2001). The solar cycle is normally included in regression analyses since many studies have shown the influence of the solar cycle on stratospheric dynamics and constituents (see *World Meteorological Organization*, 2003, Chapter 4; *Calisesi and Matthes*, 2006, and references therein). *Stahelin et al.* (2001) suggested two possible mechanisms for the link between the solar cycle and stratospheric ozone: (1) the change in the solar UV flux modulates the ozone production rate in the upper stratosphere, and (2) the change in solar energy output affects the stratospheric circulation.

Since ozone profile measurements on a global scale reach back only roughly 30 years, signals with a periodicity of about 10 years are difficult to extract with regression analyses. In *World Meteorological Organization* (2007, Chapter 3) different methods for defining solar cycle basis functions are explained, however, their use in a linear regression is not indisputable since the solar cycle signal is difficult to be distinguished from the major volcanic eruptions of the last century. Nevertheless, the F10.7 cm flux (10.7-cm radio flux) or the Mg II solar UV index as proxies in a linear regression model are still the main method to extract the solar cycle signal in ozone time series (see for example *Soukharev and Hood*, 2006).

The proxy for the solar activity which was used in the regression described

here is the F10.7cm solar flux which is available as daily data from ftp://ftp.ngdc.noaa.gov/STP/SOLAR_DATA/SOLAR_RADIO/FLUX. As for the QBO, the mean value and a possible trend in the time series was removed before use in the regression. Since the seasonal dependence was expected to be negligible, the solar cycle regression coefficient was not expanded in Fourier terms.

3.3.2.6 ENSO

The El Niño Southern Oscillation (ENSO) is a climate anomaly in the ocean and the atmosphere of the equatorial region. It is connected with pressure differences between the eastern and western Pacific Ocean which are coupled with sea-surface temperature variations. Several studies showed the influence of ENSO on total column ozone not only in the equatorial region (*Shiotani*, 1992) but worldwide (*Randel and Cobb*, 1994; *World Meteorological Organization*, 1999, Chapter 4; *Steinbrecht et al.*, 2003). While effects on zonal mean ozone values are small, for longitudinally resolved analyses the ENSO effect might be dominant in some regions.

The time series which is used as the ENSO basis function is the Southern Oscillation Index (SOI) which is a measure of the pressure gradient between Tahiti (18°S, 150°W) and Darwin (12°S, 131°E) (*Shiotani*, 1992). These data were obtained from <ftp://ftp.cpc.ncep.noaa.gov/wd52dg/data/indices/soi> where monthly mean values are made available.

No seasonal dependence in the effect of ENSO on ozone was assumed so the number of Fourier expansions for the ENSO coefficient was set to 0. The mean value of the SOI time series was removed as well as the trend before it was included in the regression.

3.3.2.7 Volcanic aerosol

The eruption of Mt. Pinatubo on June 15, 1991, significantly affected global ozone and temperatures. This was not only due to the amount of aerosol injected into the stratosphere (≈ 30 Tg, see *McCormick et al.*, 1995), but also due to the simultaneous occurrence of increased anthropogenic chlorine concentrations in the stratosphere. With heterogeneous sulfate aerosol chemistry both volcanic aerosol and chlorine work together to destroy midlatitude ozone (*Solomon*, 1999).

The basis function for the regression described here was built according to the

artificial aerosol loading function used by *Bodeker et al.* (1998) and *Liley et al.* (2000). The rapid increase in stratospheric aerosols after the eruption and the later exponential relaxation to background values, with an approximate decay time of ≈ 1 year (*McCormick et al.*, 1995), is described by the following equation:

$$\text{Pinatubo} = e^{\text{StartTime}-t} \times (1 - e^{(6 \times (\text{StartTime}-t))}). \quad (3.17)$$

StartTime describes the date when the increase in volcanic aerosol starts, t is the time of interest. Since the volcanic aerosols spread out within the stratosphere slowly (*Tie et al.*, 1994; *Rosenfield et al.*, 1997), the effects of the eruption on middle and high latitude ozone are temporally lagged to the effects observed in the tropics. The regression was therefore run with the Pinatubo basis function lagged by up to three years after to the eruption date of Mt. Pinatubo. The dispersion of the aerosol cloud in the longitudinal direction happened within a few weeks (*McCormick et al.*, 1995) so that a zonally symmetric time lag was assumed.

The Pinatubo basis function coefficient was expanded with one Fourier pair to allow for seasonally dependent effects which were shown for example by *Rosenfield et al.* (1997). No preprocessing of the basis function was done.

The second important volcanic perturbation within the analyzed ozone time period was the eruption of El Chichón in April 1982. The amount of stratospheric aerosol loading was approximately 12 Tg (*McCormick et al.*, 1995), but the effect on midlatitude ozone was significantly smaller than from Mt. Pinatubo due to the lower anthropogenic chlorine concentrations in the stratosphere at that time (*Solomon*, 1999), however, not negligible. Global measurements at this time were still sparse, with the gap between SAGE I and SAGE II stretching from November 1981 to October 1984 (*Randel and Wu*, 2007). Realistically fitting a basis function for the volcanic aerosol from El Chichón with only few ozone values available to fit to is not possible and therefore this basis function could not be included in the regression.

3.3.3 Uncertainties on the regression coefficients

The regression coefficients are calculated by minimizing the sum of the squared residuals. Residuals are the differences between the original data (in this case the monthly means calculated from the measurements) and the complete regression fit. The sum of squared residuals is determined according to Equation 3.18 (*Press*

et al., 1989) where $X_1(x), \dots, X_M(x)$ are the regression basis functions.

$$\chi^2 = \sum_{i=1}^N \left[\frac{y_i - \sum_{k=1}^M a_k X_k(x_i)}{\sigma_i} \right]^2 \quad (3.18)$$

For the calculation of χ^2 an error σ_i for each value y_i is necessary. For the observations, the error value for a particular monthly mean was obtained by error propagation of the error of each measurement within the respective month (see also Section 2.3). Error values for the chemistry-climate model simulations (described in detail in Section 5.1) are fixed to 5% of the respective monthly mean value, similar to the average error defined for ozonesondes in the stratosphere. The optimum values of the coefficients a_k are obtained by minimizing χ^2 simultaneously with respect to each coefficient (*Bevington and Robinson, 2003*). The minimum occurs where the derivative of χ^2 with respect to all M parameters a_k is zero. By using Normal Equations in matrix form, the squared uncertainties of the fitted parameters a_k are defined as the diagonal elements of the covariance matrix. For more details about the minimization by use of Normal Equations in matrix form, see *Press et al. (1989)*.

When the fit coefficient are expanded in Fourier or spherical harmonics expansions, the uncertainty on the overall fit coefficient a_i (see Equation 3.15) is a combination of the uncertainties of all expansion coefficients, calculated by error propagation. It is exemplarily shown for Fourier terms only in the equation below (Equation 3.19). The principle is the same for all additional expansions, for example expansions in Legendre polynomials or spherical harmonics.

$$\sigma_{a_i}^2 = \sigma_{a_{i0}}^2 + \sum_{k=1}^N \left[\sigma_{a_{i(2k-1)}}^2 \sin^2(2\pi k(t - 0.5)/12) + \sigma_{a_{i(2k)}}^2 \cos^2(2\pi k(t - 0.5)/12) \right] \quad (3.19)$$

3.3.4 Autocorrelation

3.3.4.1 Temporal autocorrelation

One prerequisite for the described method of calculating the uncertainties in the regression coefficients is the normal distribution of the residuals (term R in Equation 3.15) with zero mean and statistical independence in time. Since it is well known that atmospheric parameters, for example ozone, are serially correlated, the calculated uncertainties in the regression coefficients are significantly underestimated (*Tiao et al., 1990; Logan, 1994; Weatherhead et al., 1998; Staehelin*

et al., 2001). To more accurately estimate the uncertainties of the regression fit coefficients, the residuals have to be corrected for their autocorrelation. An auto-regressive process of order p (also written as ‘AR(p) process’) is generally defined as

$$R(t) = \alpha_0 + \sum_{k=1}^p \alpha_k R(t-k) + Z(t), \quad (3.20)$$

where the residual at time t can be expressed as a weighted sum of the previous k residuals plus the random component (white noise process) $Z(t)$. The weights are the auto-regressive coefficients α_k (*von Storch and Zwiers*, 2002; *Wilks*, 2006). The most frequently used AR processes are of first or second order.

As suggested in *Bodeker et al.* (1998), an AR(2) process was used in combination with the regression model described in Section 3.3.1. The auto-regression was accounted for by first fitting the regression (Eq. 3.15) to the monthly means and calculating the residuals. Then the auto-regression coefficients α_1 and α_2 are derived by regressing the residuals at time step t against the residuals at time step $t-1$ and $t-2$. The obtained coefficients are used to transform the monthly mean time series, as well as the basis functions:

$$x'(t) \longrightarrow x(t) - \alpha_1 x(t-1) - \alpha_2 x(t-2). \quad (3.21)$$

Then the regression is rerun with the transformed variables $x'(t)$. Since the monthly means calculated from the observations have data gaps this had to be considered in the calculation of α_1 and α_2 . Residuals $R(t)$ were only included in Equation 3.20 if the residuals at $t-1$ and $t-2$ were also available.

3.3.4.2 Temporal and spatial autocorrelation

With the implementation of the spherical harmonics the traditional treatment of the autocorrelation in the data is not sufficient to determine the total uncertainties on the regression coefficients. Residuals obtained by regression methods where ozone is not only a function of time but also of latitude and/or longitude could be interrelated both in space and time (*von Storch and Navarra*, 1999). Therefore a new, adjusted, auto-regressive process was developed to account for serial and spatial interrelations in the regression model (Equation 3.22).

$$R(t, s) = \alpha_0 + \sum_{l=1}^N \sum_{k=1}^M \alpha_{1 lk} R(t-1, s) + \sum_{l=1}^N \sum_{k=1}^M \alpha_{2 lk} R(t-2, s) + Z(t, s) \quad (3.22)$$

N denotes the resolution in latitude and M denotes the resolution in longitude. Equation 3.22 described the principle of the new auto-regressive process for lon-

gitudinally resolved data sets. For zonal mean data, the summation is only done over N .

In the above equation s is the geographical information about the residual. For zonal mean analyses s represents only latitudinal information, for the longitudinally resolved analyses s represents latitudinal and longitudinal information. As in Equation 3.20, the residuals of the regression at a given time t are corrected for their correlation with residuals of the two previous time steps $t-1$ and $t-2$. However, this correction is extended to not only include the residual at the same latitude and longitude at the respective previous time step but also the residuals of all other latitudes and longitudes. With a latitude resolution of N and a longitude resolution of M , all residuals at one time step can be expressed as a $N \times M$ matrix. So each residual at time t is a function of all components of the $N \times M$ matrix at time $t-1$ as well as at time $t-2$. The random component $Z(t, s)$ is the residual from the autocorrelation model.

The auto-regressive process described here was only developed theoretically. Its implementation would have exceeded the scope of this thesis, but it is planned for the future. For a realistic estimation of the uncertainties on the coefficients of the regression used here, the spatial interrelations between values should also be considered. Therefore, the significance levels of the derived EESC coefficients presented in the following chapters may be somewhat underestimated. But because most of the autocorrelation is expected to be temporal, this underestimation is expected to be small.

3.4 Summary

The current chapter presented a brief overview about the development of commonly used regression models. An attempt to apply a traditional regression approach to the vertically resolved zonal mean monthly mean data set was delineated. The missing data in this data set proved to be an insuperable problem. Therefore, the development of a new regression method which could be applied in spite of existing data gaps was necessary. The physical fundamentals of this new method, the spherical harmonics, were elucidated and their implementation in a linear regression model explained. For a realistic estimation of halogen-induced ozone changes it is indispensable to account for the most important natural sources of ozone variability in a regression. Those sources were characterized and their consideration in the new regression approach described. Although the

main focus of this thesis is a longitudinally resolved analyses of ozone data, the new method was tested and evaluated first in a zonal mean analysis which is described in the following chapter.

Chapter 4

Analysis of zonal mean data

Before the longitudinally resolved analysis of vertical ozone data is presented, a more common analysis was thought to be appropriate to get a first estimate of the performance of the new spherical harmonics regression method. Zonal mean studies of vertically resolved ozone trends, or halogen-induced changes, have been based so far mostly on satellite data with the spatial and temporal limitations of their availability (see for example Chapter 3 of *World Meteorological Organization*, 2007), or on data sets of combined sources (for example *Randel and Wu*, 2007) or on a statistically reconstructed data set (*Brunner et al.*, 2006). A comparison with the results of those studies should highlight strengths and limitations of the new regression. For this analysis, no expansion in longitude is necessary since only zonal mean data are processed. Results are presented as EESC coefficients rather than ozone trends. This is due to the fact that in reaching the maximum concentrations of EESC in the mid 1990s, ozone changes are described better by an EESC explanatory variable rather than a straight line. The EESC time series is consistent with a linear trend only up to shortly before the turnaround point which implies that only up to that point a meaningful trend value can be estimated, even if the analyzed time series might be longer. If a straight line fit were applied to a time series that extends beyond the mid 1990s, the obtained trend would be underestimated. The turnaround in EESC occurred over a decade ago so for quantifying the halogen-induced ozone changes derived from 1979 to 2006 in this study the EESC coefficients were favored over linear trends. A quantitative comparison with earlier results of linear trend analyses might be difficult to perform though since both measures, linear trend and EESC coefficient, are only related for the first part of the analyzed time period. However, qualitative assessments of the results should still be possible. Note that since the

EESC basis function is dependent on latitude and altitude in this study (see Section 3.3.2), coefficients of the same magnitude at different latitudes and/or altitudes might not always explain the same absolute change in ozone.

A regression model including spherical harmonic expansions of the regression fit coefficients, and which included the basis functions as outlined in Section 3.3, was applied to the zonal mean ozone data (see Section 2.4). The number of terms in the spherical harmonic expansions was not fixed for all pressure levels but chosen for each pressure level separately to guarantee the best possible basis function fit for the data by minimizing the number of coefficients and therefore reducing their uncertainties. Only where steep gradients and high spatial variability needed to be accounted for (lowermost and lower stratosphere) high expansions were chosen. Seasonal variability was accounted for by Fourier expansions as detailed in Section 3.3.

4.1 Vertically resolved zonal mean ozone changes

Figure 4.1 shows the EESC coefficients as a function of latitude and pressure evaluated for four months of the year. Note that the coefficients were calculated by applying the regression model simultaneously to all grid points of the latitude/longitude grid and independently at each pressure level. Since the main focus of this thesis is on stratospheric ozone changes only results for the pressure range from ~ 240 hPa to ~ 3 hPa are shown although the database covers lower altitudes.

Halogen-induced ozone changes are most pronounced in the northern high latitudes in April and the southern high latitudes in October. Negative coefficients in the northern high latitudes extend latitudinally up to 60°N - 70°N and vertically up to about 25 hPa. The most negative coefficients in this region can be found at the lowest pressure levels. In the southern high latitudes the negative coefficients cover similar pressure regions but extend further into the mid-latitudes. Most negative coefficients are found there between ~ 140 hPa and ~ 100 hPa. Although these results are resolved for specific months, regions of negative coefficients agree qualitatively well with the annual mean, global EESC coefficients described by *Brunner et al.* (2006) and the annual mean net ozone change described in *Randel et al.* (2007). However, the areas of most negative coefficients in the analysis here are slightly shifted downward compared to the results found by *Brunner et al.* (2006) and *Randel et al.* (2007), and results of the lowest pressure levels

4.1. VERTICALLY RESOLVED ZONAL MEAN OZONE CHANGES

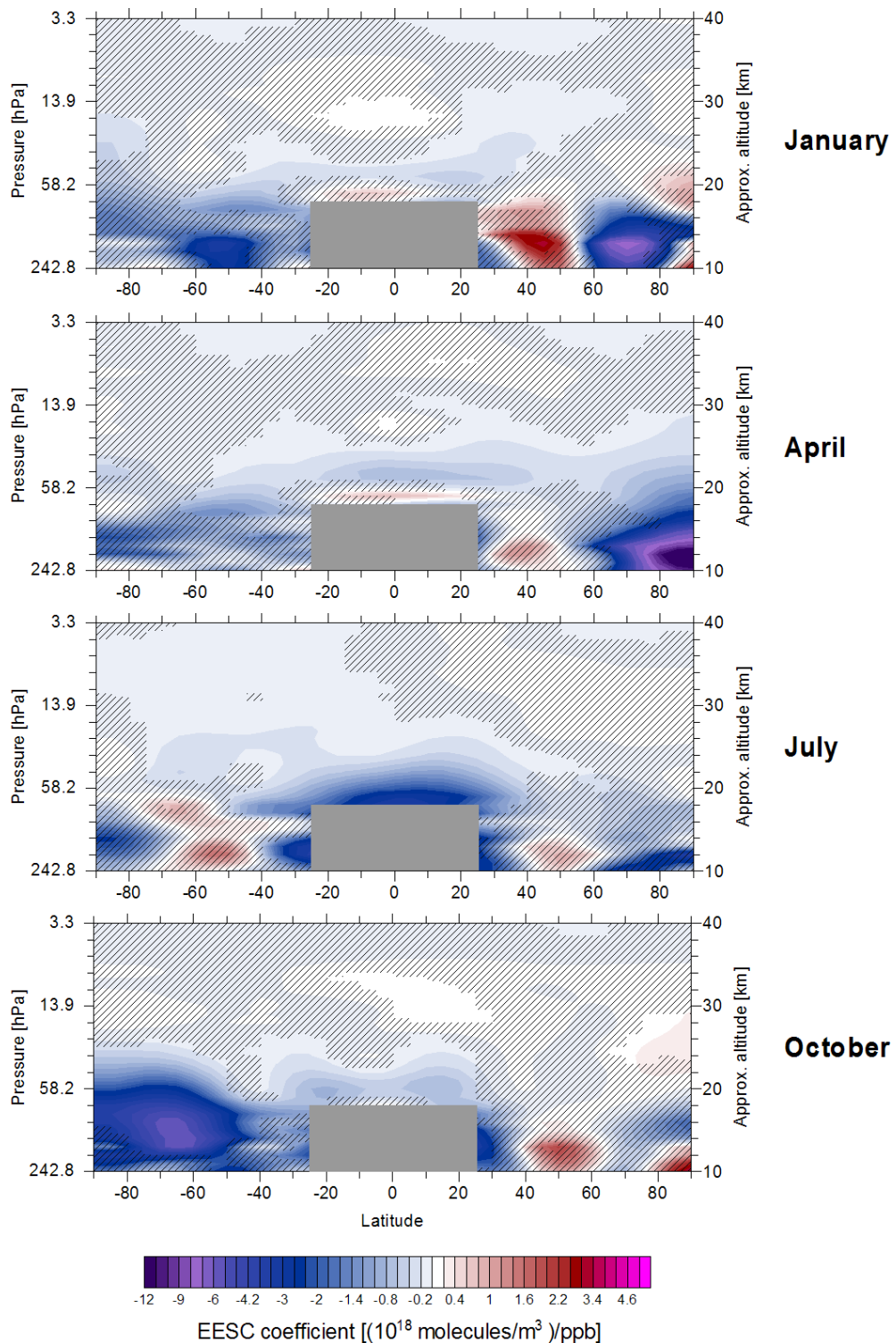


Figure 4.1: Zonal mean halogen-induced ozone changes for pressure levels from ~ 240 hPa to ~ 3 hPa and for four months of the year. Non-significant values at the 2σ level are hatched. The gray box marks pressure levels between 25°S and 25°N where EESC was not included as basis function in the regression (see Section 3.3.2).

are mainly not statistically significant. EESC coefficients in the lower stratosphere in the tropics are slightly negative, with the exception of the results of July where coefficients are more pronounced. This layer of ozone decrease due to stratospheric halogens can also be found in *Brunner et al.* (2006) and *Randel et al.* (2007). In the upper stratosphere EESC coefficients in Figure 4.1 are small, however, they are often statistically significant. This is in good agreement with results described by *Brunner et al.* (2006) where also EESC coefficients are shown, similar to Figure 4.1. In earlier studies concerning the long-term changes and variability in ozone, the upper stratosphere is the region where a strong ozone decrease was detected additionally to the decreases in the lower stratosphere in high latitudes (*Randel et al.*, 2007, and *World Meteorological Organization*, 2007, Chapter 3). This upper stratospheric ozone decrease is not apparent in Figure 4.1 since EESC coefficients are presented there rather than relative ozone changes (e.g. %/decade). However, taking into account that the EESC basis function is dependent on latitude and altitude in this study and that ozone number densities are much lower in the upper stratosphere than in the lower stratosphere, the conversion of the negative EESC coefficients in the upper stratosphere into relative ozone changes for the years where EESC increased linearly would result in a second region of strong ozone trends. Overall, the main pattern of halogen-induced ozone changes is captured by the new regression approach and results are qualitatively comparable to results of similar studies of the recent literature. *Brunner et al.* (2006) is based on statistically reconstructed data and spatial ozone variations between 60° and 90° in *Randel et al.* (2007) stay the same caused by the composition of their data set. On the contrary, the halogen-induced ozone changes presented here are based on measurements alone and the spatial variability of existing measurements between 60° and 90° is maintained, on a 5°-latitude resolution which is a clear advantage to the other two mentioned data sets.

For all four months presented high latitudinal variability of the EESC coefficients can be seen within the lowest pressure levels (from ~240 hPa to ~60 hPa). Coefficients in this region are mostly not significant, nevertheless the obtained coefficient pattern, switching quickly from very positive to very negative, might point to an unsolved problem of the analyses method. In this region about 40-50% of the zonal mean monthly means are missing in the tropics and parts of the mid-latitudes (see Figure 2.4). Fitting basis functions with high expansions for the Legendre polynomials (spherical harmonics without expansion in longitude), to capture the small-scale patterns in this region, most likely results in not enough restraint for the fit and therefore over- and undershooting of the polynomials. This leads to artefacts in the results. The less variable pattern in higher alti-

tude regions, where more data are available and the variability to be described is lower, strengthen this conclusion. Some details and absolute values of the EESC coefficient pattern might therefore be overestimated in this region. Additionally, the fact that the most negative coefficients of all four months shown occur in the northern high latitudes instead of the southern high latitudes, and that the high latitude signal is shifted slightly downward in both hemispheres might also be due to the fitting problems in this pressure region.

Figure 4.2 shows temporally and latitudinally resolved EESC coefficients for five selected pressure levels between ~ 77 hPa and ~ 25 hPa. Lowest levels where artifacts of the new regression method can be expected are omitted. An underlying similar pattern in EESC coefficients for all pressure levels is detectable: chemical ozone depletion caused by EESC in the Arctic results in large negative EESC coefficients in March and April north of $\sim 70^\circ\text{N}$, and chemical ozone depletion in the Antarctic causes the large negative coefficients between August and December from the South Pole up to about $\sim 50^\circ\text{S}$. Between June and August negative coefficients also occur in the tropics. Note however, that because ozone and EESC concentrations in the tropics are smaller than in the high latitudes (see for example Figure 3.2) large negative EESC coefficients do not describe the same change in ozone in the tropics and in polar regions. Nevertheless, the EESC coefficients in the tropics, especially during northern summer, are far larger than expected due to chemically induced ozone depletion. It might be the case that the effects of another mechanism on ozone are picked up by the EESC basis function. Note, that a linear trend is only included as basis function in the regression when EESC is not. Since changes in EESC are quasi linear until the turnaround in the mid 1990s, any effect that is not described by the other basis functions and causes a linear change in ozone could therefore be attributed to EESC. In the tropics this could be for example an increase in tropical upwelling. More ozone-poor air is transported from the troposphere into the stratosphere so that the ozone concentrations there decrease. The large negative EESC coefficients would then describe an ozone change caused by changes in transport rather than changes in chemistry. Independent of the causal mechanism, all three features show the most negative coefficients at the lowest pressure level, and for all three features coefficients get smaller with decreasing pressure. Additional small scale patterns with slightly positive coefficients can be found at all pressure levels but are mostly not statistically significant. Overall, the temporally and latitudinally resolved halogen-induced changes in ozone agree well with patterns expected from total column ozone analyses (see for example *Randel and Wu, 2007*).

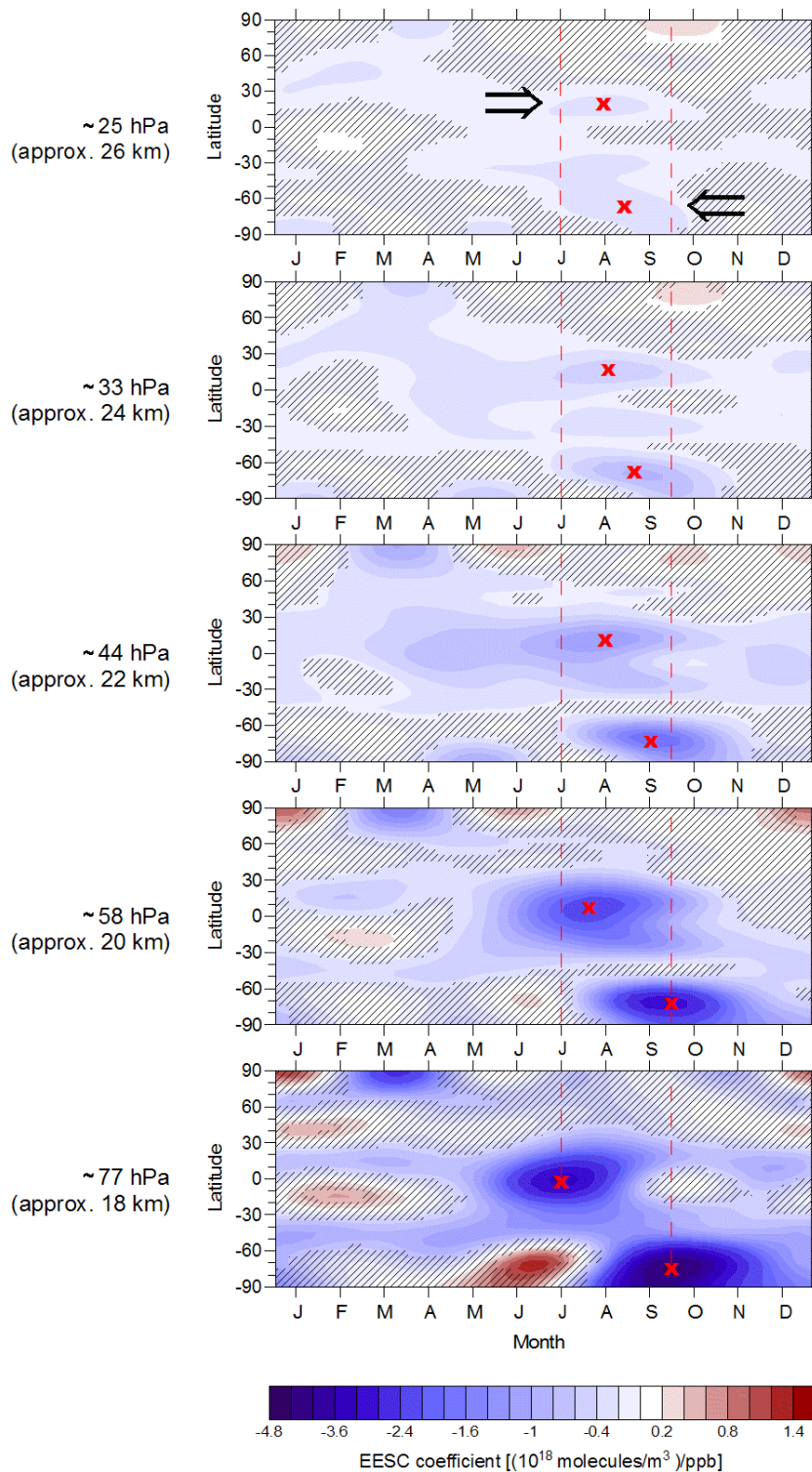


Figure 4.2: Zonal mean halogen-induced ozone changes for all months and five selected pressure levels. Non-significant values at the 2σ level are hatched. Red crosses depict the minimum coefficients in the tropics and the southern polar latitudes. Black arrows depict the change in temporal occurrence of the minimum coefficients.

4.1. VERTICALLY RESOLVED ZONAL MEAN OZONE CHANGES

Table 4.1: Time and location of minimum EESC coefficients in the tropics and southern high latitudes, and the time difference (Δ days) between their occurrences, for seven selected pressure levels.

Pressure (hPa)	Latitude band	approx. day of year	Δ days	EESC coefficient $((10^{18}\text{molec./m}^3)/\text{ppb})$
~77	75°S-70°S	269		-4.579
	5°S-0°	198	71	-3.369
~58	75°S-70°S	269		-3.123
	5°N-10°N	218	51	-2.211
~44	75°S-70°S	259		-1.821
	10°N-15°N	228	31	-1.178
~33	70°S-65°S	249		-0.873
	15°N-20°N	228	21	-0.563
~25	70°S-65°S	238		-0.406
	15°N-20°N	228	10	-0.278
~19	70°S-65°S	228		-0.226
	20°N-25°N	228	0	-0.138
~14	70°S-65°S	218		-0.213
	15°N-20°N	228	-10	-0.075

One detail in Figure 4.2 stands out: the month of the most negative coefficients in the tropics and the southern high latitudes, marked with red crosses in Figure 4.2, change for the different pressure levels shown. While the minimum coefficient in the tropics appears later in the year with increasing altitude (moving right from the left red dashed line in Figure 4.2, indicated by the left black arrow), exactly the opposite happens with the minimum coefficients in the southern polar region (moving left from the right dashed line, indicated by the right black arrow). This detail has not been described in the literature so far. The effect is quantified in Table 4.1. Note that ‘ Δ days’ always changes by a multiple of ~ 10 due to the chosen time step for the evaluation of the Fourier expanded basis functions (about every 10th day). For higher pressure levels (~ 19 hPa and ~ 14 hPa) where the date for the negative coefficients in the tropics and the southern polar regions converge

this chosen resolution of the evaluation might be the reason for the very low or even negative values for ‘ Δ days’. Keeping in mind the differences in causal mechanisms already discussed, these changes in appearance time might be connected by the Brewer-Dobson circulation (see Section 1.3): Due to atmospheric transport times, the signal of the tropical lowermost stratosphere is then shifted temporally with increasing altitude whereas it is shifted with decreasing altitude in the polar regions. Since this signal can be seen in halogen-induced ozone changes (not an ozone climatology) it could suggest an increase in tropical upwelling during the time period analyzed with a resulting strengthening of the Brewer-Dobson circulation. However, with a strengthening of the Brewer-Dobson circulation an ozone increase in the mid- to high latitudes is expected since more ozone is transported there. This cannot be seen in the results of Figure 4.2. It might be possible that the signal of the chemical ozone depletion in the high latitudes masks the transport-induced increase in ozone. But maybe the temporal development of the negative EESC coefficients in the tropics and the southern high latitudes are not connected at all: while the negative coefficients in the tropics might be caused by increased transport, the negative coefficients in the southern high latitudes are caused solely by chemical ozone depletion. The temporal development of the latter (most negative values earlier with increasing altitude) could be explained by earlier return of the solar radiation for higher altitudes. Although the newly developed regression approach has limitations describing the high ozone variability and steep horizontal gradients between ~ 240 hPa and ~ 80 hPa, the patterns in temporally and latitudinally resolved EESC coefficients are significant at the 2σ (95%) level and are reproduced for several pressure levels independently. These findings are therefore unlikely to be artefacts of the analysis method.

4.2 Did ozone from 1997 to 2007 change as expected?

Recently the focus of multi-decadal ozone time series analysis shifted from the detection and quantification of trends to the detection of a turnaround in ozone trends or even ozone recovery (*Reinsel et al.*, 2002; *Newchurch et al.*, 2003; *Dameris et al.*, 2006; *Steinbrecht et al.*, 2006; *Yang et al.*, 2006). Since reaching the maximum concentration of stratospheric halogens in the mid 1990s, ozone data sets are now sufficiently long to allow quantifications of the effects of decreasing halogen concentrations on ozone. For those estimates multiple linear regressions are applied (*World Meteorological Organization*, 2007, Chapter 6).

A small modification of the regression used in Section 4.1 allowed estimates of whether the changes in ozone in the last ten years are congruent with decreasing halogen concentrations.

4.2.1 CUSUM methodology and modification

The cumulative sum of residuals (CUSUM) method as introduced by *Reinsel et al.* (2002) assumes that ozone in the stratosphere decreases linearly (trend m_1 in Figure 4.3 (a)), after accounting for natural sources of variability, until a specified date is reached (turnaround date). This date is normally chosen according to the time of the peak in EESC (*World Meteorological Organization*, 2007, Chapter 6), around mid 1996 (*World Meteorological Organization*, 2003, Chapter 1). All data after the selected date are then evaluated for whether they show signs of a deviation away from the linear decrease m_1 (illustrated as m_2 in Figure 4.3 (a)). To quantify the deviation away from the linear decrease the CUSUM from the extrapolated decrease after the specified date is calculated, see Figure 4.3 (b). The residuals for the CUSUM calculations are determined by fitting basis functions of natural sources of variability (such as QBO or solar cycle) to the complete time series of ozone monthly means. In a next step a linear trend is fitted to the residuals up to the turnaround point and after that date extrapolated for the calculation of the CUSUM (*World Meteorological Organization*, 2007, Chapter 6).

In the regression used in this analysis, however, the influence of stratospheric chlorine and bromine is not described by a linear trend but an EESC time series (see Equation 3.15). Therefore, the CUSUM approach described above had to be slightly adjusted such that the CUSUM represents the deviation in ozone away from what would be expected from the change in EESC. Residuals were calculated for the full time period (1979 to 2007) after a complete set of basis functions, including an EESC time series, was fitted to ozone monthly means from the beginning of 1979 to the end of 1996 only (similar to the analysis described in *Brunner et al.*, 2006). The end of 1996 was chosen as the turnaround point as it was in *Newchurch et al.* (2003), *Steinbrecht et al.* (2006) and *Yang et al.* (2006). The choice of the turnaround point can affect the results, as stated in *World Meteorological Organization* (2007, Chapter 6), however, the choice of this date is most important if CUSUMs are calculated based on a linear trend (as indicated in Figure 4.3). Since the CUSUM calculations here are not based on a regression analysis including a linear trend basis function but an EESC basis function the choice of the turnaround point should not influence the results very much. If

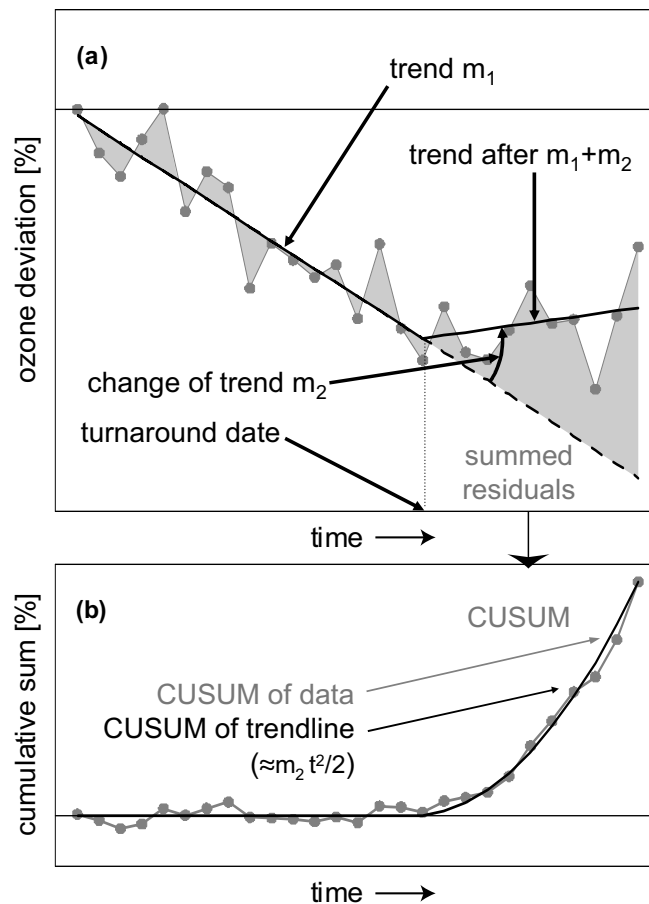


Figure 4.3: A schematic representation of the CUSUM method with (a) the idea of a change in trend, and (b) the result of the change in trend for the cumulative sum of residuals. Adapted from *World Meteorological Organization* (2007, Chapter 6).

ozone would behave as expected from the basis function fit, the CUSUM would be close to zero even in the time period after the turnaround point. Positive or negative CUSUM evolution indicates an atmospheric mechanism that influences ozone and that is not explained by the basis functions included in the regression. The significance of the deviation was tested as described in Appendix A of *Yang et al.* (2006). This test is based on three terms, the variance of the residuals up to the turnaround point, the uncertainty in the mean level of the model fit, and the uncertainty in the trend estimate for the time period up to the turnaround point. If the residuals are auto-correlated, the estimate of the uncertainty on the trend is underestimated. To account for that, the combined variances must be corrected by a factor that is determined by removing the AR(1) process (see Section 3.3.4.1) from the residuals (Appendix A3 from *Yang et al.*, 2006). If the CUSUM value at a chosen date after the turnaround then exceeds the calculated

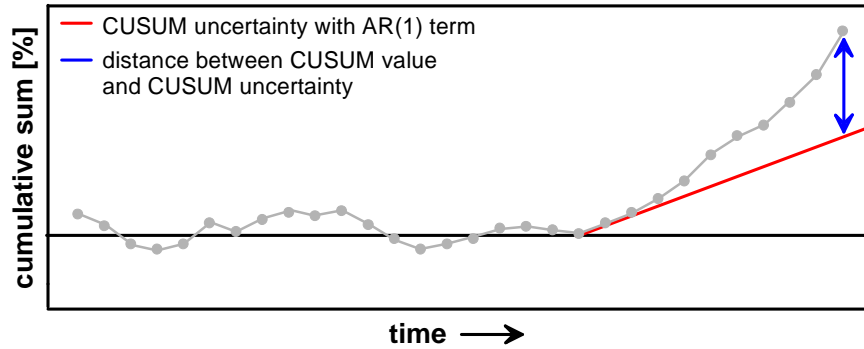


Figure 4.4: A schematic representation of the significance test for the deviation of expected ozone values calculated by the CUSUM method.

$2 \times \text{CUSUM uncertainty } (\sigma_{CU})$, the detected deviation is significant at the 95% level.

To be able to graphically distinguish between significant and non-significant CUSUM deviations, a new measure is introduced: the β value. It summarizes the distance between the calculated CUSUM value and the associated σ_{CU} at a specific date (t) (see Figure 4.4) by the following, newly developed equation:

$$\beta = 1 + (|\text{CUSUM value}(t)| - 2 \times \sigma_{CU}(t)) / (2 \times \sigma_{CU}(t)). \quad (4.1)$$

Depending on the sign of the CUSUM value (t), the β value is multiplied by -1 to differentiate between positive and negative deviations from expected ozone. For t the last available data point of the zonal mean ozone time series was chosen, December 2007. When the CUSUM value exceeds $2 \times \sigma_{CU}$ $|\beta > 1|$, the actual value indicates the factor by which σ_{CU} is exceeded. For $|\beta < 1|$ the CUSUM values are not significant at the 95% level. However, the closer the values are to 1 the closer they are to being significant. β values therefore also indicate regions where the change in ozone deviates from expectations at some level of statistical significance. Changing the length of the time period after the turnaround point could push the significance of those regions over the 95% level.

4.2.2 Results

Figure 4.5 shows the CUSUM deviation for the zonal mean ozone data set used for the analysis described in Section 4.1. Blue colors illustrate regions where ozone increased slower than expected whereas red colors indicate where ozone increased faster than expected. Where the deviation is statistically not significant at the

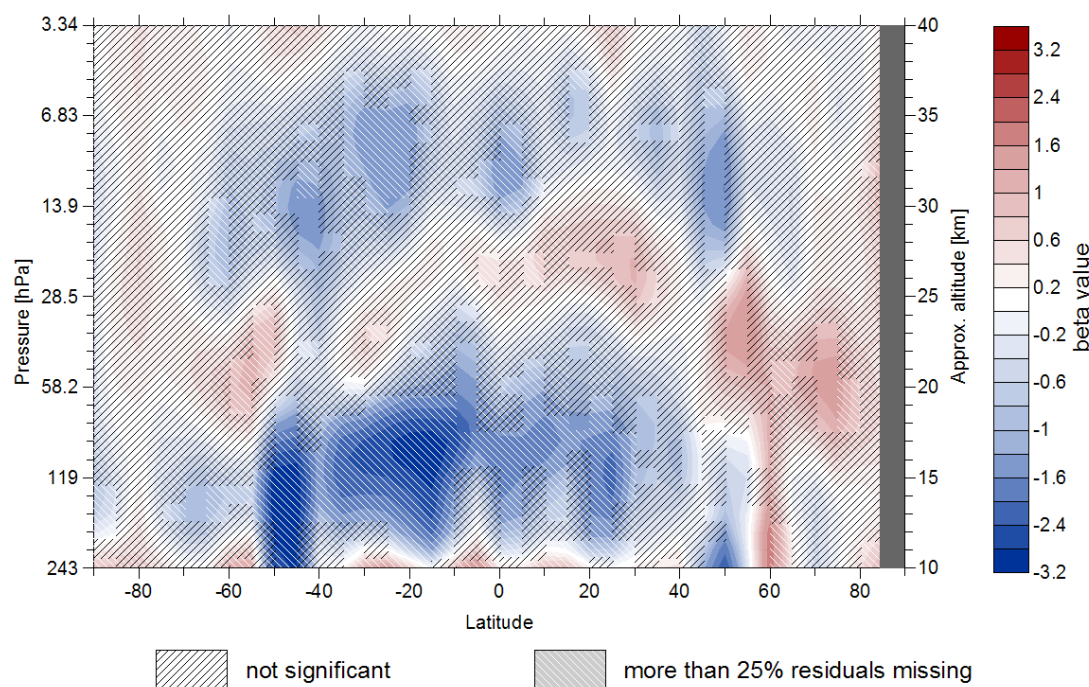


Figure 4.5: β values calculated for all latitude bands and all pressure levels. Blue colors illustrate regions where ozone increased slower than expected, red colors indicate where ozone increased faster than expected. Non-significant values on a 95% confidence level are hatched in black from lower left to upper right. In white hatched regions (upper left to lower right) more than 25% of all residuals were missing. For the latitude band 85°N to 90°N (dark gray box) no monthly means at all were available.

95% confidence level the corresponding β values are hatched in black (from lower left to upper right). Since the residuals for this analysis were calculated from the original measurements (residual = measurement - regression result), data gaps had to be accounted for in the CUSUM calculation. Whenever data were missing the corresponding residual was set to zero. Missing data were also excluded from the calculation of the variance of the residuals up to the turnaround point. Regions where more than 25% of the residuals were missing are hatched in white (from upper left to lower right) in Figure 4.5.

As seen in Figure 2.4 most measurements, and therefore most zonal monthly means, are available in the northern mid-latitudes up to ~ 10 hPa, and in the mid-stratosphere of the southern mid-latitudes. Those are the regions where less than 25% of the residuals were defined as zero. Three major regions with significant β values occur in the subtropics and mid-latitudes of both hemispheres: between 30°N and 50°S from ~ 240 hPa to ~ 60 hPa where ozone increases slower than expected from EESC decreases and where lowest values for β can be found,

between 70°N and 60°S from ~60 hPa to ~18 hPa where ozone increases faster than expected from EESC decreases, and the region between 50°N and 50°S from ~18 hPa to ~4 hPa where ozone increases again slower than expected. However, most of the β values of the middle pressure region are not statistically significant, and for most of the highest and lowest region where results are significant more than 25% of the residuals were missing.

Brunner et al. (2006) (hereafter referred to as B06) described a similar analysis, based on data gridded by equivalent latitude, where they also characterized ozone changes since 1996. They used a statistically reconstructed ozone data set at 14 pressure levels (spanning 190 hPa to 1.5 hPa) for the detection of significant deviations from ozone trends from their chosen turnaround point, end of 1995, up to December 2004. Several different regression analyses were performed, varying in the basis functions included, one with a similar set of basis functions to that used in the analysis here. The results they obtain for significant CUSUM values are similar to Figure 4.5. Three altitude regions with slower and faster than expected ozone increases can also be distinguished. Results for the middle to lower stratosphere where the increase of ozone is faster than expected are most similar. The region higher up, however, where ozone increases slower than expected, is only significant in B06's results in the southern mid-latitudes and is slightly shifted downward compared to the β value plot. Additionally, the region in the lowest stratosphere consists mainly of non-significant results in B06 whereas in the β value plot most of the results are significant. These differences could result from: (1) B06 did not consider auto-correlation in their residuals so the uncertainties on their calculated trends are underestimated, (2) the time period for calculating the CUSUM is 3 years longer for the analysis presented here during which the development of stratospheric ozone concentrations could have changed, (3) the EESC time series used here depends on pressure and latitude (see Section 3.3.1) whereas B06 used one EESC time series globally, (4) B06's analysis is based on equivalent latitude gridded data, (5) B06 chose 1995 as the turnaround point whereas here 1996 was chosen, and (6) the data sources used in the analysis can cause differences as shown by *Yang et al.* (2006).

These differences to B06 clearly show that the results of the CUSUM method depend on the quality of the regression fit, the choice of the turnaround point and the number of years of data available after the turnaround point. Mechanisms relevant for ozone deviations could change with time and could, therefore, accelerate or decelerate the increase of ozone. Such mechanisms must be important in the three regions with significant β values described above (see Figure 4.5). Only

few values of the middle stratosphere are significant though, which means that most major sources of ozone variability between 1997 and 2007 are captured by the regression model there. As indicated by the comparison of different regression results from B06, the inclusion of EESC as a regression basis function instead of a linear trend can improve the description of ozone variability significantly. The sparseness of significant ozone deviations in the β value plot in the upper and middle stratosphere, therefore, might primarily be ascribed to the age of air dependent EESC basis function in the regression model. For the most noticeable deviation from the expected ozone changes in the lowermost and upper stratosphere other processes must be delaying ozone increases (as mentioned above). What processes that could be, cannot be resolved unambiguously at this stage. For the lowermost stratosphere it also might be the case that the description of ozone changes by EESC is insufficient. It should be also kept in mind, that in the majority of the CUSUMs calculated for the lowermost and upper stratosphere, more than 25% of the residuals were missing which increases the uncertainty on the results.

4.3 Summary

A regression with spherical harmonic expansions of regression coefficients was applied to a zonal mean monthly mean ozone data set. EESC coefficients qualitatively agree with findings of recent similar analyses and expected halogen-induced ozone changes. A first estimate of the capabilities of the new regression method reveals possible problems in the basis function fits at low pressure levels. Results in this pressure region suffer from too many latitudinal expansions and resultant over- and undershooting. A small adjustment of the regression method allowed an estimate of unexpected changes in the evolution of ozone development over the last ten years. The main purpose of the zonal mean ozone analysis, i.e. testing the regression with implemented spherical harmonics of the fit coefficients on a realistic data set with a manageable number of missing data points, was successfully fulfilled. However, extending the analysis to longitudinally resolved data and, therefore, an increased number of missing data, the performance of the new regression method remains uncertain. Consequently, it is necessary to run sensitivity tests to estimate the ability of the regression with spherical harmonics to analyze longitudinally resolved data.

Chapter 5

Sensitivity tests for regression results

The analysis of the zonal mean monthly means of ozone in the previous chapter showed promising results for the use of spherical harmonics in regression analyses. However, for the zonal mean analysis, expansions only in latitude were necessary, and as can be seen in Figure 2.3, coverage for the zonal mean data set is considerably better than for the longitudinally resolved data set. To assess the performance of spherical harmonics with additional expansions in longitude it is necessary to do sensitivity tests to examine the ability of spherical harmonics to capture structures in a given data field and to evaluate the effects of missing data. As a basis for those tests a complete data set, without any missing data, is required with the same temporal and spatial characteristics as the longitudinally resolved monthly mean data set from the observations. Chemistry-Climate Model (CCM) simulations are well suited for that purpose since with multi-decadal transient simulations these criteria are all satisfied. The data set selected for this purpose is a subset of a simulation calculated with the coupled CCM E39C-A which is described in detail below.

5.1 Chemistry-climate model data set

5.1.1 The E39C-A model

The coupled chemistry-climate model ECHAM4.L39(DLR)/CHEM/ATTILA (hereafter referred to as E39C-A) was chosen to provide the multi-annual, vertically

resolved, global ozone data set which was necessary to test the newly developed analyses method. The E39C-A is an upgraded version of the ECHAM4.L39(DLR)/CHEM (E39C) chemistry climate model (*Hein et al.*, 2001; *Dameris et al.*, 2005) where the semi-Lagrangian advection scheme is replaced by the fully Lagrangian advection scheme ATTILA (*Reithmeier and Sausen*, 2002) for tracer-transport. The change in advection schemes improved the model performance substantially which is shown by *Stenke et al.* (2008b) and *Stenke et al.* (2008a). E39C itself consists of the dynamic part ECHAM4.L39(DLR) (*Land et al.*, 2002), which is a spectral GCM, and the chemistry module CHEM (*Steil et al.*, 1998). The GCM has a spectral horizontal resolution of T30 ($\approx 6^\circ$ isotropic resolution) which corresponds to approximately $3.75^\circ \times 3.75^\circ$ on the transformed latitude-longitude grid. The vertical extension of the model is defined by 39 layers, extending from the surface to the uppermost layer which is centred at 10 hPa. CHEM is based on a generalized family concept. It includes stratospheric homogeneous and heterogeneous ozone chemistry and the most relevant chemical processes for describing the tropospheric background chemistry. For more details on E39C-A see *Stenke et al.* (2008a).

5.1.2 The REF SCN2d simulation

The model data used for the analyses presented here is a CCMVal reference simulation from E39C-A. CCMVal is a chemistry-climate model validation activity of SPARC (a project of the World Climate Research Program) where process-oriented validation is facilitated (*Eyring et al.*, 2005a). Almost 20 models from research groups all over the world participate in CCMVal. Therefore simulations, for example, of the past stratospheric ozone changes or the future stratospheric composition must have exact specifications to allow comparisons of dynamical and chemical variables between the different models. In *Eyring et al.* (2005b) two reference simulations (REF runs) and additional sensitivity simulations are defined. The REF1 simulation aims to reproduce the past whereas the REF2 simulation is used to predict the future.

The classic REF1 simulation from E39C-A (running from 1960 to 2004) which would be, by its definition, the most suitable data set for the planned analyses does not cover the entire time period as is covered by the observations. However, the classic REF2 simulation does not include natural forcings such as the solar cycle or QBO, and is therefore not suitable for detailed comparisons with observations. But recently, several additional CCMVal sensitivity and control runs

for the next ozone assessment of the World Meteorological Organization (WMO) (*Eyring et al.*, 2008) were defined, of which the SCN2d simulation fulfills most necessary requirements for the planned analyses. The SCN2d simulation from E39C-A covers the time period from 1960 to 2049. It is designed to address the impact of natural variability on the REF2 simulation as close to reality as possible. Its definition is similar to the REF1 simulation, with an included solar cycle, volcanic activity and as well QBO in the past. Future forcings for the solar cycle and the QBO are estimated by repeating defined cycles from the past. No major volcanic eruption is parameterized for the future. The sea surface temperatures and sea ice coverage are prescribed according to a simulation with the HadGEM1 climate model (*Johns et al.*, 2006; *Martin et al.*, 2006), as well as concentrations of greenhouse gases and ozone depleting substances (for more details see *Garny et al.*, 2009). The transition from observed solar activity and QBO to the estimated future solar cycle and QBO could introduce minor inconsistencies in the data time series, but the effects on the results of the planned analyses should be negligible since the future forcings are only applied to the last seven years of the analyzed time period. Since both REF1 and SCN2d simulations are very similar in their definition, but the SCN2d simulation covers the entire time period as is covered by the observations, the latter was selected as basis for the following analyses.

5.1.3 Model grid adjustment

A solid comparison between observations and model simulation starts with getting the two data sets on the same temporal and spatial grid. The original temporal resolution of the E39C-A simulation is 12 hours. For the calculation of the monthly means, which are the basis for the following analyses, all 12 hourly values of the respective month were considered, no additional weighting was applied.

The ozone model output traditionally is given in mixing ratio whereas ozone in the BDBP is stored in number density. Prior to any further grid adjustments it was therefore necessary to convert the ozone model output to number density. Afterward the spatial grid adjustment could be carried out. It first dealt with the differences in the vertical: the 39 model layers (ranging from 1009 hPa to 10 hPa) were interpolated onto the defined pressure grid from the BDBP (see Section 2.1). That results in 32 adjusted model layers, which cover the atmosphere from ≈ 880 hPa to ≈ 10.5 hPa. For each of the adjusted layers the 96 longitude values had to be merged to coincide with the 6 longitude bins defined for the

longitudinally resolved observations data set. Since the model longitude grid is equally spaced (see Section 5.1.1) and the resolution is quite high, no interpolation was necessary to calculate the mean of all values within one of the observational longitude bins. For the zonal mean data set, the mean of all 96 longitude values was determined. Finally, the latitude grid was adjusted. Values from the 48 given latitudes were linearly interpolated on the 36 observational latitudes.

5.2 Methodology

Three different sensitivity tests were performed on the model data set for one selected pressure level:

1. A comparison between results from a regression analysis where the influence of EESC was calculated in every latitude and longitude grid cell separately ('traditional' regression analysis), and a regression analysis where spherical harmonics were applied so that a single fit is made to all data (full data set) to obtain the influence of EESC for all latitudes and longitudes simultaneously. This comparison enables an estimation of the ability of the spherical harmonics to capture spatial patterns. Hereafter this test is referred to as 'sensitivity test 1'.
2. A comparison between results from the spherical harmonics regression applied to the complete data set of the selected level, and results from the spherical harmonics regression applied to the model data set where values which are missing in the observations at the selected level are also defined as missing in the model data set. This second sensitivity test allows an estimation of the occurrence and location of regions where too many data gaps might change the fit of the spherical harmonics. This test is hereafter referred to as 'sensitivity test 2'.
3. A comparison of results from the traditional regression analysis with results from the regression with spherical harmonics where the data set has missing values. This test provides the most valuable information concerning the interpretation of the results from the observational data set since it allows an estimation of the combined errors introduced by the use of spherical harmonics in regression analyses and by incomplete data sets. This last test is hereafter referred to as 'sensitivity test 3'.

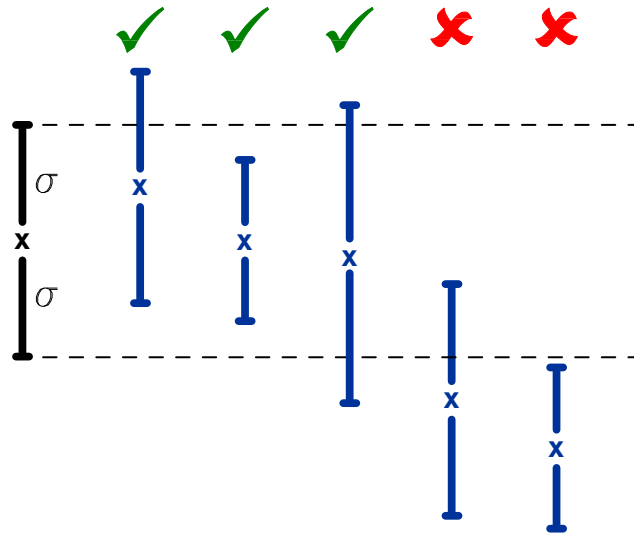


Figure 5.1: Schematic diagram of the selection criteria for comparable values. Value of the standard data set with its respective uncertainties is given in black. Values of the sensitivity data set and their uncertainties are given in blue. All sensitivity values which are within the uncertainties of the standard values are counted as comparable.

Since the goal of this study is to learn more about the longitudinal structure of halogen-induced ozone changes, the three sensitivity tests were performed on the regression coefficient for the EESC basis function (coefficient a_{2a} in Equation 3.15, page 52) at pressure level ~ 58 hPa (roughly the middle of the ozone layer in the mid-latitudes). This coefficient was evaluated for every 10th day of the year at each latitude and longitude bin separately. This results in 7776 evaluations of the seasonal, latitudinal and longitudinal pattern of the EESC coefficients which were compared in each sensitivity test. The comparison is based on two metrics which are determined for each set of EESC coefficients: the fraction of ‘comparable’ results and the fraction of ‘significant’ results. One of the two data sets to be compared is defined as the ‘standard’ against which the other (sensitivity) data set is compared. For the ‘comparability’ metric the fraction of all comparable results between the standard and the sensitivity data set is determined. A comparable result is therefore defined as an EESC coefficient of the sensitivity data set which lays within the uncertainty area of the respective EESC coefficient of the standard data set. The uncertainty area can be represented by either the 1σ or 2σ area depending on the rigor of the definition of comparable. Figure 5.1 shows schematically the selection criteria to define values as comparable. It can be expected that with increasing spherical harmonic expansions the comparability value increases since finer structures in the data can be resolved.

The significance metric describes the fraction of the EESC coefficients of the sensitivity data set which are statistically significantly different from zero at a 2σ level. The greater the number of expansions applied to the spherical harmonics, the greater the degrees of freedom in the regression model which increases the error on the derived coefficients. While the fraction of comparable results increases with increasing spherical harmonic expansions the fraction of significant results decreases so that there exists an optimal set of expansion values for each of the three sensitivity tests. For each of the sensitivity tests several expansion settings for the regression with the spherical harmonics were applied to find the optimal set of values for L (expansion in latitude) and M (expansion in longitude).

This optimal set of spherical harmonic expansions is defined as the maximum of the combined fractions of comparability and significance. The two metrics are combined by adding the number of comparable results to the number of significant results and dividing them by twice the number of overall possible results (2×7776 , see above). The optimal settings derived from all three sensitivity tests were determined at a single pressure level, i.e. ~ 58 hPa. Tests for other selected pressure levels showed similar results, although the optimal spherical harmonic expansions changed by one value of L depending on the number of missing data for the analyzed level. The more data missing the lower the expansion values for L tends to be. However, the set of optimal expansion values determined at 58 hPa was applied at all other pressure levels in the analyses for Chapter 6.

5.3 Sensitivity to the use of spherical harmonics in a regression (sensitivity test 1)

As far as I am aware, this is the first time that spherical harmonics have been used to capture the geographical structure in regression model fit coefficients. It is therefore important to assess their ability to capture patterns in spatially resolved regression applications. Results from a regression analysis where the influence of EESC was calculated for every latitude bin and every longitude bin separately (the traditional approach) were compared with results from a regression analysis where spherical harmonics were applied to describe the geographical structure in the regression fit coefficients from a single fit of the regression model to all data at a specific level.

The results of the traditional regression show a wave-like structure in the EESC coefficients in the northern high latitudes in March (Figure 5.2, left panel). Co-

5.3. SENSITIVITY TO THE USE OF SPHERICAL HARMONICS IN A REGRESSION (SENSITIVITY TEST 1)

efficients in Figure 5.2 are most negative closest to the North Pole, and they are very similar over all latitudes in the southern hemisphere. In Figure 5.3, left panel, which shows the results for September, the dominant feature is the steep meridional gradient in the coefficients starting at around 40°S which is a result of Antarctic ozone depletion. Note that all graphs in the left panels of both figures are the same since the traditional regression approach is independent of spherical harmonic expansions. All results shown are derived from regression analyses based on the E39C-A simulation.

As it can be seen in Figure 5.2 and Figure 5.3 the resolution of the spatial patterns derived from the spherical harmonic regressions increases with increasing spherical harmonic expansions. The main patterns in both figures are captured with an intermediate number of expansions, however, only with higher expansions (>L8M2) the tropical and subtropical results become similar. With the highest expansion shown (L10M2) most of the EESC coefficients are comparable. Note, comparability for this sensitivity test is determined according to the comparison based on the 1σ area (see Section 5.2). This is different to sensitivity test 2 and sensitivity test 3 where the comparability metric is based on the 2σ area. The exception for sensitivity test 1 was made since the uncertainties of the EESC coefficients from the traditional regression approach are high and results from the sensitivity data set therefore numerous comparable. In reducing the uncertainty area to only 1σ the comparability criteria is tightened and the development of the comparability metric with increasing spherical harmonic expansions is more pronounced. As expected, the significance of the EESC coefficient of the sensitivity data set is reduced with increasing expansions. Nevertheless, the degree to which the finer longitudinal structure of the EESC coefficients from the traditional regression analysis is captured with the highest shown spherical harmonic expansions, for example in Figure 5.2 in the northern high latitudes, proves that spherical harmonics implemented in a regression model indeed are able to faithfully capture geographical structures in the fit coefficients. Some of the results are not significant though, but the main features in Figure 5.2 and Figure 5.3, the wave-like pattern in the northern high latitudes and the region of the Antarctic ozone depletion, respectively, are significant and comparable.

Figure 5.4 shows the results for comparability and significance of the spherical harmonics results for different expansion settings. With six longitude bins per latitude band the highest possible expansion in longitudinal direction is $M = 2$. The number of expansion equations are always double the number chosen for M (as described in Section 3.2.1). Therefore, higher expansions than $M = 2$ are not

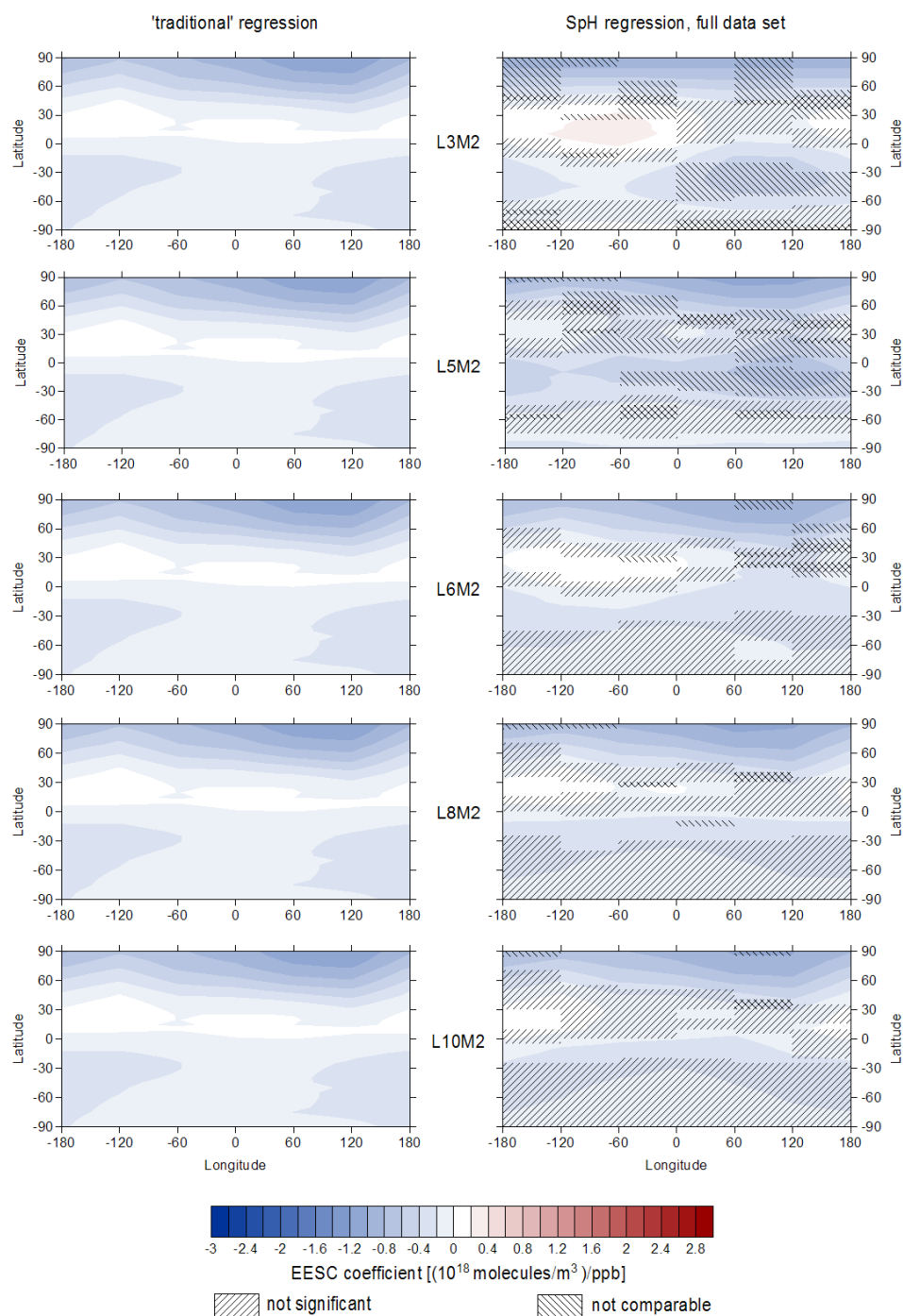


Figure 5.2: EESC coefficients evaluated March. The left column shows results for the traditional regression approach, the right column shows the results for the regression where spherical harmonics are used on a data set without gaps. Rows show results for different spherical harmonic expansions. Hatched regions indicate where the results from the regression with spherical harmonics (for the data set without gaps) are either not significant or not comparable to the results from the traditional regression approach. Note, the comparability values here are based on the 1σ area comparison.

5.3. SENSITIVITY TO THE USE OF SPHERICAL HARMONICS IN A REGRESSION (SENSITIVITY TEST 1)

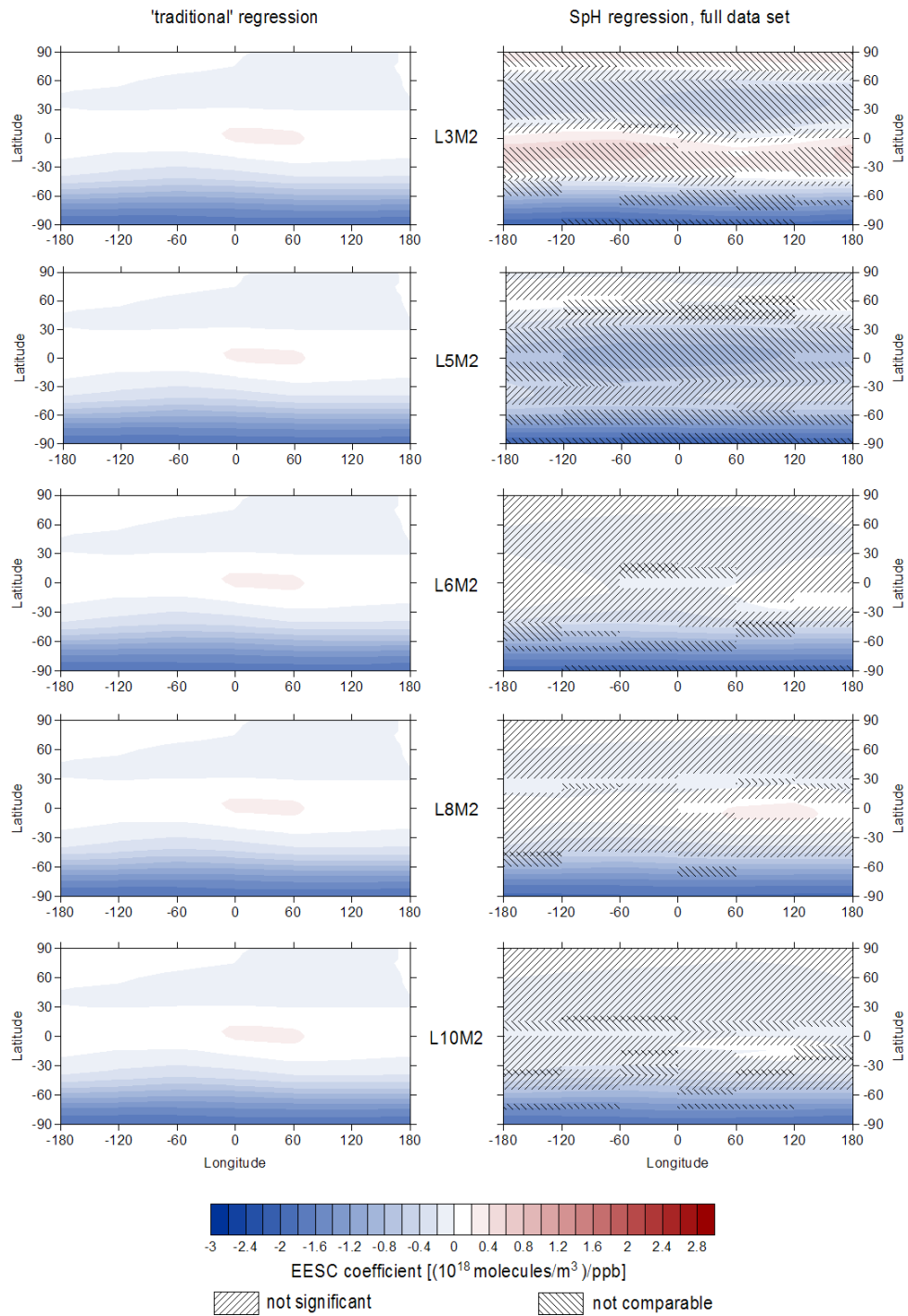


Figure 5.3: Same as for Figure 5.2, but for September.

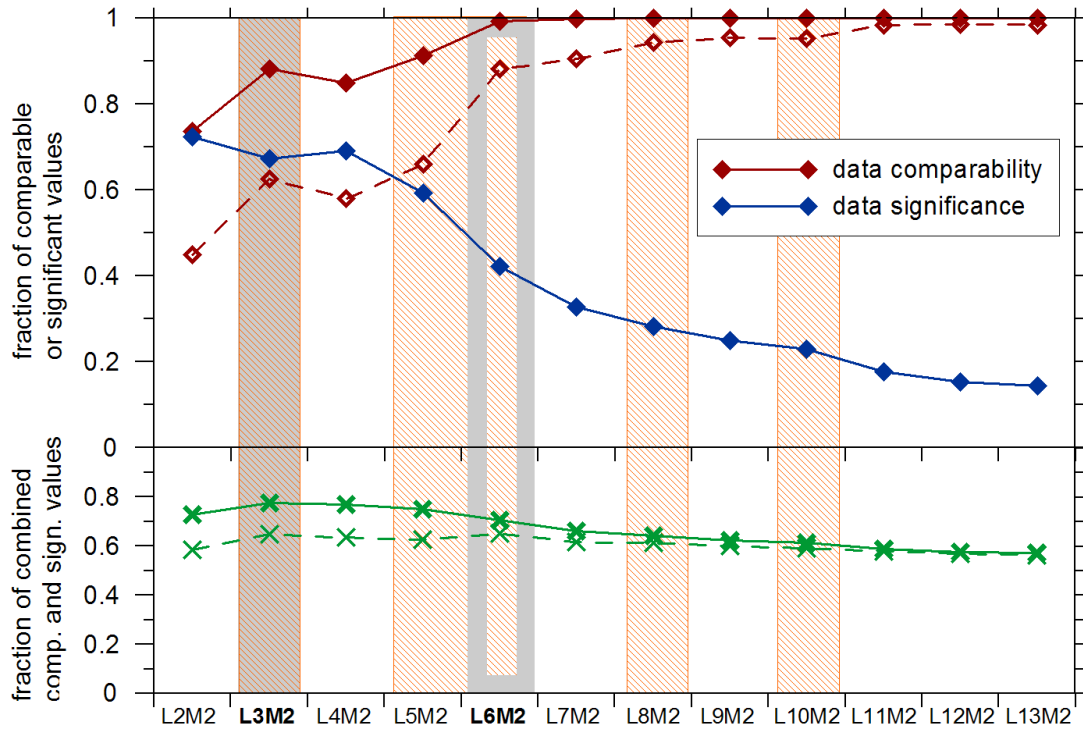


Figure 5.4: Fraction of significant (blue curve) and comparable data (red curves) for sensitivity test 1. These results are for 58 hPa, for all latitude/longitude bins, every 10th day, for several different spherical harmonic expansions. The green curves show the combined comparability and significance. Solid lines show results for the comparability test with a 2σ uncertainty, dashed lines the results for 1σ . The optimal spherical harmonic expansion for this sensitivity test is highlighted by the gray underlying box for the 2σ area comparison, the gray open box highlight the result for the 1σ area comparison. Hatched orange areas indicate the expansion settings which are shown in Figure 5.2 and Figure 5.3.

possible since the number of expansion equations would be equal or exceeding the number of available longitudinally resolved values. This would lead to overfitting. The values for L (latitudinal expansion) range between 2 and 13. For each of those expansion settings the fraction of comparable and significant values for every 10th day and all latitude/longitude bins at 58 hPa were determined. The higher those fractions the better the results from the traditional regression approach and the regression with spherical harmonics agree. As mentioned already, it can be seen that the fraction of significant values decreases whereas the fraction of comparable values increases with increasing expansions. The fraction of the combined comparable and significant values (sum of significant and comparable values divided by twice the overall values) is biggest for the expansion settings L3M2 if the comparable values are determined with the 2σ area comparison. This

is due to strong error value growth with increasing spherical harmonic expansions. The significance, therefore, decreases faster than the increase in comparable values which results in an overall decrease of interpretable values. For this sensitivity test only, the optimal expansion settings for 1σ and 2σ area comparison are not identical. The optimal settings for the 1σ area comparison are L6M2, considerably higher than for the 2σ area comparison. This is caused by the saturation of comparable values from intermediate expansion settings when evaluated with the 2σ area.

5.4 Sensitivity to data gaps (sensitivity test 2)

The main reason for implementing spherical harmonics in a regression model was the prospect of the ability to perform estimations of ozone changes on incomplete data sets. A very important test, therefore, is the estimation of how spherical harmonic expansions of the model fit coefficients react to missing data. The regression model with spherical harmonics implemented was run on a complete model data set, and a model data set where values were removed to mimic the temporal and spatial coverage of the observations.

In Figure 5.5 the EESC coefficients from both regressions are shown for March. Figure 5.6 shows the coefficients evaluated for September. As opposed to the figures from sensitivity test 1, the expansion settings are now changed for both columns which results in different spatial patterns for the different rows. This is due to the fact that results of two regression models with implemented spherical harmonics are compared.

It can be seen in Figure 5.5 that the spatial characteristics of the EESC coefficients change significantly with the lower expansions (L3M2 to L5M2), whereas the changes are only marginal with the higher expansions L7M2 and L9M2. Patterns obtained from the regression using the incomplete data set are very similar to the results from the full data set. In fact, the differences within one data set for different expansion settings exceed the differences between the complete and incomplete data set for the same settings. The number of values which are not comparable are very low for all settings, smallest for L7M2. The significance of the EESC coefficients decreases rapidly with increasing expansions as was the case for the sensitivity test 1. However, since many data are missing, the significance decreases faster compared to the results of the complete data set. Similar behavior is apparent in Figure 5.6 for September. Spatial characteristics

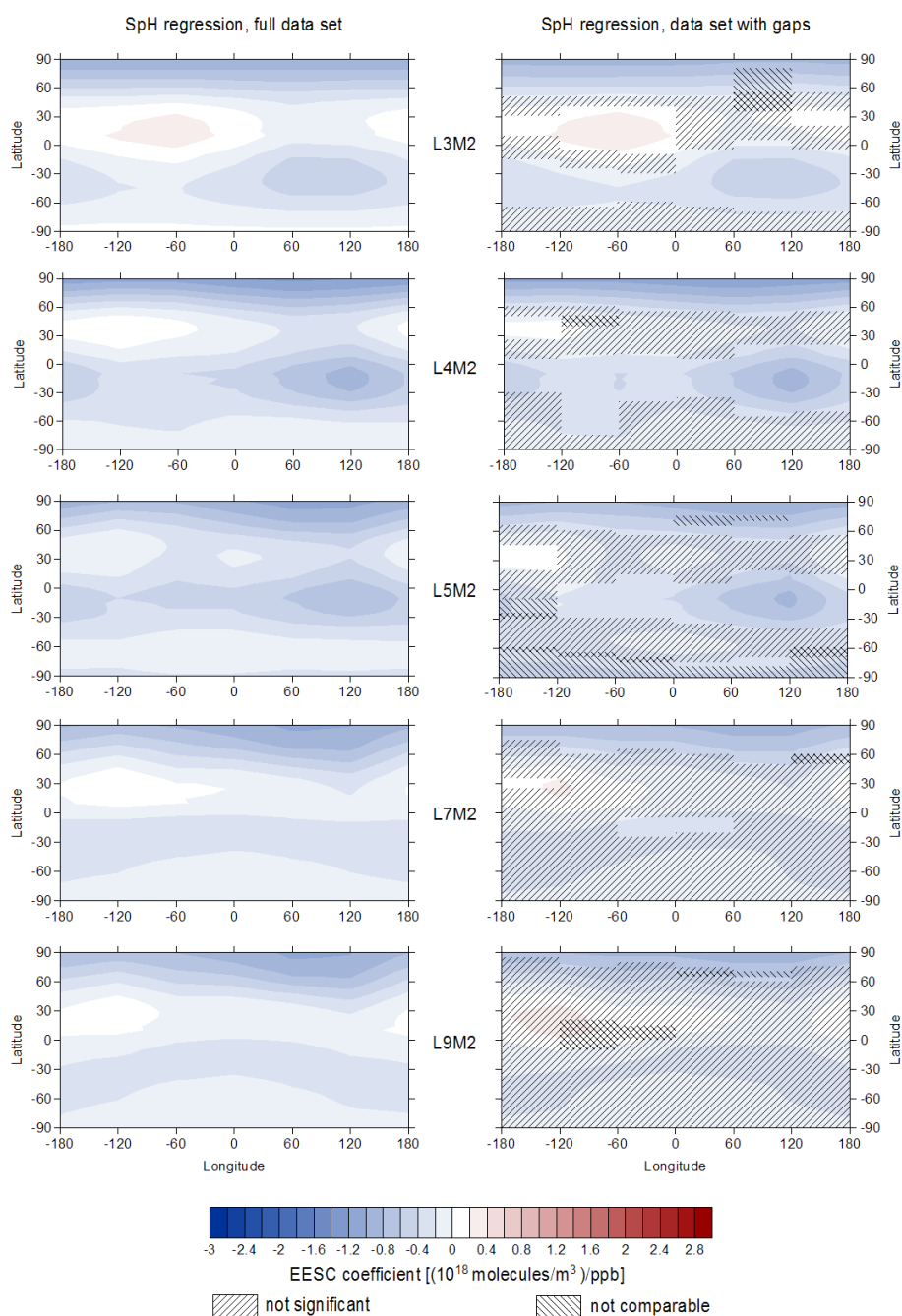


Figure 5.5: EESC coefficients evaluated for March. The left column shows results for the regression where spherical harmonics are used on a data set without gaps, the right column shows the results for the regression where spherical harmonics are used on a data set with gaps. Rows show results for different spherical harmonic expansions. Hatched regions indicate where the results from the regression with spherical harmonics for the data set with gaps are either not significant or not comparable to the results from the regression with spherical harmonics on the full data set. Note, the comparability values here are based on the 2σ area comparison.

5.4. SENSITIVITY TO DATA GAPS (SENSITIVITY TEST 2)

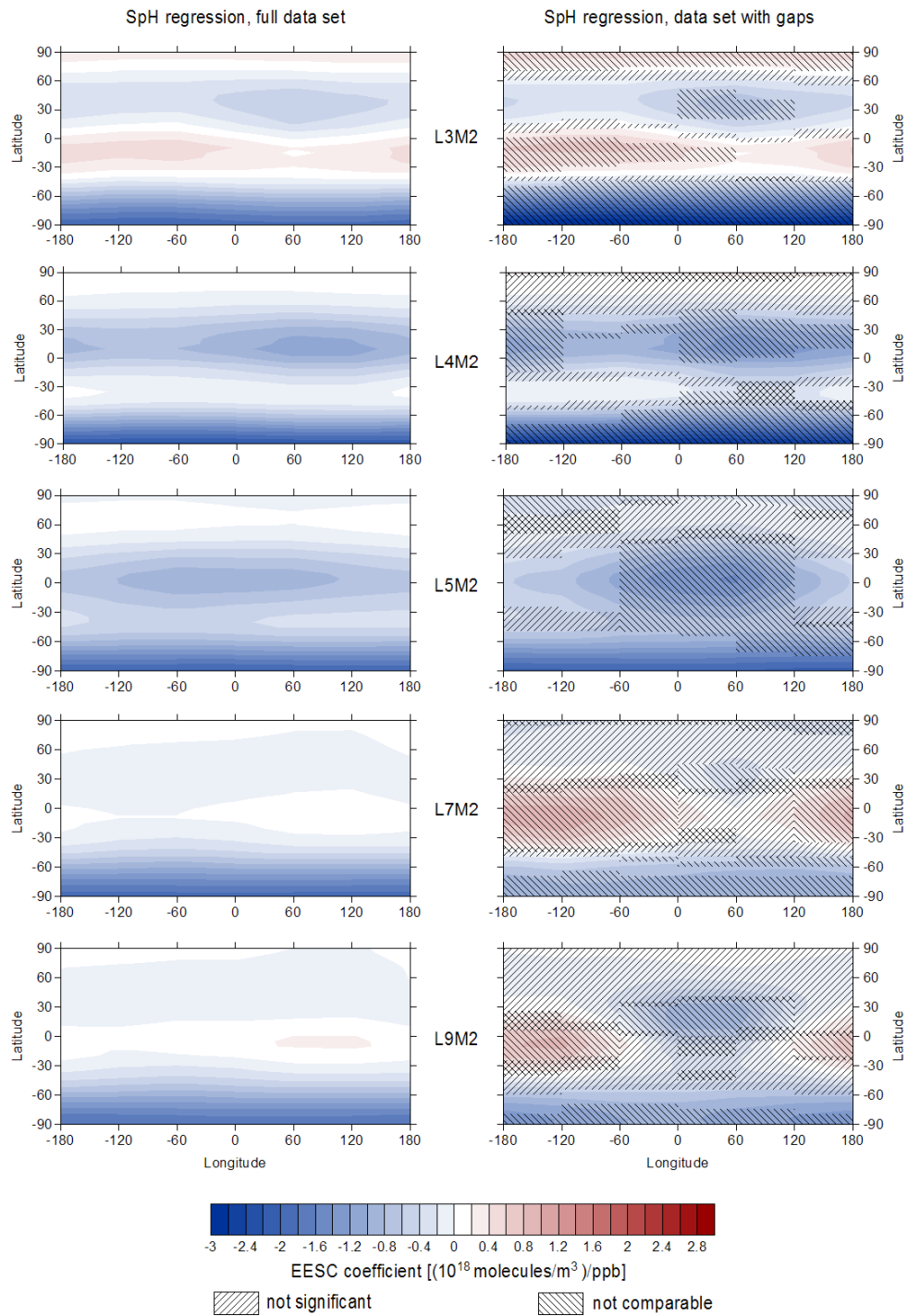


Figure 5.6: Same as for Figure 5.5, but for September.

change significantly with the lower expansions; differences between one data set for different expansions are more pronounced than differences between the data sets for the same expansion, at least for the lower expansion settings. With the higher expansions the differences between the two data sets become apparent. Due to the number of missing data, the EESC coefficient patterns, especially in the tropics and subtropics, cannot be reproduced. On the other hand, with the low expansions (L3M2 and L4M2) the Antarctic ozone depletion is significantly overestimated, whereas with the higher expansion it tends to be underestimated. As mentioned before, the number of functions with which the spherical harmonics are expanded are crucial for capturing steep meridional gradients. With data gaps it seems even more important to choose settings which are able to reproduce the spatial pattern within the data without being too loosely constrained because of the missing data. Significance decreases rapidly with increasing expansions (as mentioned before); comparability increases slightly for the low expansions and remains fairly constant for the higher expansions.

The number of missing data, therefore, definitely matters for the fitting of spherical harmonics. If data are temporally and spatially dense, high resolutions of spherical harmonics can be used. For regions and time periods where many data are missing, the higher spherical harmonics cannot be restrained enough to obtain realistic results. Figure 5.7 shows the fraction of significant and comparable data at 58 hPa and different spherical harmonic expansions. As mentioned in the previous section, the optimal set of expansions can be determined by finding the maximum of the fraction of the combined comparable and significant data. For the sensitivity test 2 this maximum is reached for the settings L3M2, as indicated by the gray box in Figure 5.7.

5.5 Sensitivity to spherical harmonics and data gaps (sensitivity test 3)

Differences between regression results where full and incomplete data sets are used become large already at low spherical harmonic expansions. However, the final test for defining the optimal set of expansion settings has to be a comparison between results from a traditional regression approach (fitting the basis functions to the time series at every latitude and longitude separately) and results from a regression where spherical harmonics are used with an incomplete data set. With that comparison the combined errors from using the spherical harmonics

5.5. SENSITIVITY TO SPHERICAL HARMONICS AND DATA GAPS
(SENSITIVITY TEST 3)

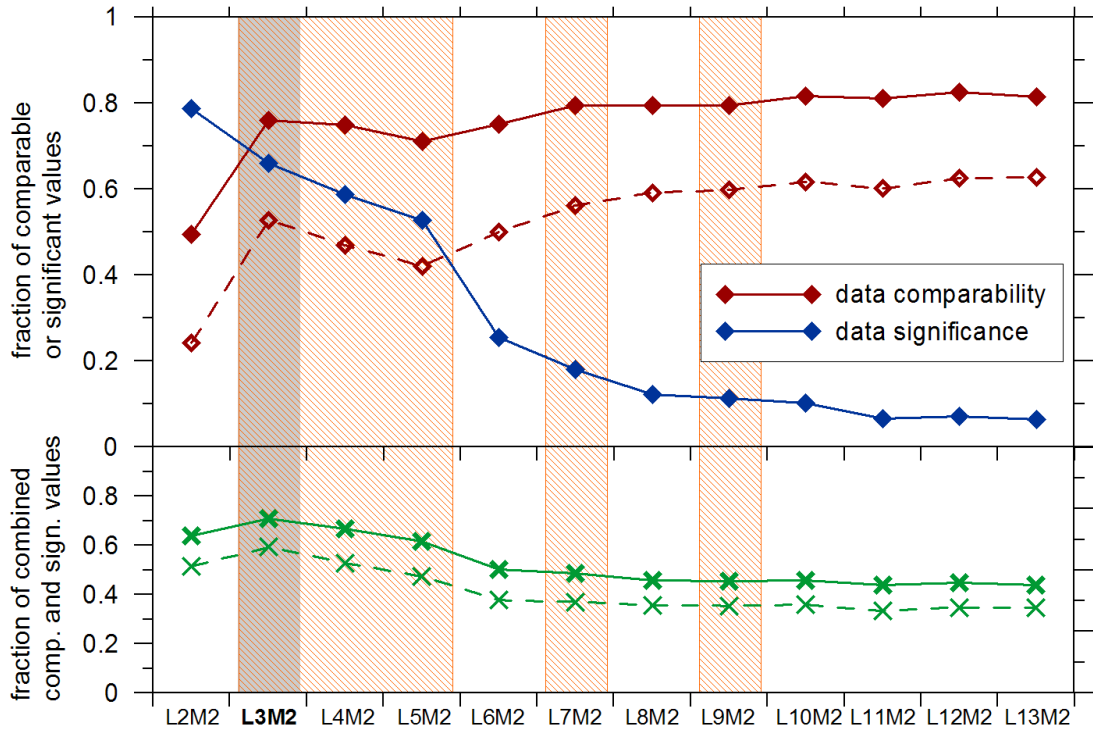


Figure 5.7: Fraction of significant (blue curve) and comparable data (red curves) for the sensitivity test 2. Data are tested at 58 hPa, for all latitude/longitude bins, every 10th day, for several different spherical harmonic expansions. The green curves show the combined comparability and significance. Solid lines show results for the comparability test with a 2σ uncertainty, dashed lines the results for 1σ . The optimal spherical harmonic expansion for this sensitivity test is highlighted by the gray underlying box for the 1σ and 2σ area comparison. Hatched orange areas indicate the expansion settings which are shown in Figure 5.5 and Figure 5.6.

in a regression and having many missing data can be evaluated and regions of non-interpretable data (either not significant, not comparable, or both) identified. Figures 5.8 and 5.9 show the results of that third sensitivity test for March and September, respectively.

As seen for the other two sensitivity tests, the structural resolution improves with increasing spherical harmonic expansions (right columns of graphs in both figures). Nevertheless, the problems of insufficient restraint for higher expansions with the incomplete data set remain (Figure 5.9, right column) which becomes obvious in direct comparison with the results of the traditional regression. As in the other two sensitivity tests, the areas where data between the two regression settings are not comparable decrease with increasing expansions, but also the overall significance of the EESC coefficients decreases. Again, the significance

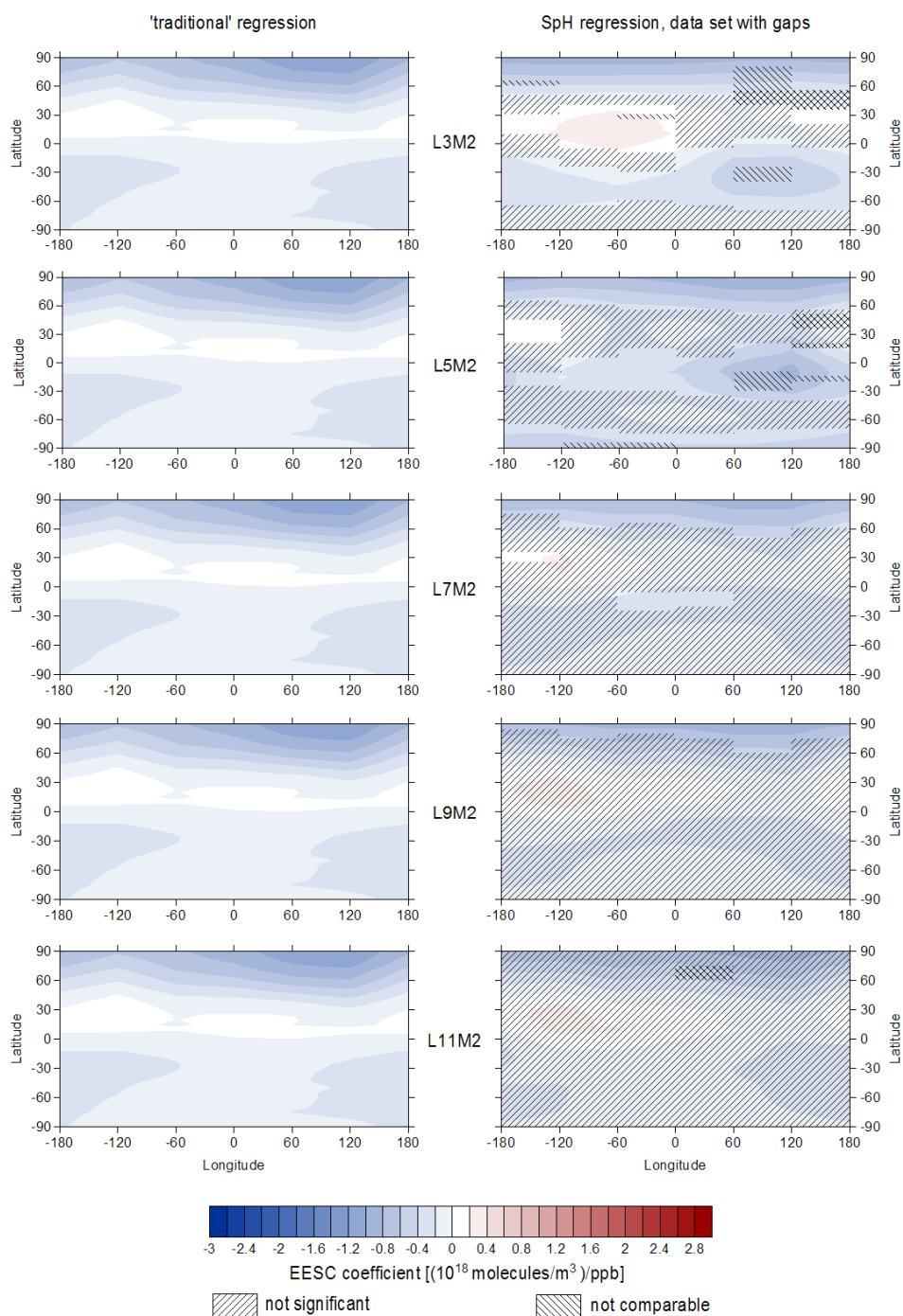


Figure 5.8: EESC coefficients evaluated for March. The left column shows results for the traditional regression approach, the right column shows the results for the regression where spherical harmonics are used on a data set with gaps. Rows show results for different spherical harmonic expansions. Hatched regions indicate where the results from the regression with spherical harmonics (for the data set with gaps) are either not significant or not comparable to the results from the traditional regression approach.

5.5. SENSITIVITY TO SPHERICAL HARMONICS AND DATA GAPS
(SENSITIVITY TEST 3)

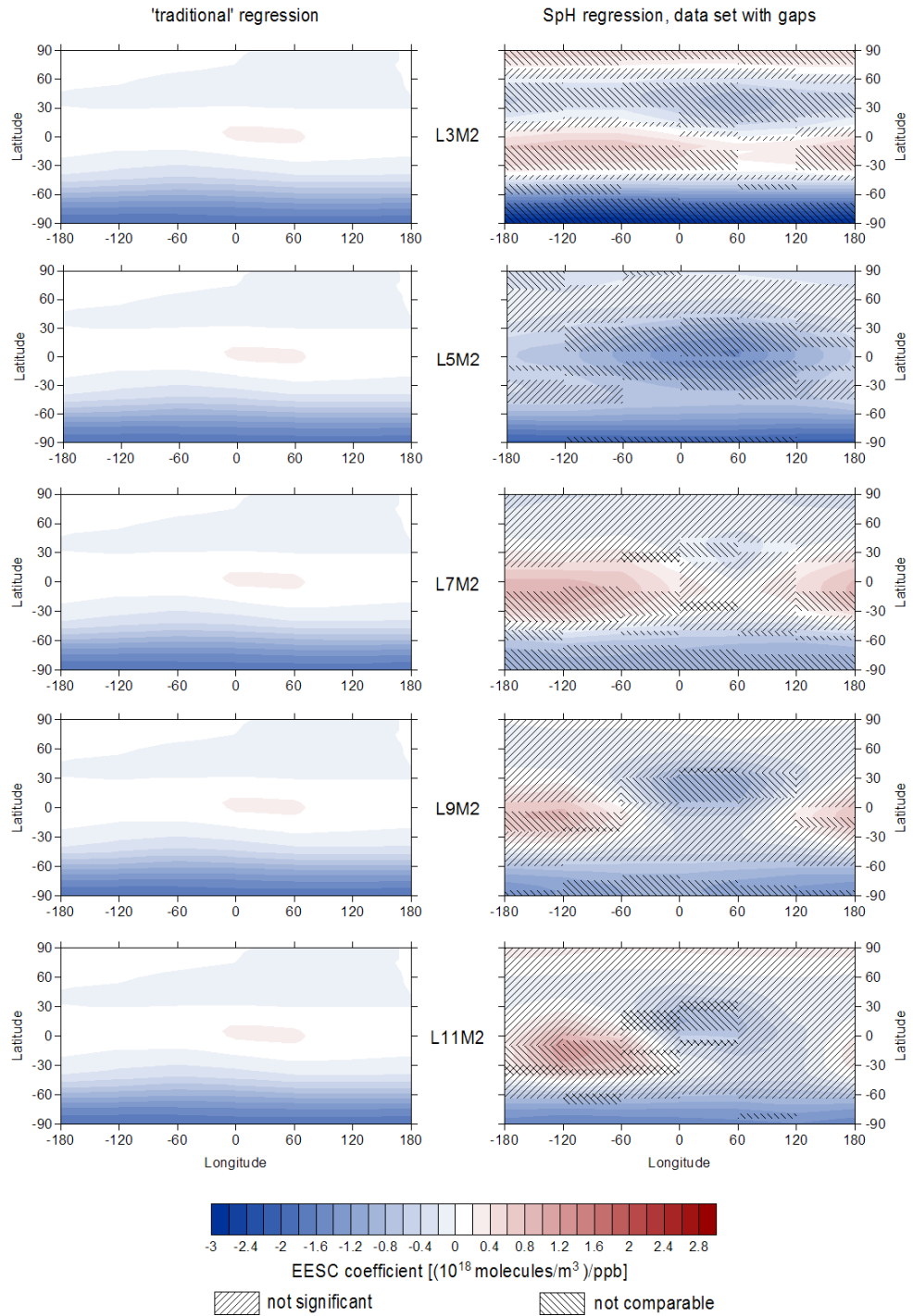


Figure 5.9: Same as for Figure 5.8, but for September.

decreases much faster than the comparability increases, so with higher expansions some days show no significant EESC coefficient at all (see Figure 5.9, right column, last row). Error values increase with higher expansions not just because of the increase in the number of coefficients to be fitted but also because of the increased uncertainty of the fit due to missing data.

Problems capturing the Antarctic ozone depletion properly were already mentioned for sensitivity test 2 (see Figure 5.6). The comparison against results from a traditional regression approach changes the areas of significant and comparable data only slightly. The most pronounced differences are areas in the tropics, especially in September, where coefficients are comparable and significant which seem by visual judgment not to be comparable at all. In those cases, the error for the coefficient from the traditional regression is very large which, therefore, includes the noticeably different coefficient in the 2σ area. Since those coefficients of the sensitivity test have very small error values themselves though, they are also counted as significant. Those regions have to be kept in mind for the interpretation of the regression analyses with the observational data set in the following chapter.

The optimal set of spherical harmonic expansions, obtained by finding the maximum of the fraction of the combined comparable and significant values (see Figure 5.10), determined by the results of sensitivity test 3, are identical to the expansions defined by sensitivity test 1 (for the 2σ area comparison) and sensitivity test 2, L3M2. Data comparability increases again only slightly with higher expansions after a first considerable improvement from expansion L2M2 to L3M2. The most pronounced reduction in significance however occurs from expansion L5M2 to L6M2 where significant values are reduced by a factor of two (from 0.528 to 0.256). The first four values (expansions L2M2 to L5M2) of the combined comparable and significant values decrease only slightly, from 0.729 to 0.697. Taking this into account and the fact that the higher spherical harmonic expansions are able to describe steeper meridional gradients more accurate and capture the spatial pattern with more detail, the expansion L5M2 was chosen as settings for the regression with the observations although the suggested optimal expansion settings by sensitivity test 3 is L3M2. With the choice of L5M2 as the final settings, the reduction of interpretable values is deliberately accepted to take the advantage of higher expansions.

Figures 5.8 and 5.9 show only two examples for sensitivity test 3, but comparisons are evaluated for every 10th day of the year. For each of those evaluations comparability and significance masks were obtained identifying regions of inter-

5.5. SENSITIVITY TO SPHERICAL HARMONICS AND DATA GAPS
(SENSITIVITY TEST 3)

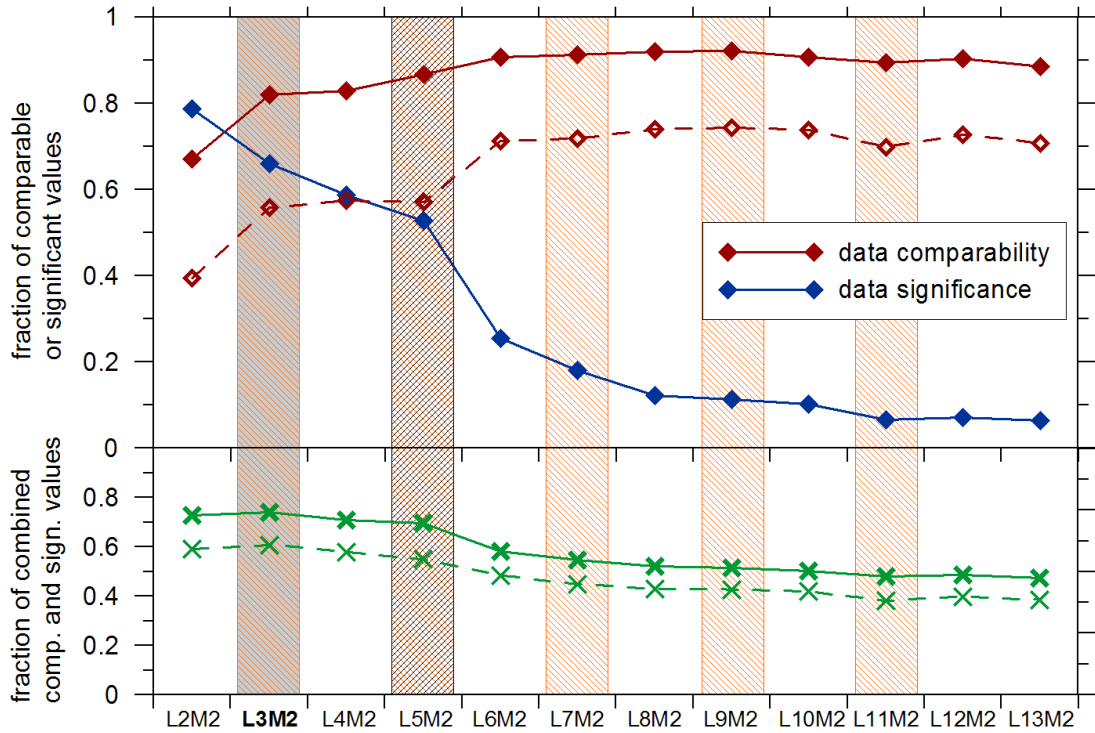


Figure 5.10: Fraction of significant (blue curve) and comparable data (red curves) for sensitivity test 3. Data are tested at 58 hPa for all latitude/longitude bins, every 10th day, for several different spherical harmonic expansions. The green curves show the combined comparability and significance. Solid lines show results for the comparability test with a 2σ error domain, dashed lines the results for 1σ . The optimal spherical harmonic expansion for this sensitivity test is highlighted by the gray underlying box for the 1σ and 2σ area comparison. Hatched orange areas indicate the expansion settings which are shown in Figure 5.8 and Figure 5.9. The black hatched area indicates the chosen settings for the regression analyses with the observations.

pretable EESC coefficients. The masks for the spherical harmonic expansion L5M2 are the most important basis for the interpretation of the regression results of the observational data which will be described in the next chapter. Only with those masks is a realistic estimation of the effects of an incomplete data set on regression results possible. The optimal expansion settings derived from all three sensitivity tests are not further considered since they were only taken as guidelines for choosing the final settings for the regression with the observations. Nevertheless, all three sensitivity tests provide deeper insight into possibilities of spherical harmonics in regression analyses, the ability to resolve spatial features and the ability to handle data gaps.

5.6 Summary

Due to the significant reduced data coverage for the longitudinally resolved data set sensitivity tests were necessary to evaluate the performance of the regression with implemented spherical harmonics of the fit coefficients with expansions in latitude and longitude, as well as the influence of missing data. For those tests a data set without gaps and with identical spatial and temporal characteristics as the observations was necessary. This data set could be obtained from chemistry-climate model output and was described in detail in this chapter. Three sensitivity tests were carried out with the model data, for several different spherical harmonic expansions: sensitivity test 1 evaluates the ability of a regression with implemented spherical harmonics of the fit coefficients to realistically capture spatial patterns, sensitivity test 2 assesses the influence of data gaps on results from spherical harmonic regressions, and with sensitivity test 3 the combined effects of spherical harmonics expanding basis functions in regressions applied on incomplete data sets are estimated. With findings of test 3 the final spherical harmonic expansions for the longitudinally resolved regression analysis were determined. Results of this longitudinally resolved regression are presented in the following chapter.

Chapter 6

Analysis of longitudinally resolved data

According to the sensitivity tests from the previous chapter, the final settings for the spherical harmonic expansions for the regression calculations were defined. Although the sensitivity tests are based on EESC coefficients only, expansions were kept the same for all basis functions. Expansions for all pressure levels analyzed were also fixed to the preferred expansion settings determined. As a result, a four dimensional field of EESC coefficients were obtained, dependent on latitude, longitude, pressure level and time. To facilitate comparisons and verifications, the complete regression (all pressure levels) was not only calculated for the observation data set, but also for the model data set where data missing in the observations were removed to match the spatial and temporal characteristics of the observation data set. Furthermore, a traditional regression was calculated individually for all latitude/longitude bins and all pressure levels from the complete model data set. With a comparison of selected subsets of all three regression analyses results, it was possible to reduce the uncertainties in the patterns obtained by the regression analysis of the observations since the influence of data gaps can be assessed as well as differences between the analyzed model simulation and reality.

6.1 Preliminary remarks

Similar to the analysis described in Section 4.1, no trends were calculated from the EESC coefficients, rather the coefficients themselves are the result of the

analysis to be presented. The significance of the coefficients is identified by their uncertainties which are derived from the individual regression approaches. The comparability, as defined in the previous chapter, is determined according to the approach of sensitivity test 3 (see Section 5.5) with the spherical harmonic expansions set to ‘L5M2’ for all pressure levels. As detailed in Section 5.5, for sensitivity test 3 the chemistry-climate model results from a traditional regression approach are compared with results from a regression with spherical harmonics implemented where all model data are removed which correspond to data missing in the actual observations. Masks of non-comparable values were derived for every pressure level separately to be able to take into account individual pressure level differences in data availability and fitting problems of the spherical harmonic approach. Note that comparability values are only available up to about 10 hPa since the E39C-A data on which they are based, exist only up to that level. Comparability masks are applied to results from the spherical harmonics regression (SpH regression) with incomplete E39C-A data and with observations.

Figure 6.1 shows the results of the comparison between the traditional regression results (based on the complete model data set) and results from the regression based on observations where the spherical harmonic settings were fixed for all pressure levels to ‘L5M2’, according to the findings from Section 5.5. Additionally, the atmospheric region of available data from the different sources is illustrated. It is possible to distinguish three pressure regions in which the number of ‘valid’ values (either comparable or significant or both) remain fairly constant: up to ~ 160 hPa (approx. 13 km), from ~ 160 hPa to ~ 77 hPa (approx. 18 km) and above ~ 77 hPa. In the lowest region, the significance is very low (not even every 10th data point is significant), but about every 2nd data point is comparable. It is the region where the tropopause is located approximately. Here ozone variability is very high due to a steep vertical gradient in ozone (see for example Figure 2.5) which complicates a good fit of the regression basis functions with the specified, small number of spherical harmonic expansions. Uncertainties on the coefficients are high and, therefore, the number of significant values is small. The high uncertainties are also the reason for the high fraction of comparable values: comparability is easily achieved since a broad area of values is embraced by the uncertainties, although the compared coefficients might not be very similar. As long as the value obtained by the regression using spherical harmonics is located within the 2σ area of the value from the traditional regression it is counted as comparable. With increasing atmospheric altitude, ozone variability decreases and the regression basis functions are more able to describe it. Therefore, the significance increases in the middle pressure region (~ 160 hPa to ~ 77 hPa). With

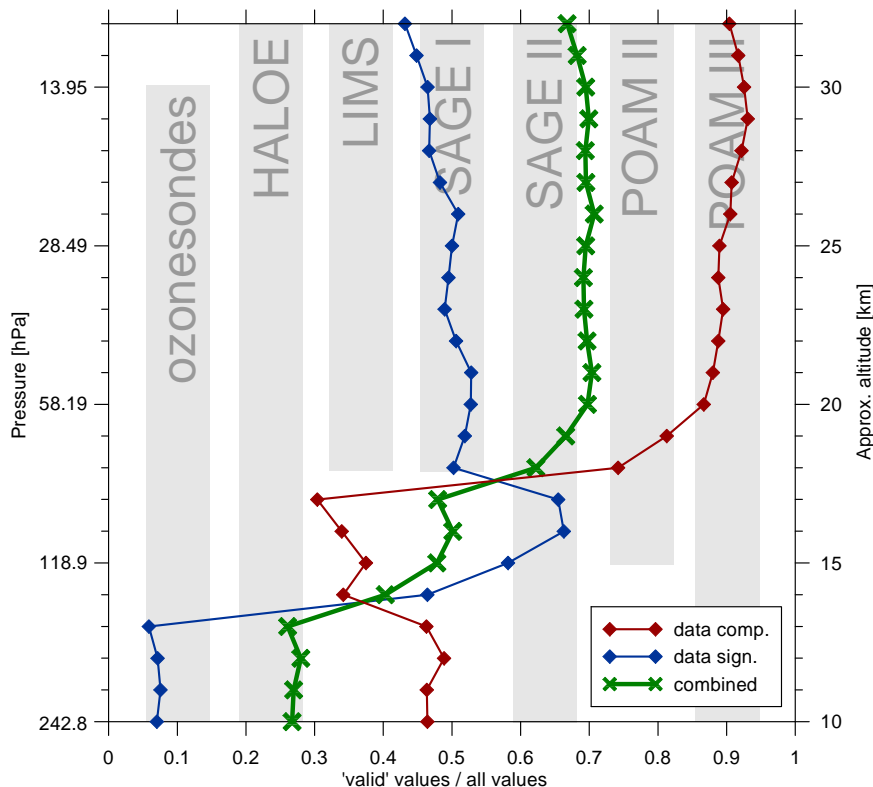


Figure 6.1: Results of the comparison between the traditional regression results and results from the spherical harmonics regression based on observations for all pressure levels: comparability (red line), significance (blue line) and values for comparability and significance combined (green line). The gray bars show the used data sources and their covered atmospheric altitude regions.

smaller uncertainties it is harder to meet the comparability criteria. Since the available data sources stay the same for the two lower pressure regions, no additional data were added to the regression analyses. The fit of the spherical harmonics might not be constrained sufficiently because there are many missing values in those regions and artificial patterns are created which do not exist in the results of the traditional regression. This is mirrored in the low comparability values. Only with the addition of more data sources which contribute to the monthly mean calculations, for example LIMS and SAGE I upward of ~ 77 hPa, is it possible to constrain the spherical harmonics well enough to obtain reliable results. In the third pressure region, the comparability therefore increases significantly with about every 2nd data point being significant.

The structure of the comparability profile is important for the subsets analyzed in the following sections since it suggests that results from pressure levels below

~ 77 hPa are considerably influenced by regression fits which are not well constrained. This was suspected already from the analysis of the zonal mean data described in Chapter 4. Non-comparable and non-significant values are, therefore, clearly marked in the following graphs of the results obtained using regressions with spherical harmonics implemented. Only the significance is flagged for results from the traditional regression. In the following sections, results for subsets from the four-dimensional, EESC coefficient field are discussed. The subsets were chosen according to regions and times with distinct zonal asymmetries in ozone in response to EESC, as described in the recent literature (see Section 1.1) and by general circulation characteristics (see Section 1.3). The results are always presented in three columns. The left column illustrates results for the complete E39C-A data set derived with a traditional regression approach (hereafter referred to as the ‘traditional regression’). The middle column displays the results for the E39C-A data set where the same data as missing in the observations were removed based on a regression using spherical harmonics (hereafter referred to as ‘SpH-Model regression’). The right column displays the results for the observations calculated with a regression using spherical harmonics (hereafter referred to as ‘SpH-Obs regression’). The model results provide valuable additional information for the interpretation of the results from the observations, but are not the main focus of this study. It also has to be kept in mind that, although a complete data set of the model data is available and effects of data gaps can therefore be eliminated, the model data do not have to match reality in all details. Differences in regression results for model data and observations, therefore, could also be caused by insufficiently explained or unexplained atmospheric mechanisms in the model.

6.2 Halogen-induced changes in the northern polar regions in spring

Strong wave activity in the Northern Hemisphere in winter and spring leads to an Arctic vortex which is often not centered above the North Pole but is displaced towards Scandinavia and Eastern Russia (*Andersen and Knudsen, 2006*). Zonal asymmetries in halogen-induced ozone changes in the Northern Hemisphere are therefore primarily expected in spring when heterogeneous chemistry within the displaced vortex has destroyed enough ozone or when the vortex breaks up and ozone-poor air is transported to lower latitudes.

Figure 6.2 shows the geographical pattern of the EESC coefficients in March for three different pressure levels: ~ 77 hPa, ~ 58 hPa and ~ 44 hPa. The results are presented in three columns as described earlier. The main feature in the traditional regression results is the wavy structure in the northern polar latitudes. The bulge of the structure, with the most negative coefficients, is located between 60°E and 180°E and extends on all pressure levels down to the mid-latitudes. However, the meridional gradient flattens with decreasing pressure levels and the magnitude of the coefficients decreases, indicating a stronger influence of EESC lower in the atmosphere. For all three pressure levels shown the influence of EESC is very small and not significant in the tropics and the Southern Hemisphere. Such a global pattern of EESC coefficients is consistent with earlier total column ozone studies (e.g. *Fioletov et al.*, 2002).

In the results from the SpH-Model regression (middle column), the wavy structure exists, the bulge of it is located between 60°E and 180°E and it extends into the mid-latitudes, however, not as far as in the results from the traditional regression. The amplitude of the wavy structure is smaller for the SpH-Model results and shows a shallower meridional gradient. The coefficients within the bulge are also slightly underestimated. The main difference between the traditional regression results and the results from the SpH-Model regression is the distinct, zonally asymmetric pattern in the tropics: there is a wave-like structure just south of the equator with the most negative EESC coefficients around 120°E . With decreasing pressure, SpH-Model results get more zonally symmetric. Since this pattern exists only in the results from the SpH-Model regression and not in the traditional regression results, and since most parts of the tropics are marked as non-comparable, this pattern is therefore most likely induced by the large amount of missing data in the tropics (see Figure 2.4). With only about 20-30% of all data points available in this region, the degrees of freedom for fitting the harmonic functions are too high and ‘overshooting’ can occur. However, this problem is not as present for higher altitude regions, either because of less missing data (both locally and globally) or because of less ozone variability which has to be explained. However, the main feature of the halogen-induced ozone changes in Northern Hemisphere spring, the wavy structure in the northern high-latitudes, is captured well with the SpH-Model regression in spite of the existing data gaps and the relatively low expansion settings chosen.

The number of non-significant values produced by the traditional regression analysis is large compared to the SpH-Model regression and it does not change much for the pressure levels presented. This could be caused by either smaller coef-

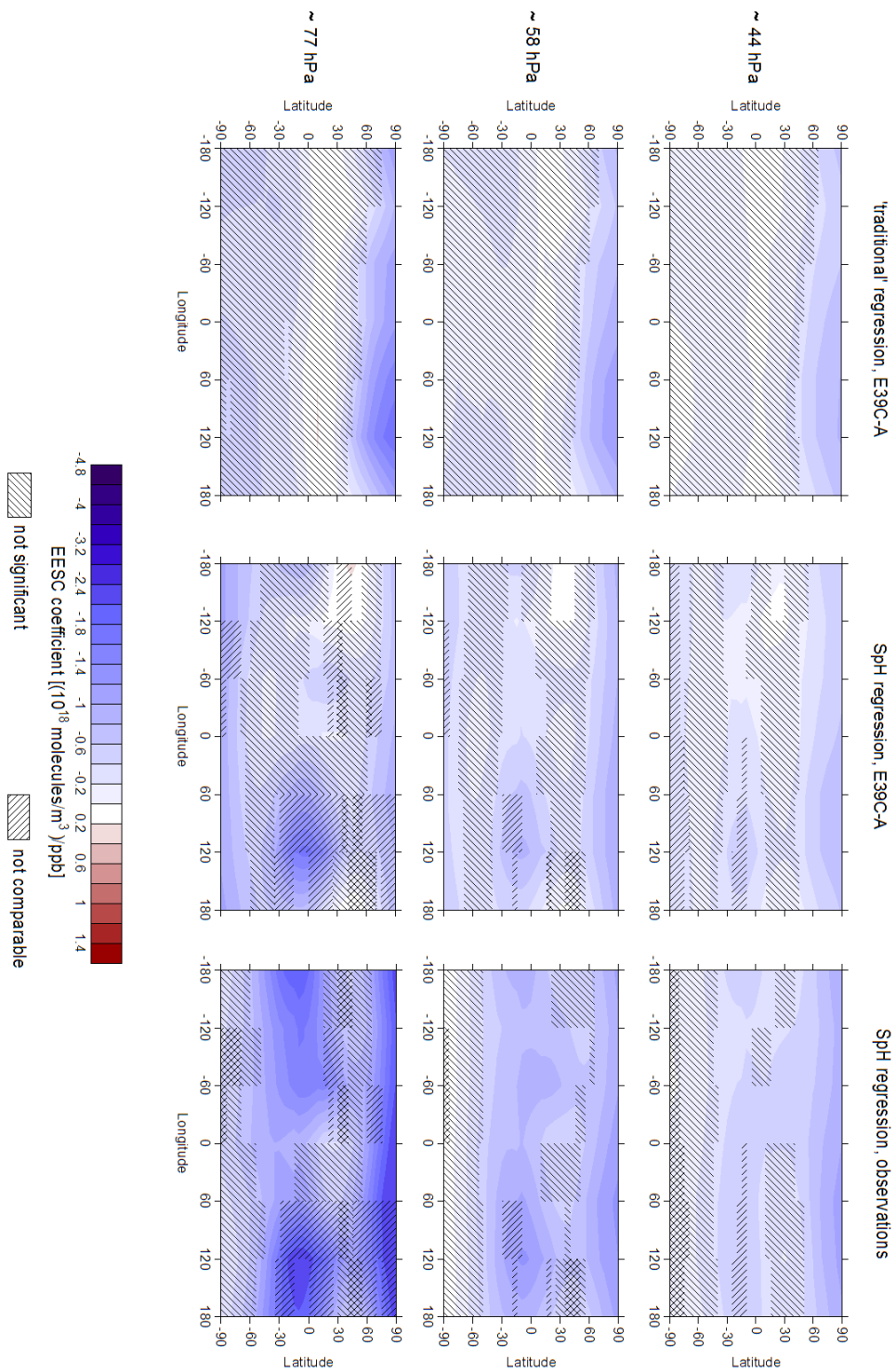


Figure 6.2: Global pattern of halogen-induced ozone changes in March for three selected pressure levels. Results are shown for the traditional regression approach based on model data (left column), for the spherical harmonics regression based on model data with data gaps (middle column) and for the spherical harmonics regression based on observations (right column). Non-significant coefficients are hatched from lower left to upper right, non-comparable coefficients are hatched from lower right to upper left.

ficients for the traditional regression with similar uncertainties compared to the SpH-Model regression or larger uncertainties on the coefficients. While the first reason surely contributes to the amount of non-significant values, the latter might also play a role. Since the calculation of the uncertainties is dependent on the number of available data in the regression (see Section 3.3.3), one of the disadvantages of the traditional regression approach compared to the regression with spherical harmonics implemented becomes apparent: the maximum number of available data for the traditional approach is, for the study here, the number of monthly means from 1979 to 2006 per latitude/longitude bin. Those monthly means are the basis for the Fourier expanded basis function fits and therefore for the determination of the basis function coefficients. With the spherical harmonic expansion, all latitude/longitude bins are fitted simultaneously which increases the number of available data by a factor of 36×6 (number of latitude bands \times number of longitude bins). Naturally, the number of fitting coefficients also increases. However, if the number of coefficients increases with a smaller factor than the data, so, overall more data per coefficient are available for the fit which decreases the uncertainty on the coefficients. In the middle and the right column of Figure 6.2, which show results of spherical harmonics based regressions, the significance increases with decreasing pressure because more data are available at higher altitudes and, therefore, the regression produces a better fit.

The results from the SpH-Obs regression are very similar to the results from the SpH-Model regression: the wave-like structure in the polar regions exists with very similar characteristics and also the signal in the tropics, caused by the spherical harmonics regression approach, is detectable. Overall the magnitude of the EESC coefficients is bigger for the SpH-Obs regression which leads to a larger number of significant results. The similarity of the SpH-Model results and the SpH-Obs results indicates that the results for the observations are realistic, at least in the northern polar regions and that E39C-A slightly underestimates the effect of EESC on ozone in March.

In Figure 6.3, latitudinally and vertically resolved results are shown for two selected longitude bins, $0^\circ\text{W}-60^\circ\text{W}$ and $120^\circ\text{E}-180^\circ\text{E}$, which are shifted by 180° . Note that comparability estimates are only available up to ~ 10 hPa since the E39C-A data on which they are based only exist up to that level. Therefore, levels of pressure smaller than ~ 10 hPa are marked with a gray box in the results based on model data. Another gray box masks out the regions in the tropics where no EESC basis function was used in the regression analysis.

The traditional regression results (left column) show a cell-like region of negative

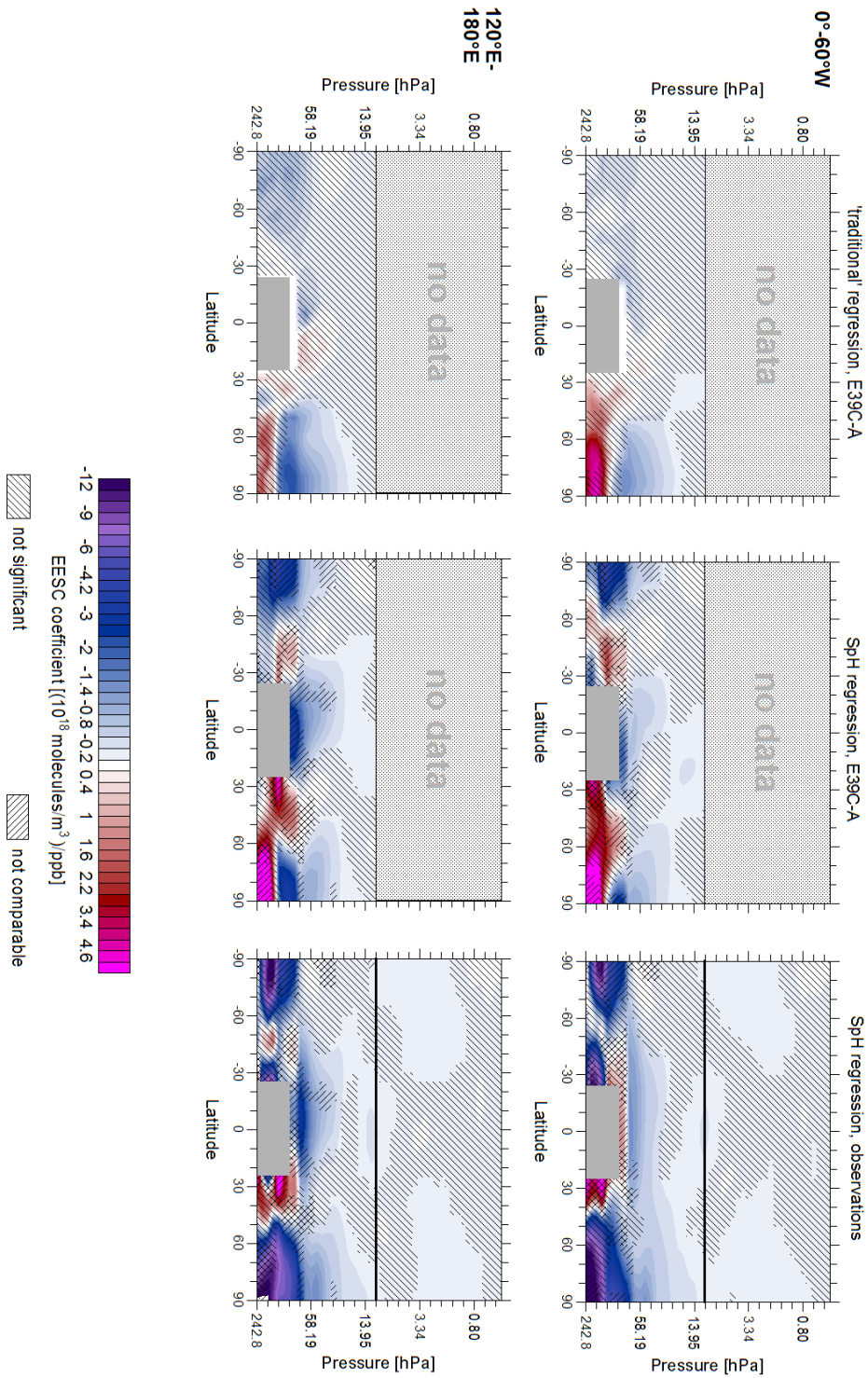


Figure 6.3: Vertically and latitudinally resolved halogen-induced ozone changes in March for two selected longitude bins. Results are shown for the three already mentioned regression analyses. Model data are only available up to ~ 10 hPa. No comparability estimates are therefore available above that pressure level (thick black line in right column). In the tropics (25°S to 25°S) an EESC basis function was not used in the regression below ~ 77 hPa (gray box).

EESC coefficients in the Arctic lower stratosphere, extending up to 50°N, with most negative coefficients between ~ 100 hPa and ~ 40 hPa. An ozone response to EESC in this latitude and altitude region in March is expected based on earlier analyses of satellite data (e.g. *Randel et al.*, 2007). However, in the lowermost stratosphere the traditional regression results show a region of positive coefficients extending far into the mid-latitudes. This signal is not expected and might be explainable by the fact that EESC as a basis function cannot realistically describe the halogen-induced changes close to the tropopause, or there might be a mechanism in the model influencing the ozone distribution in the lowermost stratosphere which causes this pattern. However, the coefficients in these low altitude regions are mostly statistically insignificant as are the results from the Southern Hemisphere and the tropics. Differences between the results of the two longitude bins are very small and are confined mainly to the magnitude of the EESC coefficients in the northern polar regions, not their distribution.

The results from the SpH-Model regression (middle column) are similar for the Northern Hemisphere middle to high latitudes, however the magnitude of the signals is slightly more pronounced: the coefficients building the cell-like structure between ~ 100 hPa and ~ 40 hPa are more negative than for the traditional regression and the positive signal of the lowermost stratosphere is also slightly stronger. But the tropospheric signal is either not significant or not comparable. Results for the Southern Hemisphere lower stratosphere and the tropics are distinctly different from the traditional regression results in these regions: a strong negative signal in the southern polar regions changes to a positive signal in the southern mid-latitudes and back to a negative signal in the tropics. Most of those results are non-comparable or non-significant, a sign that these steep meridional gradients are caused by inadequate spherical harmonics fitting, due to too many data gaps and to not enough spherical harmonic expansions, and resultant over- and undershooting. Differences between the patterns in the results from the SpH-Model regression for the two longitude bins are very small. They indicate that the regression using spherical harmonics is able to at least qualitatively capture the main features of halogen-induced ozone changes in the northern polar regions in March. Problems with insufficient spherical harmonic fittings exist, but are confined to the lower atmospheric levels.

EESC-induced changes of ozone in the observations (SpH-Obs) in the northern polar regions extend in both longitude bins far into the mid-latitudes and up to about 10 hPa. The most negative coefficients occur between ~ 240 hPa and ~ 140 hPa, close to the tropopause. With decreasing pressure the EESC coef-

ficients also decrease. This pattern is different to the pattern obtained by the SpH-Model regression. However, the results from the lowermost stratosphere in the northern high latitudes are particularly influenced by insufficient spherical harmonic fittings and are therefore marked as non-comparable. The magnitude of the EESC coefficients between ~ 80 hPa and ~ 60 hPa, where they are comparable and significant, is bigger for the results from SpH-Obs than from SpH-Model. That indicates a slight underestimation of the influence of EESC on middle stratospheric ozone by the model as mentioned above already in the discussion to Figure 6.2. The results from the lowermost stratosphere of the Southern Hemisphere and the tropics are very similar to the results from the SpH-Model regression: alternating regions of positive and negative coefficients, most of them marked as non-comparable or non-significant.

Vertically resolved zonal asymmetries in halogen-induced ozone changes in the Arctic region in spring exist. The displacement of the Arctic polar vortex and the resulting signature in EESC induced ozone changes (expressed here by EESC coefficients) is clearly detectable for different pressure levels. Results in the northern high-latitudes are significant and comparable indicating a good performance of the SpH regression in this region. However, especially in the lowermost stratosphere, unresolved problems of the SpH regression approach become apparent: with the current expansion settings steep meridional gradients cannot be resolved without compensation (over-/undershooting), therefore high spatial variability cannot be reproduced and missing data strongly influence the fit of the basis functions. At this point the question arises as to whether there is a maximum amount of missing data which can be coped with by the spherical harmonics in a regression without resulting in artifacts in the fitting coefficients. If the missing data would be evenly distributed in space and time such a limit might exist. However, since missing data in the observations are unevenly distributed it is impossible at this stage of the spherical harmonics regression development to determine this limit.

6.3 Halogen-induced changes in the southern polar regions in spring

Although the Antarctic polar vortex is much more stable than the Arctic polar vortex (see Section 1.3.2) a preferred vortex displacement location was identified towards the longitude region 0°W to 60°W by *Grytsai et al.* (2007). In this sector

low ozone is frequent in spring whereas between 90°E and 180°E ozone tends to be high. The displacement is caused by planetary waves and the resulting zonal asymmetries in ozone by depletion within the displaced vortex. Therefore, similar to the Northern Hemisphere, the main longitudinal effect of EESC on ozone is expected to show in spring, around October and November.

The same pressure levels as for Figure 6.2 are shown in Figure 6.4, only with the results for Southern Hemisphere spring (October). The results from the model data obtained by the traditional regression show negative EESC coefficients in a well-defined region from 60°S to 90°S with a steep gradient towards the pole. The distribution is zonally symmetric only for the results of the highest pressure level, ~ 44 hPa, a weak wave-like pattern is visible. A small positive, zonally asymmetric effect exists at the lowest pressure level, ~ 77 hPa, in the tropics. However, this pattern is not significant and for the higher pressure levels it vanishes completely.

In the results from the SpH-Model regression the zonally symmetric response in the southern high latitudes is almost identical to the results from the traditional regression approach. However, differences exist for the lowest pressure level: the negative coefficients extend to the southern mid-latitudes and further to the tropics where a wave-like structure exists. The higher pressure levels show a more comparable distribution of coefficients, but the zonally asymmetric effect in the tropics remains. Most of this tropical pattern is marked as non-comparable though indicating that it is caused by the combination of the spherical harmonic approach and the incompleteness of the analyzed data set. The characteristic pattern in the southern high latitudes, however, is captured well by the SpH-Model regression.

Results from the SpH-Obs regression (right column) differ with increasing altitude more and more from the results from the SpH-Model regression. While the almost zonally symmetric signal of the southern high latitudes is clearly visible at ~ 77 hPa, it becomes more and more asymmetric for the higher pressure levels. The most negative coefficients at those levels are located between 60°W and the 0° meridian. The tropical wave-like pattern detectable in the results from SpH-Model exist also in the results from SpH-Obs, however, there is a connection between the wave-pattern in the high latitudes and the pattern in the tropics in the SpH-Obs results which is missing in the SpH-Model results. While results for the mid-latitudes and tropics are mostly not comparable at ~ 77 hPa (as discussed for the SpH-Model results already), comparability in those regions increases with decreasing pressure. Overall, only the SpH-Obs results show a distinct wave-pattern in the southern polar regions and mid-latitudes around

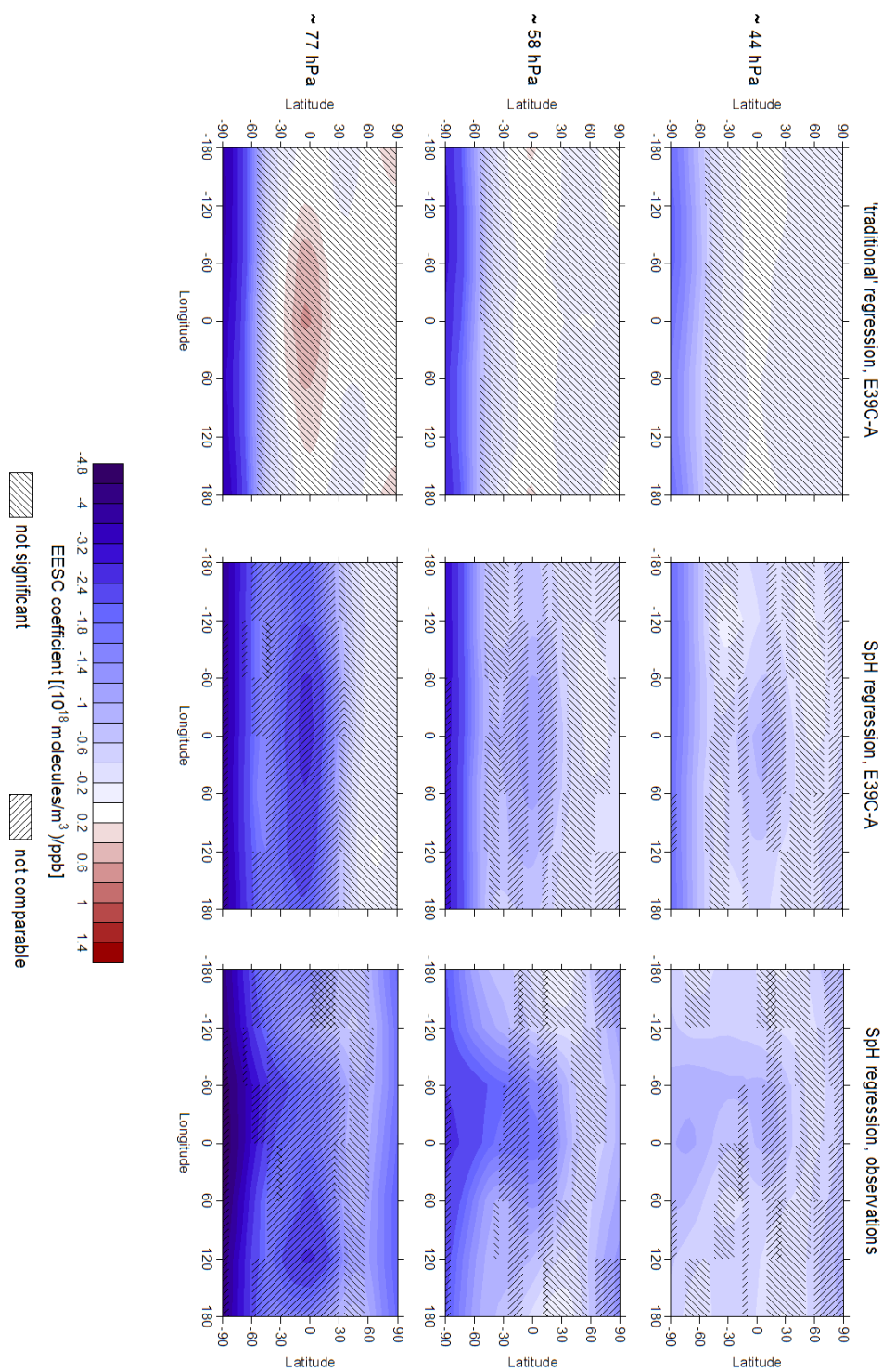


Figure 6.4: Same as Figure 6.2, only for October.

~ 58 hPa and ~ 44 hPa. The region of the bulge in the coefficients coincides there with the preferred vortex displacement location as suggested by *Grytsai et al.* (2007). This might be an indication for a more stable vortex in the model which results in October in a clear underestimation of meridional mixing of air. Results from all three regression models (traditional, SpH-Model and SpH-Obs) suggest a stronger influence of EESC on ozone in the southern hemisphere spring in the Antarctic than in the northern hemisphere spring in the Arctic (see Figure 6.2). This result is in good agreement with total column ozone analyses from *Fioletov et al.* (2002) and *Steinbrecht et al.* (2003) and strengthens again the confidence in the capability of the regression method with spherical harmonics implemented.

Figure 6.5 shows latitudinally and vertically resolved effects of halogens on ozone in October for two different longitude bins, 0°W - 60°W and 120°E - 180°E . Most negative coefficients are present in the traditional regression results in the southern polar regions. They extend to $\sim 60^\circ\text{S}$ in both longitude bins and reach in the vertical from the lowest level shown (~ 240 hPa) up to about 60 to 50 hPa. The vertical extension is slightly shifted downward to the expected main influence of EESC on ozone at about ~ 50 hPa. Results for other latitude regions than the southern high latitudes are mainly not significant for the whole pressure range shown.

Results for the SpH-Model regression (middle column) show a very similar pattern in the southern high latitudes: a region of most negative EESC coefficients from the pole to about $\sim 60^\circ\text{S}$ and from ~ 240 hPa up to about 60 to 50 hPa. The magnitude of the SpH-Model coefficients is slightly larger in the very high latitudes between ~ 100 hPa and ~ 60 hPa than the magnitude of the coefficients from the traditional regression approach. In those regions the SpH-Model coefficients are marked as non-comparable. Similar to the results shown in Figure 6.3, additional regions with negative EESC coefficients occur in the results for the SpH-Model regression in the northern high latitudes and the tropics and regions with positive EESC coefficients in the mid-latitudes of both hemispheres. Small differences between the strength of those signals exist for the two longitude bins. However, the coefficients of those signals, up to about ~ 50 hPa and in some regions even higher, are not significant or not comparable indicating again that the spherical harmonics regression approach cannot resolve the high ozone variability in this region in combination with the amount of missing data. However, the most important feature, the region of strong ozone depletion in the southern polar vortex is captured well.

In the right column of Figure 6.5 the results for the SpH-Obs regression are

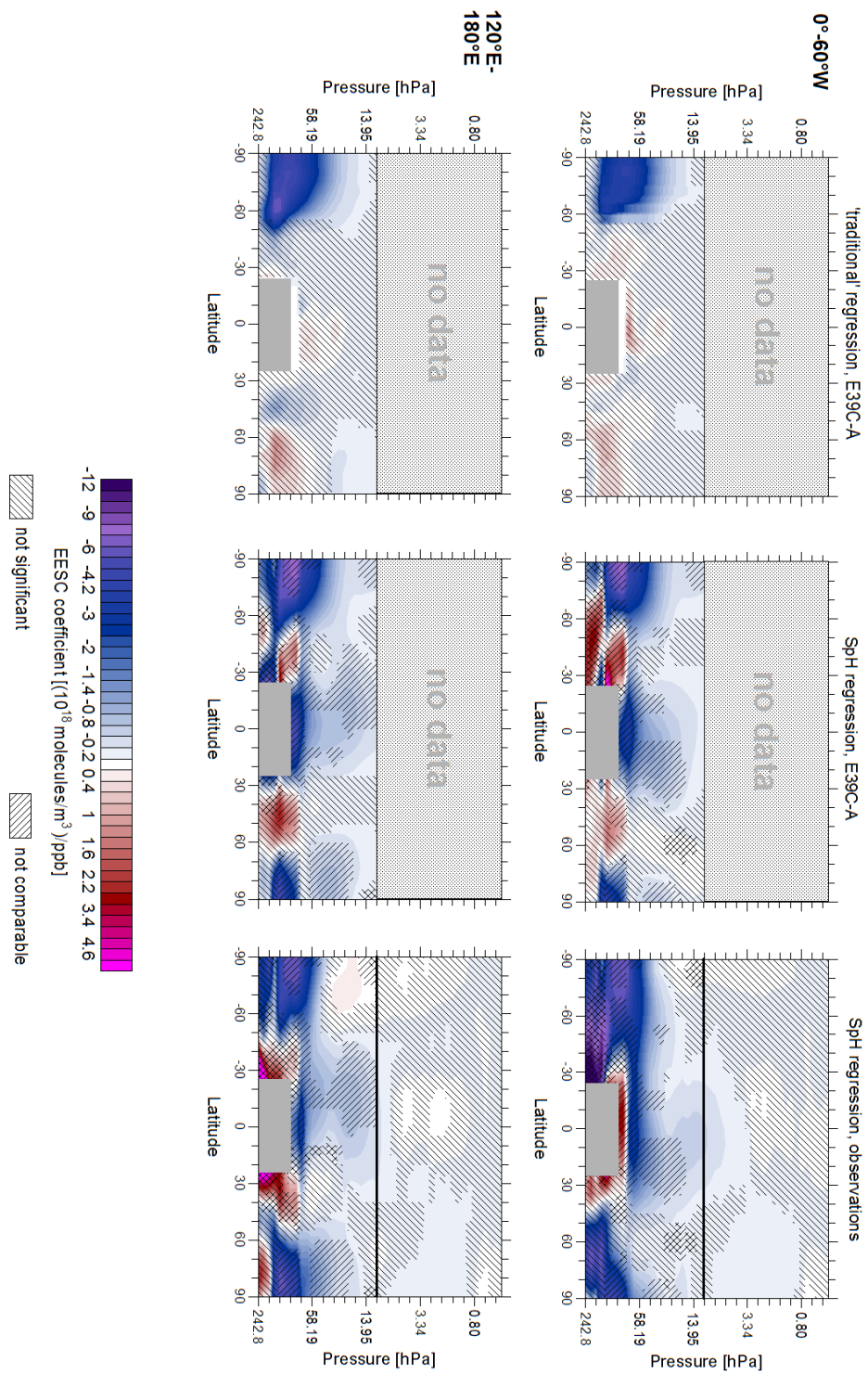


Figure 6.5: Same as Figure 6.3, only for October.

shown. The pattern of negative coefficients in the southern high latitudes exists also in these results, however, the negative coefficients for longitudes between 0°W and 60°W reach further into the mid-latitudes (up to $\sim 30^{\circ}\text{S}$). The results for the lower pressure levels indicate a high meridional variability in the EESC coefficients, similar to the results from the SpH-Model regression. Most of this pattern is marked either as insignificant or not comparable. However, around 60 hPa the results in the Southern Hemisphere are mostly statistically significant and comparable. In this pressure region an extension of the negative coefficients from the polar regions to the mid-latitudes is still detectable in the longitude bin 0°W and 60°W . That differs clearly from the SpH-Model results. The existence of this signal in the SpH-Obs results for the mentioned longitude bin and the lack of it in the 120°E and 180°E longitude bin causes the wave-like structure seen in the SpH-Obs results in Figure 6.4.

Figure 6.6 shows vertically and longitudinally resolved EESC coefficients for two latitude bands, 65°S to 60°S and 50°S to 45°S in October. The coefficients of the traditional regression are more negative for the region between 65°S and 60°S than in the region further north and the vertical extension covers many more pressure levels. There are only small differences between the longitudes in both latitude bands, indicating a very zonally symmetric response. While the negative coefficients between 65°S and 60°S are completely significant, almost all results for the latitude band 50°S to 45°S are not significant.

Results for the SpH-Model regression for the latitude band 65°S to 60°S are very similar in magnitude and vertical extension to the results from the traditional regression. Only for the lowest pressure levels do distinct differences occur (positive coefficients in results from SpH-Model) which are marked as non-comparable. The strong response of EESC in the southern high latitudes is therefore captured well with the spherical harmonics regression. For the second shown latitude band, 50°S to 45°S , results from the traditional regression and SpH-Model differ significantly within a larger pressure region: from the lowest shown level up to about 60 hPa strong positive and negative coefficients occur which are mostly non-comparable or non-significant. The spherical harmonic approach is not able to reproduce the very small coefficients which can be seen in the results from the traditional regression. The transition from steep gradients in the high latitudes to flat gradients in the mid-latitudes can obviously not be captured by the spherical harmonic expansion settings chosen in the presence of the existing data gaps.

The results for the SpH-Obs regression (right column) are similar for the more southern latitude band to the results from the SpH-Model regression, however,

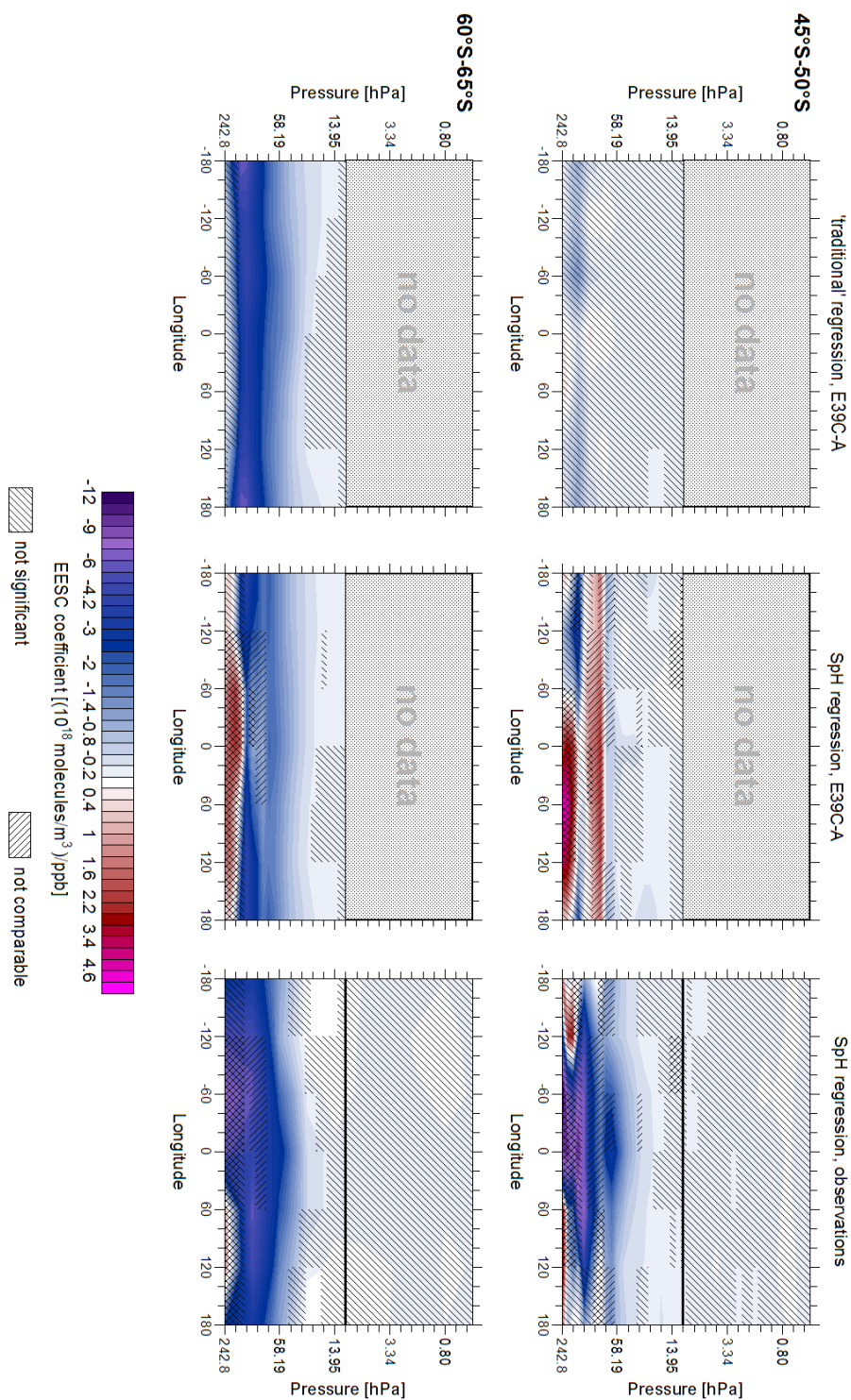


Figure 6.6: Vertically and longitudinally resolved halogen-induced ozone changes in October for two selected latitude regions, 65°S to 60°S and 50°S to 45°S. Model data are only available up to ~10 hPa. No comparability estimates are therefore available above that pressure level (thick black line in right column).

a wave-like structure is observable in pressure regions around 50 hPa which does not exist in SpH-Model results. This wave structure also exists in the latitude band from 50°S to 45°S in the same pressure region. Lower pressure regions of the results of this latitude band show also a wave-like structure, but most of the pattern is masked as not comparable. The longitudinal pattern of the SpH-Obs results in the pressure region around 50 hPa between 50°S to 45°S agrees well with the observed total column ozone zonal asymmetries described by *Grytsai et al.* (2007). The absence of this pattern in the SpH-Model and the traditional regression results might be, as already mentioned, a result of a too stable vortex in the model with less pronounced meridional mixing of air in October.

As it could be said for the northern polar regions in spring, there are also zonally asymmetric halogen-induced changes in ozone for the southern polar latitudes in spring, at least in the observations. While the analysis of observations shows the distinct wave pattern which is expected from similar total column ozone analyses, the model data show strong symmetrical features. The lack of the wave-like structure in the model results can rather be attributed more to model characteristics than shortcomings of the SpH regression approach. However, once more it became apparent that the fits of the SpH regression are poor below ~60 hPa where data coverage is fragmentary.

6.4 Halogen-induced changes in southern mid-latitudes in spring

Malanca et al. (2005) discussed the variability of Southern Hemisphere mid-latitude total column ozone between 1980 and 2000 and described a distinct zonally asymmetric pattern in ozone changes in October between 60°S and 30°S (see Figure 6.7). The reason for this zonal asymmetry was seen by *Malanca et al.* (2005) in the favored displacement of the Antarctic vortex towards Argentina and the South Atlantic which is caused by planetary wave activity. Therefore, additionally to the zonal asymmetries in ozone changes in the southern polar regions in spring (see Section before) the southern mid-latitudes in spring are investigated further here.

In Figure 6.8 (a) the latitudinally and longitudinally resolved EESC coefficients are shown at an approximate pressure of 58 hPa for the three regression analyses performed for October. In the style of *Malanca et al.* (2005) only latitudes between 60°S and 30°S are displayed. The results for the three regression analyses

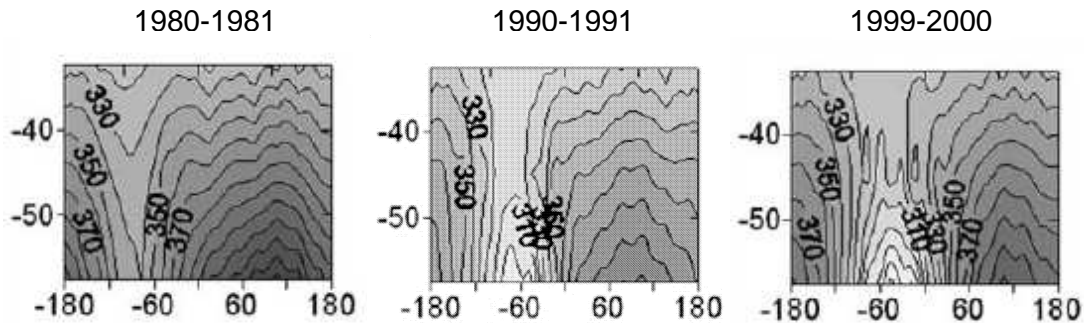


Figure 6.7: Two-year average total column ozone distribution over Southern Hemisphere mid-latitudes (60°S to 30°S) in October for three different time periods. Values are shown in DU (modified from *Malanca et al.*, 2005, Figure 2).

look quite different. There is a weak wave-structure visible in the results from the traditional regression (left column) with the bulge of the wave, with most negative coefficients, at around 60°W . Results are only significant up to about 55°S or 50°S , depending on longitude. The extension to lower latitudes, compared to the findings of *Malanca et al.* (2005) is clearly underestimated with the traditional regression, although it is based on a complete set of E39C-A data. The underestimation, therefore, is definitely caused by insufficiencies of the model data rather than the analysis method.

A wave-like structure can also be detected in the results from the SpH-Model regression (middle column). However, the bulge of the wave composed of significant and comparable negative coefficients is clearly shifted to about 60°E and extends a bit further into the mid-latitudes. These differences compared to the traditional regression results are due to the data gaps for the SpH-Model data set and the application of the spherical harmonics in a regression model. However, the SpH-Model regression captures the wavy pattern shown in the traditional regression results, although it is slightly shifted.

The results from SpH-Obs (right column) show the most distinct wave pattern of all three analyses. The most negative coefficients are located between 60°W and 0° , shifted to the pattern seen in the SpH-Model results and its amplitude is much bigger than in the SpH-Model results. The wave pattern is visible in the entire displayed latitude region with the coefficients getting smaller with decreasing latitude. The comparison between the results from *Malanca et al.* (2005) (Figure 6.7) and the SpH-Obs results presented here reveals a striking similarity: exactly where the trough in the total column ozone data is located

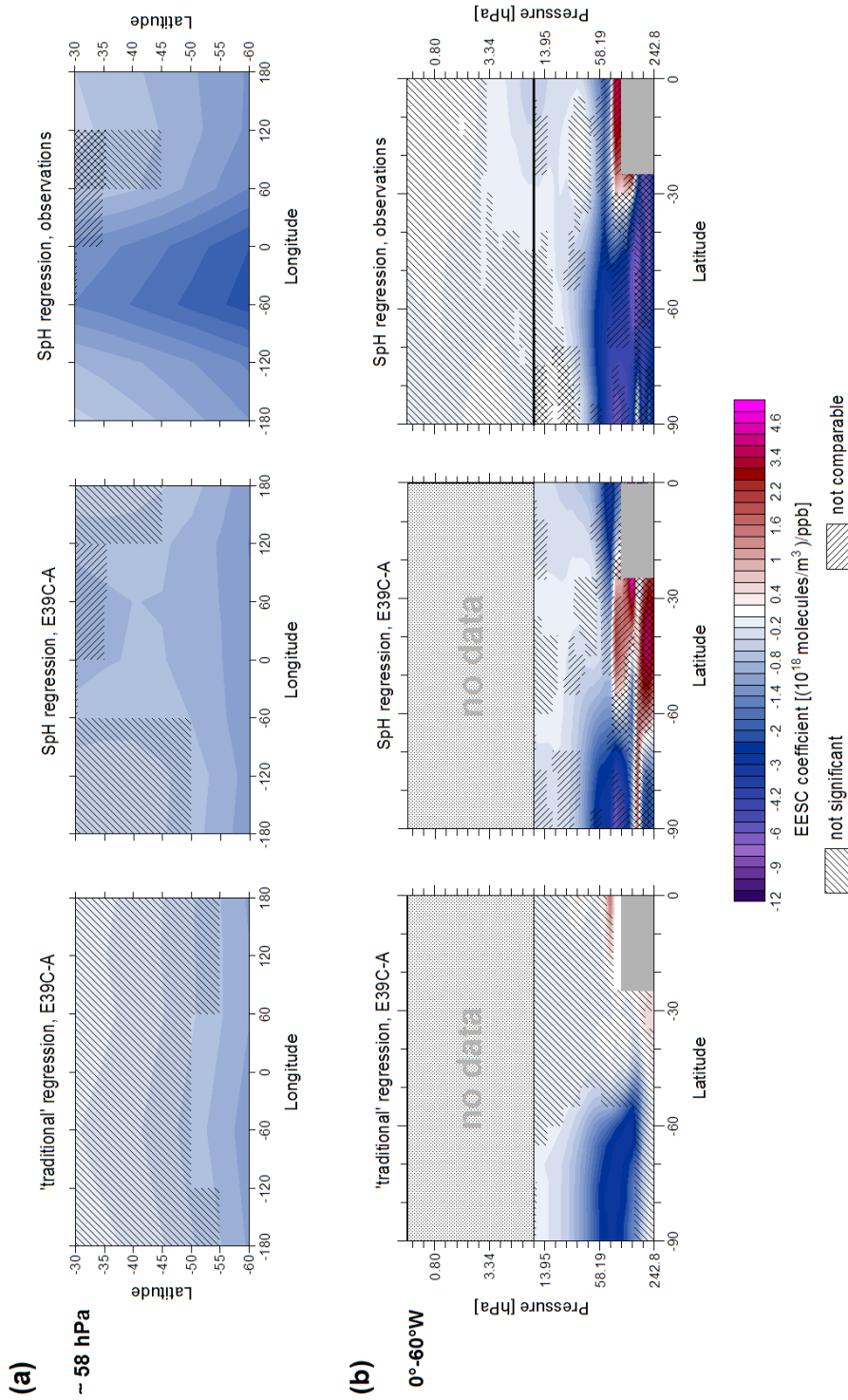


Figure 6.8: Halogen-induced ozone changes in Southern Hemisphere mid-latitudes in October. (a) Latitudinally and longitudinally resolved pattern between 60°S and 30°S at about 58 hPa, (b) vertically and latitudinally resolved pattern between 60°W and the 0° meridian. Non-significant and non-comparable coefficients are hatched. Gray boxes denote regions where no model data are available and where EESC was not included in the regression.

the most negative EESC coefficients at around 58 hPa can be found. But this striking similarity is confined to the SpH-Obs results. The zonal component is clearly overestimated in both the traditional regression and the SpH-Model regression analyses, which reduces the amplitude of the wave in the results. This is most likely caused by an overly strong zonally directed transport, for example a too stable polar vortex (*Stenke et al.*, 2008a), which reduces meridional air mass exchange. This mechanism was proposed in the previous section already and indicates a close coupling between the zonal asymmetric patterns in the southern high and mid-latitudes in spring.

Figure 6.8 (b) resolves the EESC coefficients vertically and latitudinally for the longitude region 60°W and 0° . This display is similar to the first row of graphs in Figure 6.5, but here, in Figure 6.8 (b), only the Southern Hemisphere is plotted to allow a more detailed display of the region of interest. Results from both analyses based on model data, from the traditional regression and from the SpH-Model regression, show negative coefficients in the high latitudes up to 50° and ~ 30 hPa. While the coefficients of the traditional regression are very small and not significant for the rest of the Southern Hemisphere, the lower pressure levels of the SpH-Model regression results show a region of strong positive coefficients in the mid-latitudes and another region of strong negative coefficients in the tropics. Results from both regions are mostly not comparable however. As mentioned in Section 6.3 this pattern in the SpH-Model results indicates that the spherical harmonics regression approach cannot resolve the high ozone variability in this region in combination with the amount of missing data. However, since the extension of the negative coefficients into the mid-latitudes is similar to the traditional regression results, it is not caused by the spherical harmonics regression approach but directly by the model data. The fact that the spherical harmonics regression approach actually simulates the extension into the mid-latitudes similar to the traditional regression, at least for pressure regions above ~ 60 hPa, verifies once more that the spherical harmonics regression approach can indeed capture spatial patterns in the regression fitting coefficients.

The results from the SpH-Obs regression (right column) show a much further extension of the negative EESC coefficients into the mid-latitudes compared to the SpH-Model results. Most of the results at lower pressure levels are non-comparable or non-significant, but above ~ 60 hPa they are. Those significant and comparable results of the pressure region from ~ 60 hPa to ~ 40 hPa build the distinct pattern in Figure 6.8 (right column).

The extension of the analysis of the Antarctic region in spring to the mid-latitudes

reveals a very pronounced zonally asymmetric pattern in EESC coefficients at ~ 58 hPa which is strikingly similar to changes in total column ozone described by *Malanca et al.* (2005). Therefore, it is reproduced realistically by the new regression approach despite the fitting problems of the lower altitude regions. The effects of the vortex displacement towards Argentina and the South Atlantic, with increased ozone depletion in this region, can clearly be seen in the observations but is obviously underestimated in the model results. This reinforces the already expressed surmise that the polar vortex is too stable and placed too centrally in the model.

6.5 Halogen-induced changes in northern mid-latitudes in winter

Since the early studies of *Hood and Zaff* (1995) zonal asymmetries in northern hemispheric ozone changes in winter and spring have been the main focus of longitudinally resolved ozone change studies. This is due to the distinctly observable pattern, the good data coverage, and the expected strong wave activity and clear vortex displacement which cause the zonal asymmetries. While the vortex displacement is most important for explaining the spring ozone changes, in winter rather wave activity is responsible for longitudinal differences. In addition to the analysis of northern high-latitude ozone changes in spring (see Section 6.2) an analysis of northern high-latitude ozone changes in winter might be promising for the detection of zonal asymmetries.

Figure 6.9 and Figure 6.10 show the Northern Hemisphere patterns of EESC coefficients in January for six different pressure levels, reaching from ~ 44 hPa to ~ 10 hPa. Note that only results for the Northern Hemisphere are displayed. Results for the traditional regression approach (left column) show a distinct wave-like pattern for all six pressure levels which changes its extension from being confined to the high latitudes at around 44 hPa to a full hemispheric presence near ~ 10 hPa. The most negative coefficients can always be found in the very high latitudes, changing location from 0° to 120°E to about 120°W to 0° . However, the overall size of the coefficients decreases with decreasing pressure. Coefficients in the tropics and adjacent parts of the mid-latitudes are mostly not significant.

Results from the SpH-Model regression also display a wave-like structure for all six pressure levels, but these are not confined to a certain latitude region. The amplitude of the structure decreases with decreasing pressure. The region of

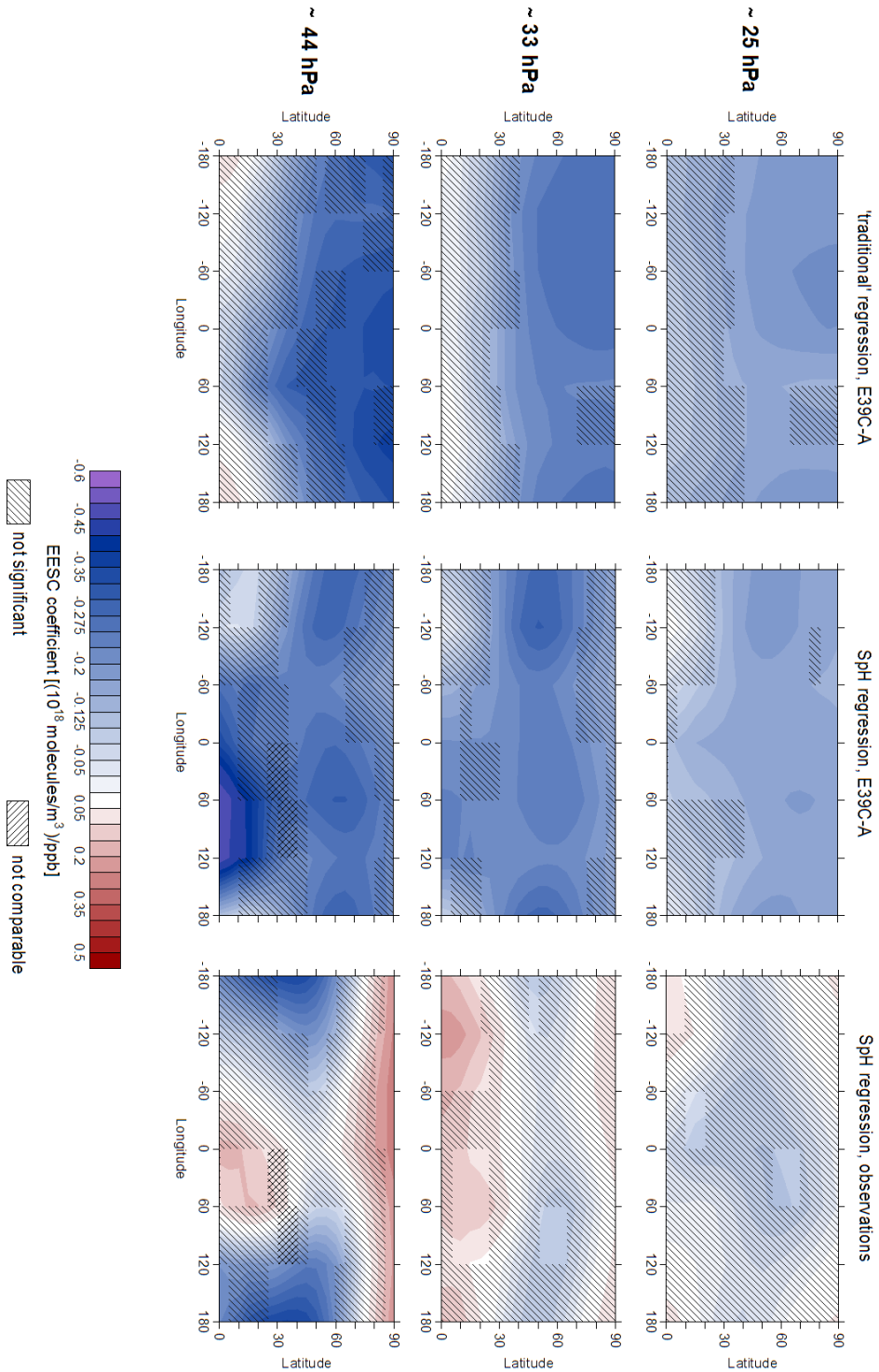


Figure 6.9: Global pattern of halogen-induced ozone changes in January for three selected pressure levels, ~ 44 hPa, ~ 33 hPa and ~ 25 hPa. Results are shown for the traditional regression approach based on model data (left column), for the SpH regression based on model data with data gaps (middle column) and for the SpH regression based on observations (right column). Non-significant and non-comparable coefficients are hatched.

6.5. HALOGEN-INDUCED CHANGES IN NORTHERN MID-LATITUDES
IN WINTER

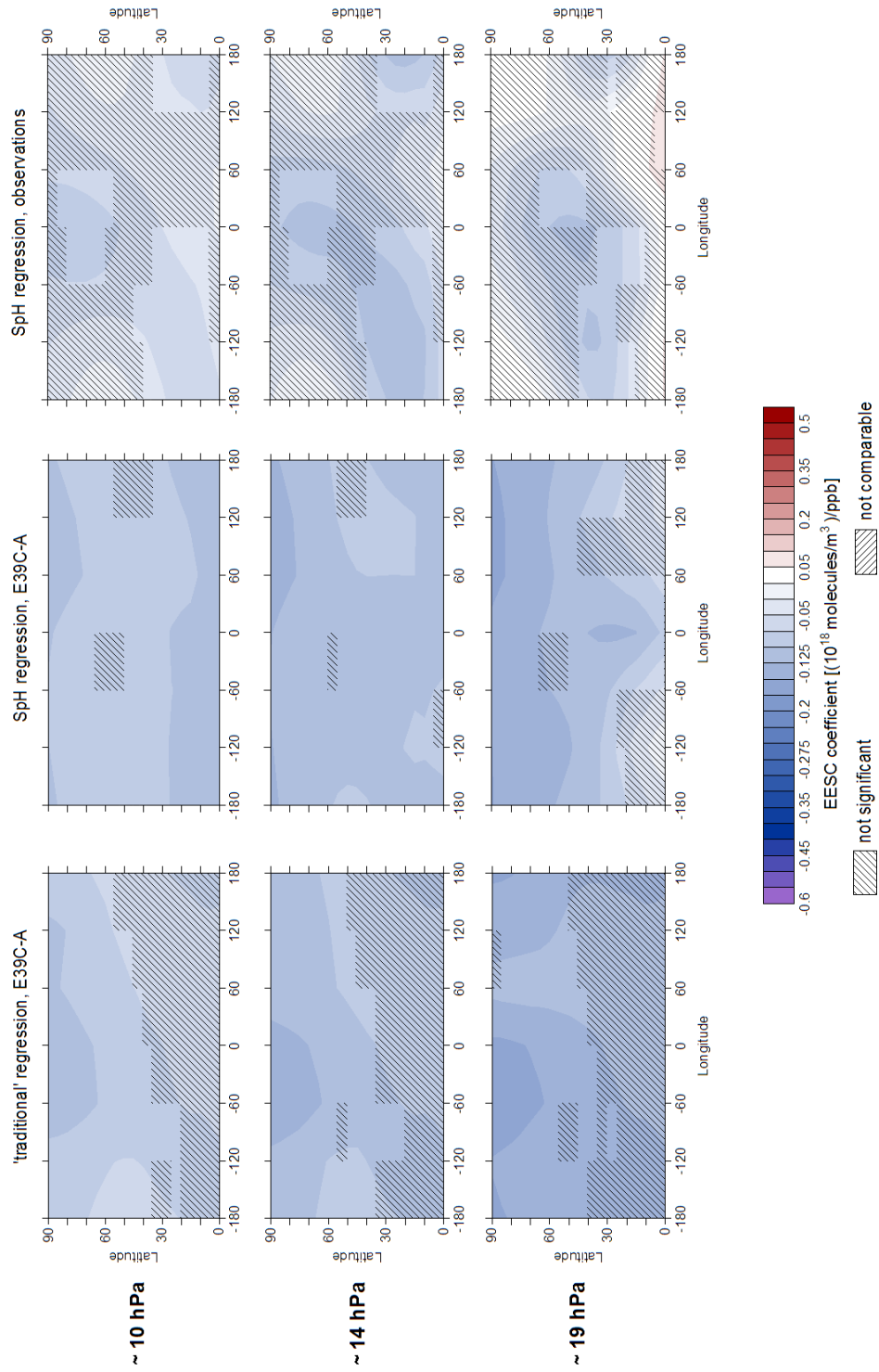


Figure 6.10: Same as Figure 6.9, only for the pressure levels ~19 hPa, ~14 hPa and ~10 hPa.

most negative coefficients also shifts to higher latitudes with decreasing pressure. While it is located around 60°N between ~ 44 hPa and ~ 25 hPa it is close to the pole for the three higher levels. Areas of significant values shift with the negative coefficients and increase noticeably with increasing altitude. Overall, the size of the coefficients from the SpH-Model regression and the traditional regression agree very well, only for the lowest level shown are the coefficients derived from the traditional regression approach clearly more negative in the polar regions. The spherical harmonic approach captures the wave patterns in EESC coefficients well and may only overestimate the waves' amplitude slightly.

Results from the SpH-Obs regression are distinctly different from the results from the SpH-Model regression for the lower three levels (Figure 6.9). Although there are wave-like patterns at all three pressure levels of the results from the SpH-Obs regression, the locations of the structures are not consistent and their phases shift by about 180° throughout the pressure region from ~ 44 hPa to ~ 25 hPa. Even regions with positive coefficients occur close to the tropics and the northern high latitudes. Overall, the coefficients are smaller than for the SpH-Model regression results which is mirrored in the smaller number of coefficients which are significant. Results for the three higher levels, ~ 19 hPa to ~ 10 hPa (Figure 6.10), are in better agreement with results from the SpH-Model regression. The magnitudes of the SpH-Obs coefficients are only slightly smaller than those from the SpH-Model regression. The area of most negative coefficients in the SpH-Obs results extends from the mid-latitudes at roughly 180°E east- and northward to the polar regions where most negative coefficients are then located around the 0° meridian. However, only a fraction of the coefficients contributing to this pattern is significant. The differences between SpH-Obs and SpH-Model results for the lower pressure levels are caused by differences in observations and model data since results from the traditional regression and the SpH-Model regression (both based on model data) resemble each other more than results from the SpH-Obs and the SpH-Model regression which both use the spherical harmonic approach. The differences in observations and model data might be caused by atmospheric mechanisms varying in strength between the two data sets: this could be, for example, the strength of wave activity which would cause different changes in ozone or the stability and strength of the polar vortex margins. Whatever the causes are, they are less important or not present for the three higher pressure levels where SpH-Obs results and SpH-Model results become more alike.

Figure 6.11 shows the vertically and longitudinally resolved EESC coefficients in January for three mid- to high latitude regions, 50°N to 55°N , 60°N to 65°N

6.5. HALOGEN-INDUCED CHANGES IN NORTHERN MID-LATITUDES IN WINTER

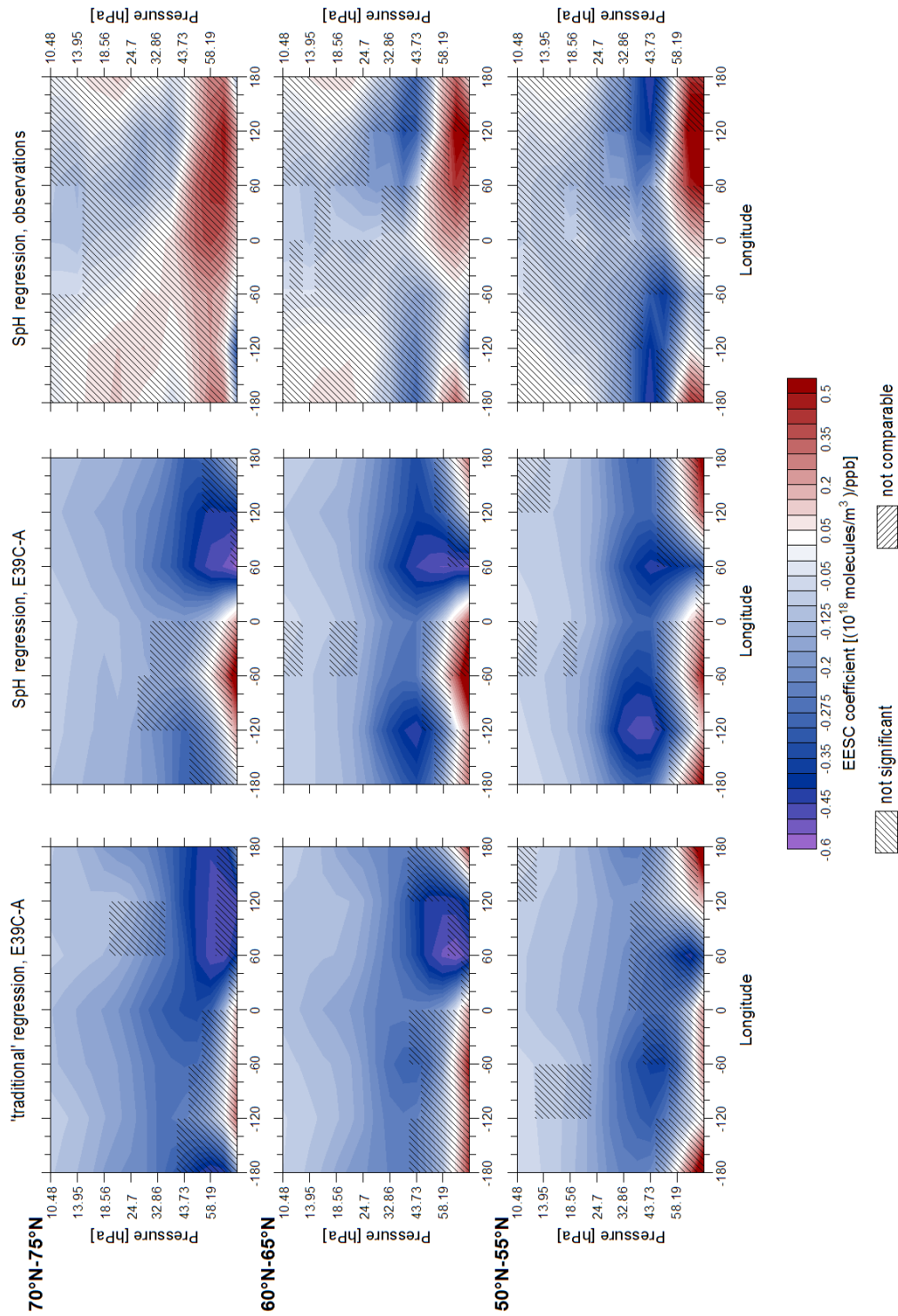


Figure 6.11: Vertically and longitudinally resolved halogen-induced ozone changes in the northern high latitudes in January, shown for three latitude regions: 50°N to 55°N, 60°N to 65°N and 70°N to 75°N. Non-significant and non-comparable coefficients are hatched.

and 70°N to 75°N. In the vertical, EESC coefficients are shown from ~ 77 hPa to ~ 10 hPa. Results from the traditional regression show a distinct wave pattern in the EESC coefficients for all three latitude bands throughout the whole pressure region shown. There is a region with a minimum of negative coefficients around 60°E and a second region with a minimum of negative coefficients around 60°W. Coefficients for all three latitude bands are mostly significant for pressure levels higher than ~ 40 hPa.

The SpH-Model regression results are very similar to the results of the traditional regression for the magnitude of the coefficients and the presence of a wave structure throughout the whole pressure region presented. The amplitude of the wave is slightly underestimated for the higher pressure levels in the SpH-Model results. Most results from the SpH-Model regression are significant, but a few exceptions exist for the lowest levels, especially in the western part of the hemisphere. Overall, the similarity of the pattern in the EESC coefficients derived with the traditional regression and the SpH-Model regression is very high for all three latitude bands presented. The spherical harmonics in the SpH-Model regression capture the pattern of halogen-induced ozone changes in Northern Hemisphere winter well in spite of missing data.

Results from the SpH-Obs regression show a wave pattern for all three latitude bands presented and all pressure regions displayed. Negative EESC coefficients are mostly located around 33 hPa, between 150°E and 150°W, in 50°N to 55°N. With increasing latitude, these negative coefficients shift westward and to higher altitude regions, therefore being located between 70°N and 75°N at around 30°E at roughly 10 hPa. An additional hemispheric- and pressure-level-spanning feature is visible in the most northern latitude band. Positive EESC coefficients spiral through all longitudes from about 60 hPa to roughly 14 hPa. Most of the negative and positive EESC coefficients are not significant though. Differences between SpH-Obs results (right column) and SpH-Model results (middle column) are most distinct for the lower pressure levels. As already mentioned, the similarity of the traditional regression results and the SpH-Model regression results suggest that the differences between the SpH-Obs results and the SpH-Model results are most likely caused by mechanisms represented differently in the model than in reality. In higher altitude regions, differences become smaller and the size of the coefficients more comparable.

It could be shown that zonal asymmetries in halogen-induced ozone changes exist in northern high latitudes in winter. Model results and observations differ substantially for lower altitude regions but become more comparable with increasing

altitude. The reasons for this cannot be determined unequivocally. Differences in atmospheric mechanisms between the model and in the atmosphere which are more pronounced at lower altitudes were suggested. Besides, comparisons with zonally asymmetric total column ozone changes described in the literature (*Hood and Zaff*, 1995; *Peters and Entzian*, 1999; *Peters et al.*, 2008) raise another question. *Hood and Zaff* (1995) saw a negative trend in total column ozone from 1979 to 1991 in the mid- to high latitudes over Europe, that was even stronger over Russia and the western Pacific. While the latter is also detectable in the observation results of this study, no decrease in ozone over Europe is detectable. In *Peters and Entzian* (1999) a similar total column ozone trend pattern to *Hood and Zaff* (1995) was found, although the analysis was based on the total column ozone years from 1979 to 1992. The analysis of decadal total column ozone changes in *Peters et al.* (2008) also showed negative changes over Europe as well as Russia and the western Pacific. The shorter time period for the total column ozone trend determination in the analyses from *Hood and Zaff* (1995) and *Peters and Entzian* (1999) compared to the time period analyzed in this study could cause the detected differences in halogen-induced ozone changes. However, the total column ozone trend over Europe was also detected by *Peters et al.* (2008) who used data from 1960 to 2000. Therefore the missing trend over Europe in the analysis presented here might have to be attributed to a different source. To obtain a comparable signal over Europe in vertically resolved ozone data fields as seen in the total column ozone analyses, a substantial ozone decrease would have to occur in the region of maximum ozone concentrations, around 70 hPa to 40 hPa. The lack of this ozone decrease in the SpH-Obs results of the study here and the presence of it in the SpH-Model results at the expense of the signal further east might, therefore, be a further sign of a shortcoming in the new regression model. The two regions of ozone decrease described cannot be resolved with the chosen spherical harmonic settings which consequently results in a pattern modification. However, with increasing altitude, the negative EESC coefficients shift westward and therefore the results at ~ 10 hPa show greater similarity with the patterns derived from ERA-40 reanalyses by *Gabriel et al.* (2007). Although the pattern of ozone change linked to a change in wave activity by several studies could not be reproduced in detail, zonally asymmetric ozone changes in northern high latitudes in winter were definitely detected.

6.6 Halogen-induced changes in the tropics in northern summer

In the analysis of the zonal mean data in Section 4.1 a possible connection between the halogen-induced changes in the tropics and those a few months later in the southern high latitudes was described (see Figure 4.2). With increasing altitude the temporal offset between the changes in the two regions decrease and at around 14 hPa both are present in August. To further investigate the findings from Section 4.1, Figure 4.2, results from August at ~ 14 hPa from the longitudinally resolved analyses were examined. The additional results of the E39C-A data could help to better evaluate the findings from the zonal mean ozone analysis, especially the changes noted in the tropics.

Figure 6.12 illustrates the global halogen-induced ozone changes in August for the three pressure levels ~ 19 hPa, ~ 14 hPa and ~ 10 hPa. Note that the coefficients are small for all three regression analyses appropriate to the lower ozone number densities in this atmospheric region. Therefore, the spatial gradients shown in Figure 6.12 are not very steep and the zonal asymmetric patterns weak. The traditional regression results show only a very weak wave-like structure in the tropics and more and more zonally symmetric patterns in the mid-latitudes. Most of these signals are not significant though. An additional region of small negative coefficients is visible in the southern high latitudes, also with a wave-like structure, with the bulge of the most negative coefficients between 150°W and 60°W . For all three pressure levels shown, the coefficients in this region are significant. This pattern in the southern high latitudes might be caused by early ozone depletion at the top of the Antarctic polar vortex.

Results from the SpH-Model regression show a significant wave pattern in the tropics with the bulge of the most negative coefficients located roughly between 60°E and 180°E . While this pattern is symmetric with respect to the equator on the higher pressure levels it is slightly shifted to the Northern Hemisphere at ~ 19 hPa. These tropical results are mostly significant as well as comparable. The wave-pattern which can be seen in the results from the traditional regression in the southern high latitudes does not exist in the results from the SpH-Model regression. The overall pattern of the EESC coefficients derived from the traditional regression is, therefore, not very well captured by the spherical harmonics regression. The fact that the wave-like structure in the tropics is not marked as non-comparable might be caused by the magnitude of the uncertainties on the traditional regression results and therefore does not necessarily indicate a realistic

6.6. HALOGEN-INDUCED CHANGES IN THE TROPICS IN NORTHERN SUMMER

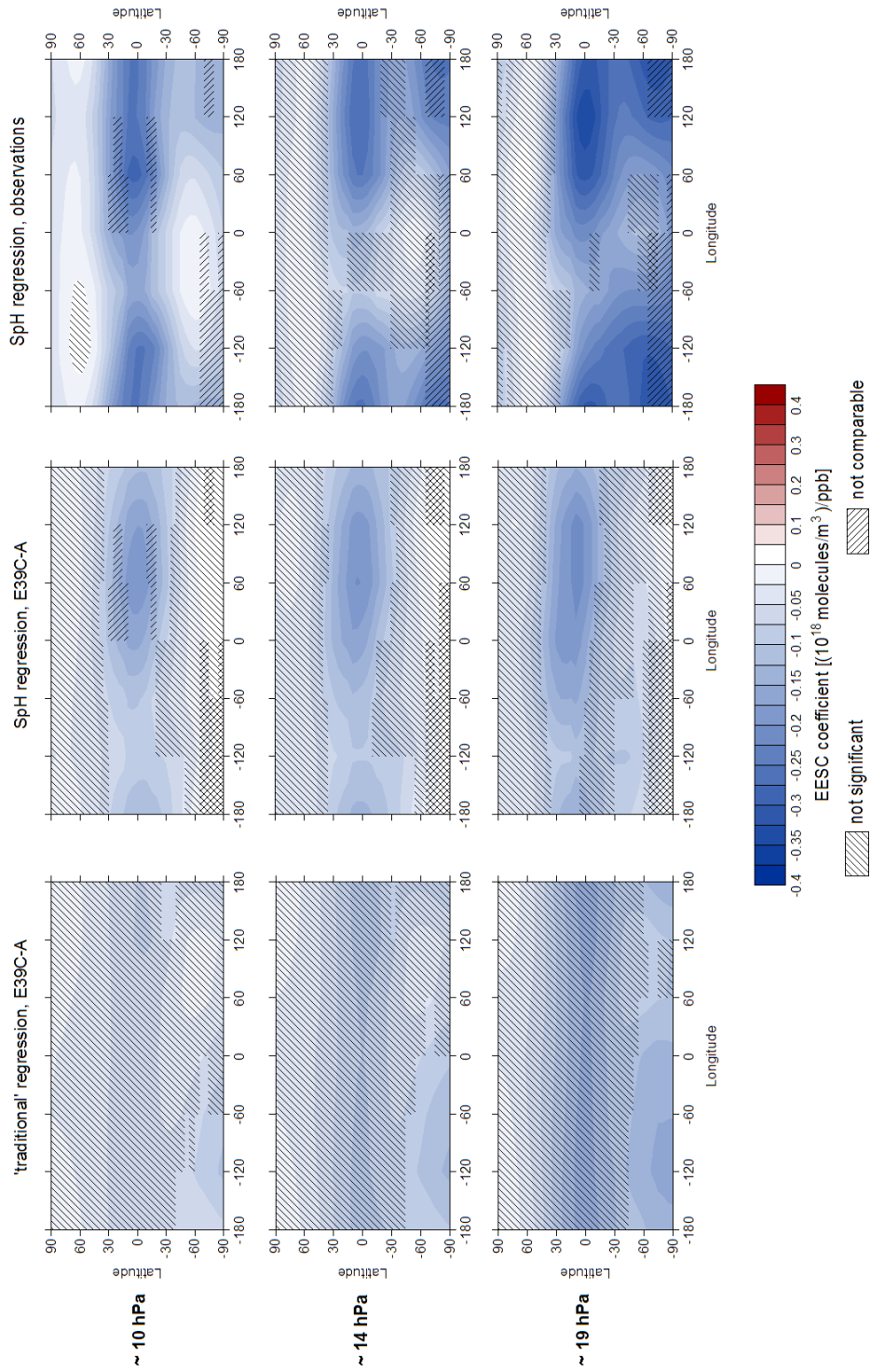


Figure 6.12: Global pattern of halogen-induced ozone changes in August for three selected pressure levels. Results are shown for the traditional regression approach based on model data (left column), for the spherical harmonics regression based on model data with data gaps (middle column) and for the spherical harmonics regression based on observations (right column). Non-significant and non-comparable coefficients are hatched.

pattern. In fact, taking into account that the tropical data coverage is scarce and that similar tropical patterns were shown in results for October (see Section 6.3) which were identified as methodological artifacts, it seems likely that the tropical wave-like structure in the SpH-Model results in August are also artifacts.

SpH-Obs results show distinct wave patterns in the tropics at all three pressure levels with a larger amplitude than shown in the SpH-Model results. The bulge of the wave, with the most negative coefficients, is located roughly between 60°E and 180°E and the pattern is more or less symmetric to the equator. Most of the pattern is comparable and significant for the three pressure levels shown. Unlike the SpH-Model results, the SpH-Obs results show a second region of negative coefficients in the southern high latitudes also with a wave-like structure. The location of the most negative coefficients is slightly shifted to the East compared to the structure in the tropics. The coefficients of the southern high latitude signal are mostly significant but not comparable. Chances of detecting a significant, longitudinally resolved signal in the EESC coefficients in the tropics in August were small since spatial and temporal coverage for the longitudinally resolved data set can be poor, especially in the tropics. Overall, an influence of EESC on ozone in the southern high latitudes could not be confirmed with the SpH-Obs regression and the wave-like structures in the tropics in the SpH-Obs regression results are most likely an artifact of the regression method.

A realistic signal in the pressure region around 14 hPa in the tropics and the southern high latitudes where a signal could be seen in the zonal mean data set could not be derived from the longitudinally resolved data set with the existing data gaps and the chosen spherical harmonic expansions. Coefficients in this pressure region are small since ozone variability is low and the influence of EESC on ozone is weak, and uncertainties on the coefficients are large. Nevertheless, the signal might exist in the data but with the current stage of development of the spherical harmonics regression it cannot be unambiguously extracted.

6.7 Summary

Subsets of latitudinally, longitudinally, vertically and temporally resolved EESC coefficient data fields were analyzed to identify regions of zonal asymmetric ozone changes. The subsets were chosen according to reported longitudinal differences in total column ozone trends, regions and times of most pronounced wave activity and findings from the zonal mean analysis presented earlier in this thesis.

Distinct wave patterns were verified with the spherical harmonics regression approach in EESC coefficients in the northern and southern high latitudes, as well as in southern mid-latitudes, in spring. Wave structures in EESC coefficients are weaker in the northern high-latitudes in winter. In the tropics no wave structures in EESC coefficients could be unambiguously identified. For all described analyses applies that the patterns in the lower altitude regions are most likely influenced by inadequate regression fits. Nevertheless, at higher altitudes zonal asymmetries in vertically resolved, halogen-induced changes can be realistically identified and shown in more detail than ever before.

Chapter 7

Conclusion and Outlook

The aim of this thesis was to verify the occurrence of zonal asymmetries in vertically resolved halogen-induced stratospheric ozone changes on a global scale and link them to atmospheric processes. The first challenge associated with accomplishing this goal was the lack of a suitable data basis with an adequate temporal and spatial coverage. To this end a new data set was developed where many different vertically well-resolved data sources were combined. This data set is described in detail in *Hassler et al. (2008)* and attracted enough attention within the scientific community that it has already been used elsewhere (see for example *McKenzie et al., 2008*, *Stenke et al., 2008a*, *Bodeker et al., 2009*, and *Karpechko et al., 2009*, submitted). However, even with the newly developed data set, coverage in some regions of the globe is insufficient to allow the application of traditional regression analysis methods. To meet this second major challenge a new statistical approach was developed which is largely insensitive to data gaps. A combination of orthogonal trigonometric functions (spherical harmonics) were implemented in a regression model to facilitate an estimation of spatial patterns in regression basis functions by fitting them to the available values. Since the missing data were still numerous enough to influence the quality of the regression fit significantly, sensitivity tests assessing the general performance of spherical harmonics in regression methods as well as the effect of incomplete data sets were indispensable. With the exception of a newly introduced latitudinally and vertically dependent EESC time series, the explanatory variables used in this new regression model are largely well-established. Coefficients for EESC were calculated with the new regression application resulting in a four dimensional, longitude-, latitude- pressure-, and seasonally-dependent coefficient field. Finally, subsets of this field which display zonal asymmetries were discussed, com-

pared to findings of related literature and linked to atmospheric processes which could be possible reasons for those longitudinal differences.

7.1 Conclusion

The development of the new database and the implementation of the spherical harmonics in a regression model is advanced enough to allow longitudinally resolved analyses of ozone changes. However, there are many areas where both the database and regression model could or should be improved.

Highly vertically resolved ozone measurements of optimal quality are necessary for analyses such as these presented in this thesis. Without sufficient temporal and spatial coverage a global examination of halogen-induced changes in ozone profiles is not possible. The new analysis method can better accommodate missing data although the significance and validity of the results can be considerably affected. Ozonesondes are still the main source of high quality ozone measurements in the troposphere and lower stratosphere. The 136 ozonesonde stations are not uniformly distributed around the globe with the result that the coverage is not dense enough for global analyses on a $5^\circ \times 60^\circ$ grid. Irregular sounding schedules, short time periods in which stations are operational, and only few measurements from ocean areas, confound analyses for atmospheric regions where only ozonesonde data are available. Satellite-based measurements are more dense and frequent, however, especially for the early and late years of the period from 1979 to 2006, coverage is only fragmentary due to the lack of suitable data. Only with the continuation of high quality measurements of ozone profiles, by ozonesondes and satellite-based instruments, can robust analyses of vertically and longitudinally resolved ozone changes (see Chapter 6), or estimates of the development of the ozone distribution (see Section 4.2) be achieved.

Since the peak of anthropogenic halogen loading of the stratosphere was reached in the mid- to late 1990s, a singular linear trend as a basis function in a regression model to describe halogen-induced ozone changes is no longer appropriate. Therefore either the global mean time series of EESC (*World Meteorological Organization*, 2007, Chapter 6) or a two-trend approach where the second trend basis function is set to 0 before a defined turnaround date and is proportional to time after the turnaround point is used as the explanatory variable. However, the EESC concentrations in the stratosphere depend on transport and mixing and cannot be described correctly by a singular time series. Rather individual EESC

time series for which the latitude and altitude dependence is considered must be implemented in regression models. Halogen-induced ozone changes over the last 25 years can then be captured well.

Analyses and sensitivity tests performed in this thesis showed that it is possible to implement spherical harmonic expansions of fit coefficients in a regression model and successfully describe spatial patterns of halogen-induced ozone changes, as comparisons with results of a traditional regression approach confirmed. It is important to choose enough spherical harmonic expansions to capture steep gradients and small-scale variability. A big advantage of the spherical harmonics regression is that neighboring latitudes and longitudes are connected by the expansion functions and calculated results ‘know’ about their surroundings, as it is in reality. Therefore, the influence of EESC on ozone in regions with data gaps can be evaluated with the coefficients obtained by fitting the expanded EESC basis function to the available data. Now regression analyses are possible in areas where a traditional approach would be limited.

However, if the areas of missing values are too frequent or too large, the data might not contain enough information to sufficiently constrain the spherical harmonic expansions of the fit coefficients. This results in inadequate fitting and overshooting. The number of missing data is large for some regions and some time periods and it is there that problems associated with the spherical harmonic expansions are expected. But other regions could also be affected. To identify regions where the effects of missing data on the calculation of EESC coefficients are largest, sensitivity tests with a complete data set (in this case from a chemistry-climate model) were necessary. Although model results and observations can differ in the representation of atmospheric dynamics and the distribution of chemical constituents, without these sensitivity tests, an appropriate interpretation of the results would not be possible.

A small number of spherical harmonics was chosen in this study to maximize the statistical significance of the results by keeping artifacts in the results due to insufficient basis function fits to a minimum. While the chosen settings are problematic for the regression within the lowermost stratosphere, above ~ 60 hPa regression results improve. In those regions gradients are not as steep and the small-scale ozone fluctuations decrease, to reveal only the global scale pattern. These can be described more realistically with the chosen settings. A successful application of spherical harmonics in a regression with the chosen expansion settings is limited for this reason to the mid- and upper stratosphere as long as the number of missing data is not reduced in the lower stratosphere.

Longitudinal differences in halogen-induced ozone changes exist not only in total column ozone but also in ozone profiles. This was shown for the first time on a global scale and results are in good agreement with findings for total column ozone and regionally confined ozone profile analyses. Zonal asymmetries normally range over several pressure levels and can show a considerable amplitude in the magnitude of the EESC coefficients, dependent on latitude and season. They occur mainly in times and regions of strong atmospheric wave activity and regions of polar vortex displacements, as suggested by several previous studies. Taking those findings into account it seems not appropriate anymore to employ zonal mean vertical ozone data sets for radiative transfer calculations and climate change estimations.

7.2 Outlook

The work for this thesis includes two main features which are newly developed, the database for the analysis and the regression method with spherical harmonics implemented. Although much progress was made in developing a high quality database and a regression technique that can handle a database with incomplete temporal and spatial coverage, there is still room for further developments and improvements.

A problem for the regression approach remains the number of missing data. Reducing the missing data in some way would reduce the degrees of freedom for the regression fit and would, therefore, increase the significance of the regression results. The addition of satellite data sets, for example such as SAGE III, ILAS I and II, GOMOS, OSIRIS or ACE-FTS*, would substantially increase the available data for monthly mean calculations and would improve the longitudinally resolved coverage. Especially data from instruments which are still operational could fill data gaps for the period from mid-2005 onwards which is so far only represented by ozonesonds. By extending the database beyond 2006 (latest data so far in the database) with both satellite and ozonesonde profiles, it would be possible to enlarge the regression analyses by two and a half years, therefore allowing the regression a more accurate fit. There is also a possibility to further improve the data quality of the monthly mean calculated from the database. As stated in Section 2.3 problems of inhomogeneities between the different data sources have not been dealt with so far. While the method applied here to address this issue

*Abbreviations are explained in Appendix A

(discarding the lowest and highest quartile of the error weighted and sorted individual measurements, see Section 2.3) is sufficient to allow the analyses for this study, the data quality could definitely be improved by correcting the offsets and drifts between the data sources before calculating the monthly means. However, this was beyond the intended scope of this thesis.

As seen in Chapters 4 and 6 the regression with spherical harmonic expansions of the fit coefficients still has some shortcomings. Since this method is new, many modifications and improvements were tested and implemented. However, some alterations could eliminate some problems. In Section 3.3.4.2 it was stated that the autocorrelation in the data could be underestimated for the spherical harmonics regression since so far only the temporal dependence is incorporated in the auto-regressive process. Adding the spatial dependence would allow a more realistic estimate of the uncertainties on the coefficients.

Another area where problems associated with the new regression method were highlighted was the number of data which were not statistically significant or were affected by fitting problems of the regression basis functions. A method to reduce the number of these non-significant and non-comparable results could be to define an optimal set of spherical harmonic expansions for every pressure level individually. So far the settings are optimized for the pressure region of ~ 58 hPa for the EESC basis function (see Chapter 5) and applied uniformly to all other pressure levels and basis functions. However, the results suggest that the spherical harmonic expansions might not have been suitable for pressure levels of the lowermost stratosphere where high spatial ozone variability with steep gradients requires expansions of higher orders to capture the spatial pattern. Using expansions of higher order could enhance the number of comparable values provided that not too many data are missing for the regression fit. However, expansions of higher order mean more coefficients to be determined (with the same number of data) which causes a decrease in the number of significant values since uncertainties on the coefficients grow. Higher in the atmosphere it could be possible to reduce the number of expansions without losing the ability of the spherical harmonics to reproduce spatial response patterns. Gradients in these altitude regions flatten and, therefore, fewer equations are required to describe them. The reduction in expansions would reduce the number of coefficients to be determined and significance of the results would be increased by retaining the level of comparability.

Although the regression method implemented with spherical harmonic expansions of the fit coefficients can deal with a certain amount of missing data, expansion

settings are limited by the data gaps with a resultant reduction of the ability to capture spatial patterns. Since increasing the temporal and spatial coverage of the input database is not easily achieved, an improvement of the spherical harmonics regression, for obtaining estimates of halogen-induced ozone changes, could be achieved by simplifying the spatial pattern to be described. This could be possible by adding an additional spatial pattern to the expansions of the EESC basis function which characterizes the halogen-induced global changes of total column ozone. Most steep gradients would then already be captured by this additional pattern and only the deviations to this pattern would need to be generated by the spherical harmonics. The number of available data could be sufficient to achieve this. Especially the problems of capturing the steep gradients in ozone changes in the lower stratosphere might be significantly reduced in this way.

So far the focus of all analyses were halogen-induced changes of ozone only. However, with the applied regression, a global, vertically resolved estimate of the influence of all other basis functions on ozone would also be possible. It is known from *Steinbrecht et al. (2003)* that QBO and also solar cycle cause zonally asymmetric patterns in total column ozone and lower stratospheric temperature. Model results from *Schmidt and Brasseur (2006)* reveal distinct longitudinal differences in the stratospheric temperature response to solar variability which could also have an effect on the ozone distribution. A detailed analysis of the vertically resolved influence of those basis functions could, therefore, help identifying regions of strongest coupling with ozone and help quantifying the effects of those basis functions on ozone variability.

Finally, the vertically and longitudinally resolved results for the observations could be compared to chemistry-climate model results analyzed with the same method. A first step in this direction was already taken by using the E39C-A model output to validate the significance and robustness of the observation-based results. In some cases differences between model and observation based results could not be attributed to artifacts of the new regression method but are caused by differences in stratospheric mechanisms. This comparison could be extended by including results from additional chemistry-climate models to assess those differences. However, for a full and detailed evaluation, process-oriented model analyses are necessary. The findings of those analyses might lead to an improvement of model performances and ultimately to a more accurate prediction of the stratospheric ozone development in coming decades.

Appendix A

Acronyms and Abbreviations

ACE-FTS	Atmospheric Chemistry Experiment - Fourier Transform Spectrometer
AOGCM	Atmosphere-ocean general circulation model
BDBP	Binary Database of Profiles
BM	Brewer-Mast ozonesonde
CCM	Chemistry-Climate Model
CCMVal	Chemistry-Climate Model Validation
CHEM	Chemistry module of the CCM E39C-A
CFC	Chlorofluorocarbon
CI	Carbon-Iodine ozonesonde
CUSUM	Cumulative sum of residuals
ECC	Electrochemical concentration cell (ozonesonde)
ECHAM	European Centre Hamburg Model
ECMWF	European Centre for Medium-Range Weather Forecasts
EESC	Equivalent effective stratospheric chlorine
ENSO	El Niño Southern Oscillation
ERA-40	ECMWF 40 Year Re-analysis
GCM	General circulation model
GOMOS	Global Ozone Monitoring by Occultation of Stars
HALOE	Halogen Occultation Experiment

APPENDIX A. ACRONYMS AND ABBREVIATIONS

ILAS	Improved L imb A tmospheric S pectrometer
IPCC	Intergovernmental P anel on C limate C hange
LIMS	L imb I nfrared M onitor of the S tratosphere
NASA	National A eronautics and S pace A dministration
NCEP	National C enter for E nvironmental P rediction
NDACC	Network for the D etection of A tmospheric C omposition C hange
NF	Normalization factor
NIWA	National I nstitute of W ater & A tmospheric R esearch
NMC	National M eteorological C enter
NOAA	National O ceanic and A tmospheric A dministration
NRL	Naval R esearch L aboratory
ODS	O zone-depleting substances
OSIRIS	O ptical S pectrograph and I nfrared I maging S ystem
POAM	P olar O zone and A erosol M easurement I nstrument
PSC	P olar stratospheric cloud
QBO	Q uasi-biennial oscillation
REF	CCM r eference simulations
SAGE	S tratospheric A erosol and G as E xperiment
SHADOZ	S outhern H emisphere A dditional O zonesondes
SOI	S outhern O scillation I ndex
SPARC	S tratospheric P rocesses A nd their R ole in C limate
SpH	S pherical h armonics
TOMS	T otal O zone M apping S pectrometer
UKMO	U K M et O ffice
UV	U ltra-violet
WMO	W orld M eteorological O rganization
WOUDC	W orld O zone and U ltraviolet R adiation D ata C entre

Bibliography

- Ahrens, C. D. (1994), *Meteorology today - An introduction to weather, climate and the environment*, 5th ed., West Publishing Company, St. Paul.
- Andersen, S., and B. Knudsen (2006), The influence of polar vortex ozone depletion on NH mid-latitude ozone trends in spring, *Atmos. Chem. Phys.*, *6*, 2837–2845.
- Andrews, D. G. (2000), *An Introduction to Atmospheric Physics*, Cambridge University Press, UK.
- Andrews, D. G., J. R. Holton, and C. B. Leovy (1987), *Middle atmosphere dynamics*, Academic Press Inc., London.
- Appenzeller, C., A. K. Weiss, and J. Staehelin (2000), North Atlantic Oscillation modulates total ozone winter trends, *Geophys. Res. Lett.*, *27*(8), 1131–1134.
- Arfken, G. (1970), *Mathematical Methods for Physicists*, 2nd ed., Academic Press, New York.
- Baldwin, M. P., and T. J. Dunkerton (1999), Downward propagation of the Arctic Oscillation from the stratosphere to the troposphere, *J. Geophys. Res.*, *104*, 30,937–30,946.
- Baldwin, M. P., L. J. Gray, T. J. Dunkerton, K. Hamilton, P. H. Haynes, W. J. Randel, J. R. Holton, M. J. Alexander, I. Hirota, T. Horinouchi, D. B. A. Jones, J. S. Kinnnersley, C. Marquardt, K. Sato, and M. Takahasi (2001), The Quasi-Biennial Oscillation, *Rev. Geophys.*, *39*(2), 179–229.
- Baldwin, M. P., M. Dameris, and T. Shepherd (2007), How will the stratosphere affect climate change?, *Science*, *316*, 1576–1577.
- Bevington, P. R., and D. K. Robinson (2003), *Data Reduction and Error Analysis for the Physical Sciences*, 3rd ed., McGraw-Hill, New York.

BIBLIOGRAPHY

- Bhatt, P. P., E. E. Remsberg, L. L. Gordley, J. M. McInerney, V. G. Brackett, and J. M. Russell III (1999), An evaluation of the quality of Halogen Occultation Experiment ozone profiles in the lower stratosphere, *J. Geophys. Res.*, *104*(D08), 9261–9275.
- Bodeker, G. E., I. S. Boyd, and W. A. Matthews (1998), Trends and variability in vertical ozone and temperature profiles measured by ozonesondes at Lauder, New Zealand: 1986–1996, *J. Geophys. Res.*, *103*(D22), 28,661–28,681.
- Bodeker, G. E., S. Solomon, and B. Hassler (2009), Report on SPARC Ozone Database Workshop, *SPARC Newsletter*, *32*, 23–25.
- Bojkov, R., L. Bishop, W. J. Hill, G. C. Reinsel, and G. C. Tiao (1990), A statistical trend analysis of revised Dobson total ozone data over the Northern Hemisphere, *J. Geophys. Res.*, *95*(D7), 9785–9807.
- Brasseur, G., and S. Solomon (1986), *Aeronomy of the Middle Atmosphere*, 2nd ed., D. Reidel Publishing Company, Dordrecht.
- Brewer, A. W. (1949), Evidence for a world circulation provided by the measurements of helium and water vapour distribution in the stratosphere, *Q. J. R. Meteorol. Soc.*, *75*, 351–363.
- Brewer, A. W., and J. R. Milford (1960), The Oxford-Kew Ozone sonde, *Proc. R. Soc. London*, *A256*, 470–495.
- Brönnimann, S., J. Luterbacher, C. Schmutz, H. Wanner, and J. Staehelin (2000), Variability of total ozone at Arosa, Switzerland, since 1931 related to atmospheric circulation differences, *Geophys. Res. Lett.*, *27*(15), 2213–2216.
- Brunner, D., J. Staehelin, J. A. Maeder, I. Wohltmann, and G. E. Bodeker (2006), Variability and trends in total and vertically resolved stratospheric ozone based on the CATO ozone data set, *Atmos. Chem. Phys.*, *6*, 4985–5008.
- Butkov, E. (1968), *Mathematical Physics*, Addison-Wesley Publishing Company, Reading.
- Byerly, W. E. (2007), *An elementary treatise on fourier's series and spherical, cylindrical, and ellipsoidal harmonics*, Cosimo Classics, New York.
- Calisesi, Y., and K. Matthes (2006), The middle atmospheric ozone response to the 11-year solar cycle, *Space Science Reviews*, *125*, 273–286.

- Charney, J., and P. Drazin (1961), Propagation of planetary-scale disturbances from the lower into the upper atmosphere, *J. Geophys. Res.*, *66*, 83–109.
- Cicerone, R. J., R. S. Stolarski, and S. Walters (1974), Stratospheric ozone destruction by man-made chlorofluoromethanes, *Science*, *185*, 1165–1167.
- Crook, J. A., N. P. Gillett, and S. P. E. Keeley (2008), Sensitivity of Southern Hemisphere climate to zonal asymmetry in ozone, *Geophys. Res. Lett.*, *35*(L07806), doi:10.1029/2007GL032698.
- Cunnold, D. M., W. P. Chu, R. A. Barnes, M. P. McCormick, and R. E. Veiga (1989), Validation of SAGE II Ozone Measurements, *94*(D06), 8447–8460.
- Cunnold, D. M., H. J. Wang, L. W. Thomason, J. M. Zawodny, J. A. Logan, and I. A. Megretskaya (2000), SAGE (version 5.96) ozone trends in the lower stratosphere, *J. Geophys. Res.*, *105*(D4), 4445–4457.
- Dameris, M., V. Grewe, M. Ponater, R. Deckert, V. Eyring, F. Mager, S. Matthes, C. Schnadt, A. Stenke, B. Steil, C. Brühl, and M. A. Giorgetta (2005), Long-term changes and variability in a transient simulation with a chemistry-climate model employing realistic forcing, *Atmos. Chem. Phys.*, *5*, 2121–2145.
- Dameris, M., S. Matthes, R. Deckert, V. Grewe, and M. Ponater (2006), Solar cycle effect delays onset of ozone recovery, *Geophys. Res. Lett.*, *33*(L03806), doi:10.1029/2005GL024741.
- Dessler, A. E. (2000), *The Chemistry and Physics of Stratospheric Ozone*, Academic Press, San Diego.
- Dobson, G. M. B. (1956), Origin and distribution of polyatomic molecules in the atmosphere, *Proc. Royal Soc. London*, *A236*, 187–193.
- Efstathiou, N., C. Varotsos, R. Singh, A. Cracknell, and C. Tzanis (2003), On the longitude dependence of total ozone trends over middle-latitudes, *Int. J. Rem. Sens.*, *24*, 1361–1367.
- Eyring, V., N. R. P. Harris, M. Rex, T. G. Shepherd, D. W. Fahey, G. T. Amantidis, J. Austin, M. P. Chipperfield, M. Dameris, P. M. Forster, A. Gettelman, H.-F. Graf, T. Nagashima, P. A. Newman, S. Pawson, M. J. Prather, J. A. Pyle, R. J. Salawitch, B. D. Santer, and D. W. Waugh (2005a), A Strategy for Process-Oriented Validation of Coupled Chemistry-Climate Models, *Bull. Amer. Meteorol. Soc.*, *86*, 1117–1133.

BIBLIOGRAPHY

- Eyring, V., D. E. Kinnison, and T. G. Shepherd (2005b), Overview of planned coupled chemistry-climate simulations to support upcoming ozone and climate assessments, *SPARC Newsletter*, *25*, 11–17.
- Eyring, V., M. P. Chipperfield, M. A. Giorgetta, D. E. Kinnison, E. Manzini, K. Matthes, P. A. Newman, S. Pawson, T. G. Shepherd, and D. W. Waugh (2008), Overview of the New CCMVal reference and sensitivity simulations in support of upcoming Ozone and Climate Assessments and the Planned SPARC CCMVal Report, *SPARC Newsletter*, *30*, 20–26.
- Farman, J. C., R. J. Murgatroyd, A. M. Silnickas, and B. A. Thrush (1985), Ozone photochemistry in the Antarctic stratosphere in summer, *Q. J. R. Meteorol. Soc.*, *111*, 1013–1028.
- Fioletov, V. E., G. E. Bodeker, A. J. Miller, R. D. McPeters, and R. S. Stolarski (2002), Global and zonal total ozone variations estimated from ground-based and satellite measurements: 1964-2000, *J. Geophys. Res.*, *107*, D22(4647), doi:10.1029/2001JD001350.
- Forster, P. M. d. F., and K. P. Shine (1997), Radiative forcing and temperature trends from stratospheric ozone changes, *J. Geophys. Res.*, *102*(D9), 10,841–10,855.
- Fortuin, J. P., and H. Kelder (1998), An ozone climatology based on ozonesonde and satellite measurements, *J. Geophys. Res.*, *103*(D24), 31,709–31,734.
- Gabriel, A., D. Peters, I. Kirchner, and H.-F. Graf (2007), Effect of zonally asymmetric ozone on stratospheric temperature and planetary wave propagation, *Geophys. Res. Lett.*, *34*(L06807), doi:10.1029/2006GL028998.
- Garny, H., M. Dameris, and A. Stenke (2009), Impact of prescribed SSTs on climatologies and long-term trends in CCM simulations, *Atmos. Chem. Phys. Discuss.*, *9*, 4489–4524.
- Gille, J. C., and J. M. Russell III (1984), The Limb Infrared Monitor of the Stratosphere: Experiment Description, Performance, and Results, *J. Geophys. Res.*, *89*(D4), 5125–5140.
- Gillett, N. P., J. F. Scinocca, D. A. Plummer, and M. C. Reader (2009), Sensitivity of climate to dynamically-consistent zonal asymmetries in ozone, *Geophys. Res. Lett.*, *36*(L10809), doi:10.1029/2009GL037246.

- Glaccum, W., R. Lucke, R. M. Bevilacqua, E. P. Shettle, J. S. Hornstein, D. T. Chen, J. D. Lumpe, S. S. Krigman, D. J. Debrestian, M. D. Fromm, F. Dalaudier, E. Chassefiere, C. Deniel, C. E. Randall, D. W. Rusch, J. J. Olivero, C. Brogniez, J. Lenoble, and R. Kremer (1996), The Polar Ozone and Aerosol Measurement (POAM II) Instrument, *J. Geophys. Res.*, *101*(D9), 14,479–14,487.
- Grytsai, A., O. Evtushevsky, O. Agapitov, A. Klekociuk, and G. Milinevsky (2007), Structure and long-term change in the zonal asymmetry in Antarctic total ozone during spring, *Ann. Geophys.*, *25*, 361–374.
- Harris, N. R. P., G. Ancellet, L. Bishop, D. J. Hofmann, J. B. Kerr, R. D. McPeters, M. Prendez, W. J. Randel, J. Staehelin, B. H. Subbaraya, A. Volz-Thomas, J. Zawodny, and C. S. Zerefos (1997), Trends in stratospheric and free tropospheric ozone, *J. Geophys. Res.*, *102*(D1), 1571–1590.
- Hassler, B., G. E. Bodeker, and M. Dameris (2008), Technical Note: A new global database of trace gases and aerosols from multiple sources of high vertical resolution measurements, *Atmos. Chem. Phys.*, *8*, 5403–5421.
- Hassler, B., G. E. Bodeker, I. Cionni, and M. Dameris (2009, accepted), A vertically resolved, monthly mean, ozone database from 1979 to 2100 for constraining global climate model simulations, *Int. J. Rem. Sens.*
- Haynes, P. H. (2005), Stratospheric Dynamics, *Annu. Rev. Fluid Mech.*, *37*, 263–293, doi:10.1146/annurev.fluid.37.061903.175710.
- Haynes, P. H., C. J. Marks, M. E. McIntyre, T. G. Shepherd, and K. P. Shine (1991), On the “downward control” of extratropical diabatic circulations by eddy-induced mean zonal forces, *J. Atmos. Sci.*, *48*, 651–678.
- Hein, R., M. Dameris, C. Schnadt, C. Land, V. Grewe, I. Köhler, M. Ponater, R. Sausen, B. Steil, J. Landgraf, and C. Brühl (2001), Results of an interactively coupled atmospheric chemistry-general circulation model: Comparison with observations, *Ann. Geophys.*, *19*, 435–457.
- Hervig, M., and M. McHugh (1999), Cirrus detection using HALOE measurements, *Geophys. Res. Lett.*, *26*(6), 719–722.
- Hill, W. J., P. N. Sheldon, and J. J. Tiede (1977), Analysing worldwide total ozone for trends, *Geophys. Res. Lett.*, *4*(1), 21–24.

BIBLIOGRAPHY

- Hollandsworth, S. M., R. D. McPeters, L. E. Flynn, W. Planet, A. J. Miller, and S. Chandra (1995), Ozone trends deduced from combined Nimbus 7 SBUV and NOAA 11 SBUV/2 data, *Geophys. Res. Lett.*, *22*(8), 905–908.
- Holton, J. R. (2004), *An Introduction to Dynamic Meteorology*, 4th ed., Elsevier Academic Press, Burlington, USA.
- Holton, J. R., P. H. Haynes, M. E. McIntyre, A. R. Douglass, R. B. Rood, and L. Pfister (1995), Stratosphere-troposphere exchange, *Rev. Geophys.*, *33*(4), 403–440.
- Hood, L. L., and D. A. Zaff (1995), Lower stratospheric stationary waves and the longitude dependence of ozone trends in winter, *J. Geophys. Res.*, *100*(D12), 25,791–25,800.
- Hoppel, K., R. Babilacqua, D. R. Allen, G. E. Nedoluha, and C. Randall (2003), POAM III observations of the anomalous 2002 Antarctic ozone hole, *Geophys. Res. Lett.*, *30*(1394), doi:10.1029/2003GL016899.
- Johns, T. C., C. F. Durman, H. T. Banks, M. J. Roberts, A. J. McLaren, J. K. Ridley, C. A. Senior, K. D. Williams, A. Jones, G. J. Rickard, S. Cusack, W. J. Ingram, M. Crucifix, D. M. H. Sexton, M. M. Joshi, B.-W. Dong, H. Spencer, R. S. R. Hill, J. M. Gregory, A. B. Keen, A. K. Pardaens, J. A. Lowe, A. Bodas-Salcedo, S. Stark, and Y. Searl (2006), The New Hadley Centre Climate Model (HadGEM1): Evaluation of Coupled Simulations, *J. Climate*, *19*, 1327–1353.
- Jukes, M. N., and M. E. McIntyre (1987), A high-resolution on-layer model of breaking planetary waves in the stratosphere, *Nature*, *328*, 590–596.
- Karpechko, A. Y., N. P. Gillett, B. Hassler, K. H. Rosenlof, and E. Rosanov (2009, submitted), Objective assessment of ozone in chemistry-climate model simulations, *Atmos. Chem. Phys. Discuss.*
- Kirchner, I., and D. Peters (2003), Modelling the wintertime response to upper tropospheric and lower stratospheric ozone anomalies over the North Atlantic and Europe, *Atmos. Environ.*, *21*, 2107–2118.
- Knudsen, B. M., and S. B. Andersen (2001), Longitudinal variation in springtime ozone, *Nature*, *413*, 699–700.
- Komhyr, W. D. (1965), A carbon-iodine sonde sensor for atmospheric soundings, in *Proc. Ozone Symp., Albuquerque*, p. 26, Geneva.

- Komhyr, W. D. (1969), Electrochemical concentration cells for gas analysis, *Ann. Geophys.*, *25*, 203–210.
- Komhyr, W. D., S. J. Oltmans, A. N. Chopra, and P. R. Franchois (1985), Performance characteristics of high-altitude ECC ozonsondes, in *Atmospheric Ozone, Proceedings of the Quadrennial Ozone Symposium*, Greece.
- Land, C., J. Feichter, and R. Sausen (2002), Impact of vertical resolution on the transport of passive tracers in the ECHAM4 model, *Tellus B*, *54*, 344–360.
- Liley, J. B., P. V. Johnston, R. L. McKenzie, A. J. Thomas, and I. S. Boyd (2000), Stratospheric NO₂ variations from a long time series at Lauder, New Zealand, *J. Geophys. Res.*, *105*(D9), 11,633–11,640.
- Liu, X., K. Chance, C. E. Sioris, T. P. Kurosu, and M. J. Newchurch (2006), Intercomparison of GOME, ozonesonde, and SAGE II measurements of ozone: Demonstration of the need to homogenize available ozonesonde data sets, *J. Geophys. Res.*, *111*(D14305), doi:10.1029/2005JD006718.
- Logan, J. A. (1994), Trends in the vertical distribution of ozone: an analysis of ozonesonde data, *J. Geophys. Res.*, *99*(D12), 25,553–25,585.
- Logan, J. A., I. A. Megretskaya, A. J. Miller, G. C. Tiao, D. Choi, L. Zhang, R. S. Stolarski, G. J. Labow, S. M. Hollandsworth, G. E. Bodeker, H. Claude, D. Demuer, J. B. Kerr, D. W. Tarasick, S. J. Oltmans, B. Johnson, F. Schmidlin, J. Staehelin, P. Viatte, and O. Uchino (1999), Trends in the vertical distribution of ozone: a comparison of two analyses of ozonesonde data, *J. Geophys. Res.*, *104*, 26,373–26,399.
- Lucke, R. L., D. Korwan, R. M. Bevilacqua, J. S. Hornstein, E. P. Shettle, D. T. Chen, M. Daehler, J. D. Lumpe, M. D. Fromm, D. Debrestian, B. Neff, M. Squire, G. König-Langlo, and J. Davies (1999), The Polar Ozone and Aerosol Measurement (POAM III) Instrument and Early Validation Results, *J. Geophys. Res.*, *104*(D15), 18,785–18,799.
- Lumpe, J. D., R. M. Bevilacqua, K. W. Hoppel, S. S. Krigman, D. L. Kriebel, C. E. Randall, D. W. Rusch, C. Brogniez, R. Ramanananaherosa, E. P. Shettle, J. J. Olivero, J. Lenoble, and P. Pruvost (1997), POAM II Retrieval Algorithm and Error Analysis, *J. Geophys. Res.*, *102*(D19), 23,593–23,614.
- Lumpe, J. D., R. M. Bevilacqua, K. W. Hoppel, and C. E. Randall (2002), POAM III Retrieval Algorithm and Error Analysis, *J. Geophys. Res.*, *107*(D21), doi:10.1029/2002JD002137.

BIBLIOGRAPHY

- Lumpe, J. D., R. M. Bevilacqua, C. E. Randall, G. Nedoluha, K. W. Hoppel, J. Russel, V. L. Harvey, C. Schiller, B. Sen, G. Taha, G. Toon, and H. Vömel (2006), Validation of Polar Ozone and Aerosol Measurement (POAM) III version 4 stratospheric water vapor, *J. Geophys. Res.*, *111*(D11301), doi:10.1029/2005JD006763.
- Mäder, J. A., J. Staehelin, D. Brunner, W. A. Stahel, I. Wohltmann, and T. Peter (2007), Statistical modeling of total ozone: Selection of appropriate explanatory variables, *J. Geophys. Res.*, *112*(D11108), doi:10.1029/2006JD007694.
- Malanca, F., P. Canziani, and G. Argüello (2005), Trends evolution of ozone between 1980 and 2000 at midlatitudes over the Southern Hemisphere: Decadal differences in trends, *J. Geophys. Res.*, *110*(D05102), doi:10.1029/2004JD004977.
- Margenau, H., and G. M. Murphy (1956), *The Mathematics of Physics and Chemistry*, 2nd ed., D. van Nostrand Company, New York.
- Martin, G. M., M. A. Ringer, V. D. Pope, A. Jones, C. Dearden, and T. J. Hinton (2006), The Physical Properties of the Atmosphere in the New Hadley Centre Global Environmental Model (HadGEM1). Part I: Model Description and Global Climatology, *J. Climate*, *19*, 1274–1301.
- Mayer, B., and A. Kylling (2005), Technical note: The libRadtran software package for radiative transfer calculations - description and examples of use, *Atmos. Chem. Phys.*, *5*, 1855–1877.
- McConnell, J. C., and J. J. Jin (2008), Stratospheric Ozone Chemistry, *Atmosphere-Ocean*, *46*(1), 69–92.
- McCormick, M. P., J. M. Zawodny, R. E. Veiga, J. C. Larsen, and P. H. Wang (1989), An overview of SAGE I and SAGE II ozone measurements, *Planet. Space Sci.*, *37*(12), 1567–1586.
- McCormick, M. P., L. W. Thomason, and C. R. Trepte (1995), Atmospheric effects of the Mt Pinatubo eruption, *Nature*, *373*, 399–404.
- McKenna, D. S., J.-U. Groöf, G. Günther, P. Konopka, R. Müller, G. Carver, and Y. Sasano (2002), A new Chemical Lagrangian Model of the Stratosphere (CLaMS) 2. Formulation of chemistry scheme and initialization, *J. Geophys. Res.*, *107*, doi:10.1029/2000JD000113.

- McKenzie, R. L., C. Weinreis, P. V. Jonston, B. Liley, H. Shiona, M. Kotkamp, D. Smale, N. Takegawa, and Y. Kondo (2008), Effects of urban pollution on UV spectral irradiances, *Atmos. Chem. Phys.*, *8*, 5683–5697.
- McPeters, R. D., D. J. Hofmann, M. Clark, L. Flynn, L. Froidevaux, M. Gross, B. Johnson, G. Koenig, X. Liu, S. McDerimid, T. McGee, F. Murcray, M. J. Newchurch, S. J. Oltmans, A. Parrish, R. Schnell, U. Singh, J. J. Tsou, T. Walsh, and J. M. Zawodny (1999), Results from the 1995 Stratospheric Ozone Profile Intercomparison at Mauna Loa, *J. Geophys. Res.*, *104*(D23), 30,505–30,514.
- McPeters, R. D., G. J. Lebow, and J. A. Logan (2007), Ozone climatological profiles for satellite retrieval algorithms, *J. Geophys. Res.*, *112*(D05308), doi:10.1029/2005JD006823.
- Miller, A. J., G. C. Tiao, G. C. Reinsel, D. Wuebbles, L. Bishop, J. Kerr, R. M. Nagatani, J. J. DeLuisi, and C. L. Mateer (1995), Comparisons of observed ozone trends in the stratosphere through examination of Umkehr and balloon ozonesonde data, *Journal of Geophysical Research*, *100*(D6), 11,209–11,217.
- Miller, R. L., G. A. Schmidt, and D. T. Shindell (2006), Forced annular variations in the 20th century Intergovernmental Panel on Climate Change Fourth Assessment Report models, *J. Geophys. Res.*, *111*(D18101), doi:10.1029/2005JD006323.
- Molina, L. T., and M. J. Molina (1987), Production of Cl₂O₂ from the self-reaction of the ClO radical, *J. Phys. Chem.*, *91*(2), 433–436.
- Molina, M. J., and F. S. Rowland (1974), Stratospheric sink for chlorofluoromethanes: chlorine atom catalyzed destruction of ozone, *Nature*, *249*, 810–812.
- Müller, R., J.-U. Grooß, K. Lemmen, D. Heinze, M. Dameris, and G. E. Bodeker (2008), Simple measures of ozone depletion in the polar stratosphere, *Atmos. Chem. Phys.*, *8*, 251–264.
- Nazaryan, H., and M. P. McCormick (2005), Comparisons of Stratospheric Aerosol and Gas Experiment (SAGE II) and Solar Backscatter Ultraviolet Instrument (SBUV/2) ozone profiles and trend estimates, *J. Geophys. Res.*, *110*(D17302), doi:10.1029/2004JD005483.

BIBLIOGRAPHY

- Nazaryan, H., M. P. McCormick, and J. M. Russell III (2005), New studies of SAGE II and HALOE ozone profile and long-term change comparisons, *J. Geophys. Res.*, *110*(D09305), doi:10.1029/2004JD005425.
- Nazaryan, H., M. P. McCormick, and J. M. Russell III (2007), Comparative analysis of SBUV/2 and HALOE ozone profiles and trends, *J. Geophys. Res.*, *112*(D10304), doi:10.1029/2006JD007367.
- Newchurch, M. J., E.-S. Yang, D. M. Cunnold, G. C. Reinsel, J. M. Zawodny, and J. M. Russell III (2003), Evidence for slowdown in stratospheric ozone loss: First stage of ozone recovery, *J. Geophys. Res.*, *108*(D16), doi:10.1029/2003JD003471.
- Newman, P. A., J. S. Daniel, D. W. Waugh, and E. R. Nash (2007), A new formulation of equivalent effective stratospheric chlorine (EESC), *Atmos. Chem. Phys.*, *7*, 4537–4552.
- Nikulin, G., and A. Karpechko (2005), The mean meridional circulation and midlatitude ozone buildup, *Atmos. Chem. Phys.*, *5*, 3159–3172.
- Niu, X., J. E. Frederick, M. L. Stein, and G. C. Tiao (1992), Trends in column ozone based on TOMS Data: Dependence on Month, Latitude and Longitude, *J. Geophys. Res.*, *97*(D13), 14,661–14,669.
- Oehlert, G. W. (1986), Trends in Dobson total ozone: an update through 1983, *J. Geophys. Res.*, *91*(D2), 2675–2679.
- Paradine, C. G., and B. H. Rivett (1964), *Statistical methods for technologists*, 3rd ed., The English Universities Press LTD., London.
- Peters, D., and G. Entzian (1999), Longitude-Dependent Decadal Changes of Total Ozone in Boreal Winter Months during 1979-92, *J. Climate*, *12*, 1038–1048.
- Peters, D., A. Gabriel, and G. Entzian (2008), Longitude-dependent decadal ozone changes and ozone trends in boreal winter months during 1960-2000, *Ann. Geophys.*, *26*, 1275–1286.
- Pipes, L. A. (1958), *Applied Mathematics for Engineers and Physicists*, 2nd, international student edition ed., McGraw-Hill, New York, Kōgakusha Company, Tokyo.
- Plumb, R. A. (1996), A “tropical pipe” model of stratospheric transport, *J. Geophys. Res.*, *101*, 3957–3972.

- Press, W. H., B. P. Flannery, S. A. Teukolsky, and W. T. Vetterling (1989), *Numerical Recipes in Pascal - The Art of Scientific Computing*, Cambridge University Press.
- Randall, C. E., D. W. Rusch, R. M. Bevilacqua, K. W. Hoppel, J. D. Lumpe, E. Shettle, E. Thompson, L. Deaver, J. Zawodny, E. Kyrö, B. Johnson, H. Kelder, V. M. Dorokhov, G. König-Langlo, and M. Gil (2003), Validation of POAM III ozone: Comparisons with ozonesonde and satellite data, *J. Geophys. Res.*, *108*(D12), doi:10.1029/2002JD002944.
- Randel, W. J., and J. B. Cobb (1994), Coherent variations of monthly mean total ozone and lower stratospheric temperature, *J. Geophys. Res.*, *99*(D3), 5433–5447.
- Randel, W. J., and F. Wu (1996), Isolation of the ozone QBO in SAGE II data by singular-value decomposition, *J. Atmos. Sci.*, *53*, 2546–2559.
- Randel, W. J., and F. Wu (2007), A stratospheric ozone profile data set for 1979–2005: Variability, trends, and comparisons with column ozone data, *J. Geophys. Res.*, *112*(D06313), doi:10.1029/2006JD007339.
- Randel, W. J., M. Park, F. Wu, and N. Livesey (2007), A Large Annual Cycle in Ozone above the Tropical Tropopause Linked to the Brewer-Dobson Circulation, *J. Atmos. Sci.*, *64*, 4479–4488.
- Reid, S. J. (2000), *Ozone and Climate Change - A Beginner's Guide*, Gordon and Breach Science Publishers, Amsterdam.
- Reinsel, G. C. (1981), Analysis of total ozone data for the detection of recent trends and the effects of nuclear testing during the 1960's, *Geophys. Res. Lett.*, *8*, 1227–1230.
- Reinsel, G. C., G. C. Tiao, A. J. Miller, D. J. Wuebbles, P. S. Connell, C. L. Mateer, and J. J. DeLuisi (1987), Statistical analysis of total ozone and stratospheric Umkehr data for trends and solar cycle relationship, *J. Geophys. Res.*, *92*(D2), 2201–2209.
- Reinsel, G. C., E. C. Weatherhead, G. C. Tiao, A. J. Miller, R. Nagatani, D. J. Wuebbles, and L. E. Flynn (2002), On detection of turnaround and recovery in trend for ozone, *J. Geophys. Res.*, *107*(D10), doi:10.1029/2001JD000500.
- Reinsel, G. C., A. J. Miller, E. C. Weatherhead, L. E. Flynn, R. M. Nagatani, G. C. Tiao, and D. J. Wuebbles (2005), Trend analysis of total ozone data

BIBLIOGRAPHY

- for turnaround and dynamical contributions, *J. Geophys. Res.*, *110*(D16306), doi:10.1029/2004JD004662.
- Reithmeier, C., and R. Sausen (2002), ATTILA: atmospheric tracer transport in a Lagrangian model, *Tellus B*, *54*, 278–299.
- Remsberg, E. E., and L. E. Deaver (2005), Interannual, solar cycle, and trend terms in middle atmospheric temperature time series from HALOE, *J. Geophys. Res.*, *110*(D06106), doi:10.1029/2004JD004905.
- Remsberg, E. E., G. Lingenfelter, M. Natarajan, L. L. Gordley, B. T. Marshall, and E. Thompson (2007), On the quality of the Nimbus 7 LIMS version 6 ozone for studies of the middle atmosphere, *JQSRT*, *105*(3), 492–518.
- Rind, D., J. Lerner, and J. Zawodny (2005), A complementary analysis for SAGE II data profiles, *Geophys. Res. Lett.*, *32*(L07812), doi:10.1029/2005GL022550.
- Ronnebeck, K., and D. Sonntag (1976), Eine weiterentwickelte elektrochemische Ozonradiosonde, *Z. Meteorol.*, *26*, 15–19.
- Rosenfield, J. E., D. B. Considine, P. E. Meade, J. T. Bacmeister, C. H. Jackman, and M. R. Schoeberl (1997), Stratospheric effects of Mount Pinatubo aerosol studied with a coupled two-dimensional model, *J. Geophys. Res.*, *102*(D3), 3649–3670.
- Rowland, T. S., N. R. P. Harris, R. D. Bojkov, and P. B. Bloomfield (1988), Statistical error analysis of ozone trends - winter depletion in the northern hemisphere, in *Ozone in the Atmosphere*, edited by R. D. Bojkov and P. Fabian, pp. 71–75, A. Deepak Publishing, Hampton, Virginia.
- Russell III, J. M., L. L. Gordley, J. H. Park, S. R. Drayson, D. H. Hesketh, R. J. Cicerone, A. F. Tuck, J. E. Frederick, J. E. Harries, and P. Crutzen (1993), The Halogen Occultation Experiment, *J. Geophys. Res.*, *98*(D6), 10,777–10,797.
- Schmidt, H., and G. P. Brasseur (2006), The response of the middle atmosphere to solar cycle forcing in the Hamburg Model of the Neutral and Ionized Atmosphere, *Space Science Reviews*, *125*, 345–356.
- Shepherd, T. G. (2008), Dynamics, Stratospheric Ozone, and Climate Change, *Atmosphere-Ocean*, *46*(1), 117–138.
- Shiotani, M. (1992), Annual, quasi-biennial, and El Nino-southern oscillation (ENSO) time-scale variations in equatorial ozone, *J. Geophys. Res.*, *97*(D7), 7625–7633.

- Shreedharan, C. R. (1968), An Indian electrochemical ozonesonde, *J. Phys. E. Sci. Instrum. Ser2*, pp. 995–997.
- Smit, H. G. J., and D. Kley (1996), Jülich Ozone Sonde Intercomparison Experiment (JOSIE), 5 February - 8 March 1996, *Tech. Rep. Report No. 130*, WMO.
- Smit, H. G. J., W. Straeter, B. J. Johnson, S. J. Oltmans, J. Davies, D. W. Tarasick, B. Hoegger, R. Stubi, F. J. Schmidlin, T. Northam, A. M. Thompson, J. C. Witte, I. Boyd, and F. Posny (2007), Assessment of the performance of ECC-ozonesondes under quasi-flight conditions in the environmental simulation chamber: Insights from the Juelich Ozone Sonde Intercomparison Experiment (JOSIE), *J. Geophys. Res.*, *112*(D19306), doi:10.1029/2006JD007308.
- Solomon, K. R. (2008), Effects of Ozone Depletion and UV-B Radiation on Humans and the Environment, *Atmosphere-Ocean*, *46*(1), 185–202.
- Solomon, S. (1999), Stratospheric ozone depletion: a review of concepts and history, *Rev. Geophys.*, *37*(3), 275–316.
- Soukharev, B. E., and L. L. Hood (2006), Solar cycle variation of stratospheric ozone: Multiple regression analysis of long-term satellite data sets and comparisons with models, *J. Geophys. Res.*, *111*(D20314), doi:doi:10.1029/2006JD007107.
- SPARC/IOC/GAW (1998), Assessment of trends in the Vertical Distribution of Ozone, Chap. 1, *WMO Ozone Research and Monitoring Project Report No. 43 Report No.1*, World Climate Research Programme.
- St. John, D. S., S. P. Bailey, W. H. Fellner, J. M. Minor, and R. D. Snee (1981), Time series search for trend in total ozone measurements, *J. Geophys. Res.*, *86*(C8), 7299–7311.
- Staehelin, J., N. R. P. Harris, C. Appenzeller, and J. Eberhard (2001), Ozone trends: a review, *Rev. Geophys.*, *39*(2), 231–290.
- Steil, B., M. Dameris, C. Brühl, P. J. Crutzen, V. Grewe, M. Ponater, and R. Sausen (1998), Development of a chemistry module for GCMs: First results of a multiannual integration, *Ann. Geophys.*, *16*, 205–228.
- Steil, B., C. Brühl, E. Manzini, P. J. Crutzen, J. Lelieveld, P. J. Rasch, E. Roeckner, and K. Krüger (2003), A new interactive chemistry-climate model: 1. Present-day climatology and interannual variability of the middle atmosphere

BIBLIOGRAPHY

- using the model and 9 years of HALOE/UARS data, *J. Geophys. Res.*, *109*(D9), doi:10.1029/2002JD002971.
- Steinbrecht, W., H. Claude, U. Köhler, and K. P. Hoinka (1998), Correlations between tropopause heights and total ozone: Implications for long-term changes, *J. Geophys. Res.*, *103*(D15), 19,183–19,192.
- Steinbrecht, W., H. Claude, U. Köhler, and P. Winkler (2001), Interannual changes of total ozone and northern hemisphere circulation patterns, *Geophys. Res. Lett.*, *28*(7), 1191–1194.
- Steinbrecht, W., B. Hassler, H. Claude, P. Winkler, and R. S. Stolarski (2003), Global distribution of total ozone and lower stratospheric temperature variations, *Atmos. Chem. Phys.*, *3*, 1421–1438.
- Steinbrecht, W., H. Claude, F. Schönenborn, I. McDermid, T. Leblanc, S. Godin, T. Song, D. Swart, Y. Meijer, G. Bodeker, B. Connor, N. Kämpfer, K. Hocke, Y. Calisesi, N. Schneider, J. de la Noë, A. Parrish, I. Boyd, C. Brühl, B. Steil, M. Giorgetta, E. Manzini, L. Thomason, J. Zawodny, M. McCormick, J. Russell III, P. Bhartia, R. S. Stolarski, and S. Hollandsworth-Frith (2006), Long-term evolution of upper stratospheric ozone at selected stations of the Network for the Detection of Stratospheric Change (NDSC), *J. Geophys. Res.*, *111*(D10308), doi:10.1029/2005JD006454.
- Stenke, A., M. Dameris, V. Grewe, and H. Garny (2008a), Implications of Lagrangian transport for coupled chemistry-climate simulations, *Atmos. Chem. Phys. Discuss.*, *8*, 18,727–18,764.
- Stenke, A., V. Grewe, and M. Ponater (2008b), Lagrangian transport of water vapour and cloud water in the ECHAM4 GCM and its impact on the cold bias, *Clim. Dyn.*, *31*, 491–506(16).
- Stolarski, R. S., R. Bojkov, L. Bishop, C. Zerefos, J. Staehelin, and J. Zawodny (1992), Measured trends in stratospheric ozone, *Science*, *256*, 342–349.
- Thompson, A. M., J. C. Witte, S. J. Oltmans, F. Schmidlin, J. A. Logan, M. Fujiwara, V. W. J. H. Kirchhoff, F. Posny, G. J. R. Coetzee, B. Hoegger, S. Kawakami, T. Ogawa, J. Fortuin, and H. Kelder (2003a), Southern Hemisphere Additional Ozonesondes (SHADOZ) 1998-2000 tropical ozone climatology 2. Tropospheric variability and the zonal wave-one, *J. Geophys. Res.*, *108*(8241), doi:10.1029/2002JD002241.

- Thompson, A. M., J. C. Witte, R. D. McPeters, S. J. Oltmans, J. A. Schmidlin, J. A. Logan, M. Fujiwara, V. W. J. H. Kirchhoff, F. Posny, G. J. R. Coetzee, B. Hoegger, S. Kawakami, T. Ogawa, B. J. Johnson, H. Vömel, and G. Labow (2003b), Southern Hemisphere Additional Ozonesondes (SHADOZ) 1998-2000 tropical ozone climatology - 1. Comparison with Total Ozone Mapping Spectrometer (TOMS) and ground-based measurements, *J. Geophys. Res.*, *108*, D2(8238), doi:10.1029/2001JD000967.
- Tiao, G. C., G. C. Reinsel, J. H. Pedrick, G. M. Allenby, C. L. Mateer, A. J. Miller, and J. J. DeLuisi (1986), A statistical trend analysis of ozonesonde data, *J. Geophys. Res.*, *91*, 13,121–13,136.
- Tiao, G. C., G. C. Reinsel, D. Xu, J. H. Pedrick, X. Zhu, A. J. Miller, J. J. DeLuisi, G. M. Mateer, and D. J. Wuebbles (1990), Effects of autocorrelation and temporal sampling schemes on estimates of trend and spatial correlation, *J. Geophys. Res.*, *95*(D12), 20,507–20,517.
- Tie, X., G. P. Brasseur, B. Briegleb, and C. Granier (1994), Two-dimensional simulation of Pinatubo aerosol and its effect on stratospheric ozone, *J. Geophys. Res.*, *99*(D10), 20,545–20,562.
- Tung, K. K., and H. Yang (1994), Global QBO in circulation and ozone. Part I: reexamination of observational evidence, *J. Atmos. Sci.*, *51*, 2699–2707.
- Veiga, R. E., D. M. Cunnold, W. P. Chu, and M. P. McCormick (1995), Stratospheric aerosol and gas experiments I and II comparisons with ozonesondes, *J. Geophys. Res.*, *100*(D5), 9073–9090.
- von Storch, H., and A. E. Navarra (1999), *Analysis of Climate Variability - Applications of Statistical Techniques: Proceedings of an Autumn School Organized by the Commission of the European Community on Elba from October 30 to November 6, 1993*, 2nd, updated and extended ed., Springer Verlag, Berlin.
- von Storch, H., and F. W. Zwiers (2002), *Statistical Analysis in Climate Research*, Cambridge University Press, Cambridge.
- Wang, H. J., D. M. Cunnold, and X. Bao (1996), A critical analysis of Stratospheric Aerosol and Gas Experiment ozone trends, *J. Geophys. Res.*, *101*(D7), 12,495–12,514.
- Wang, H. J., D. M. Cunnold, L. W. Thomason, J. M. Zawodny, and G. E. Bodeker (2002), Assessment of SAGE version 6.1 ozone data quality, *J. Geophys. Res.*, *107*(D23), doi:10.1029/2002JD002418.

BIBLIOGRAPHY

- Wang, P.-H., D. M. Cunnold, C. R. Trepte, H. J. Wang, P. Jing, J. Fishman, V. G. Brackett, J. M. Zawodny, and G. E. Bodeker (2006a), Ozone variability in the midlatitude upper troposphere and lower stratosphere diagnosed from a monthly SAGE II climatology relative to the tropopause, *J. Geophys. Res.*, *111*(D21304), doi:10.1029/2005JD006108.
- Wang, P.-H., J. Fishman, V. L. Harvey, and M. H. Hitchman (2006b), Southern tropical upper tropospheric zonal ozone wave-1 from SAGE II observations (1985-2002), *J. Geophys. Res.*, *111*(D08305), doi:10.1029/2005JD006221.
- Waugh, D. W., and T. M. Hall (2002), Age of stratospheric air: theory, observations and models, *Rev. Geophys.*, *40*(4), doi:10.1029/2000RG000101.
- Weatherhead, E. C., G. C. Reinsel, G. C. Tiao, X.-L. Meng, D. Choi, W.-K. Cheang, T. Keller, J. DeLuisi, D. J. Wuebbles, J. B. Kerr, A. J. Miller, S. J. Oltmans, and J. E. Frederick (1998), Factors affecting the detection of trends: Statistical considerations and applications to environmental data, *J. Geophys. Res.*, *103*(D14), 17,149–17,161.
- Weatherhead, E. C., G. C. Reinsel, G. C. Tiao, C. H. Jackman, L. Bishop, S. M. Hollandsworth-Frith, J. DeLuisi, T. Keller, S. J. Oltmans, E. L. Fleming, D. J. Wuebbles, J. B. Kerr, A. J. Miller, J. Herman, R. D. McPeters, R. M. Nagatani, and J. E. Frederick (2000), Detecting the recovery of total column ozone, *J. Geophys. Res.*, *105*(D17), 22,201–22,210.
- Wilks, D. (2006), *Statistical methods in the atmospheric sciences*, International Geophysics Series, 2nd ed., Elsevier, Academic Press, Amsterdam.
- Wohltmann, I., R. Lehmann, M. Rex, D. Brunner, and J. A. Mäder (2007), A process-oriented regression model for column ozone, *J. Geophys. Res.*, *112*(D12304), doi:10.1029/2006JD007573.
- World Meteorological Organization (1989), Scientific Assessment of Stratospheric Ozone: 1989, Vol. 1, *Tech. Rep. Report No. 20*, Global Ozone Research and Monitoring Project, Geneva, Switzerland.
- World Meteorological Organization (1999), Scientific Assessment of Ozone Depletion: 1998, *Tech. Rep. Report No. 44*, Global Ozone Research and Monitoring Project, Geneva, Switzerland.
- World Meteorological Organization (2003), Scientific Assessment of Ozone Depletion: 2002, *Tech. Rep. Report No. 47*, Global Ozone Research and Monitoring Project, Geneva, Switzerland.

- World Meteorological Organization (2007), Scientific Assessment of Ozone Depletion: 2006, *Tech. Rep. Report No. 50*, Global Ozone Research and Monitoring Project, Geneva, Switzerland.
- Yang, E.-S., D. M. Cunnold, R. J. Salawitch, M. P. McCormick, J. Russell III, J. M. Zawodny, S. Oltmans, and M. J. Newchurch (2006), Attribution of recovery in lower-stratospheric ozone, *J. Geophys. Res.*, *111*(D17309), doi: 10.1029/2005JD006371.
- Yu, J. R., and C. Y. She (1995), Climatology of a midlatitude mesopause region observed by a lidar at Fort Collins, Colorado (40.6°N, 105°W), *J. Geophys. Res.*, *100*(D4), 7441–7452.

Acknowledgments

Since I first started working with stratospheric ozone data at the Meteorological Observatory in Hohenpeißenberg in 2001, many years passed by in which I learned immensely much about an interesting and important topic, in which I met many people who endorsed me in my undertaking, who made me think, and who made my days at work so enjoyable, and in which the plans for this PhD thesis changed uncountable times. That the thesis ultimately evolved to the study presented here is connected to the following people:

First of all I want to thank my PhD supervisor Prof. Dr. Martin Dameris who never showed any doubt in spite of many adverse conditions that I would finish this thesis in the end, who found several times money to support me and who motivated me with his inexhaustible optimism and his enthusiasm for science and ozone research. A huge thank-you also goes to my supervisor in New Zealand, Dr. Greg Bodeker, who not only taught me how to program properly, and not to cling too much to research plans (there is always a plan B), but also had an answer to every question I asked, offered solutions for unsolvable problems and patiently explained and introduced me to the deeper secrets of science. Unforgettable, of course, are also the possibilities to experience farming first-hand and the free lectures about the many ways of conquering the world. I also want to say a big thank-you to Prof. Dr. Bernhard Mayer who agreed to be my second official supervisor although we had never met before. Prof. Dr. Ulrich Schumann agreed without hesitation to employ me at DLR Oberpfaffenhofen for two months in 2008 and for six months in 2009, so that my living was secured and I could continue my work. This is highly appreciated.

I also want to express my gratitude towards the institutions where I worked during the last years: the Meteorological Observatory Hohenpeißenberg, the NIWA station in Lauder and the IPA of DLR in Oberpfaffenhofen. All of these institutions have great technical support which I was allowed to make use of. And the fantastic working atmosphere with the friendly and helpful colleagues in all three institutions made it a pleasure for me to come to work every day and do the science presented here in this thesis.

I am very grateful that I was selected by the DAAD to be a recipient of the DAAD PhD studentship which allowed me to live and work in New Zealand for one year. I also want to thank NIWA New Zealand for hosting me during my DAAD studentship and the year after. That is much appreciated.

I used data from several satellite instruments and ozone sounding stations. The people involved in doing the measurements and the processing of the data are too numerous to be acknowledged by name, but I want to express my gratitude to all of them and acknowledge their work. I further want to thank the people from IPA of DLR Oberpfaffenhofen for providing and preprocessing the chemistry-climate model output which I used for the sensitivity test.

I also owe my parents and my sisters a huge thank-you for always being supportive, for accepting the stay in New Zealand without too much complaining, for sending me letters, postcards, parcels and emails to keep me happy and working, and for always having the time and nerve to listen to my problems and complaints. My flatmates from Hostel 3 in Lauder deserve also special thanks. Without their pleasant and motivating presence in the hostel working would have been so much harder! A big thank-you goes, of course, also to my friends from all over the world who never had any doubt that I would actually finish the PhD one day, who kept in touch although I was not very responsive, who were always willing to discuss my work, who kept me mentally sane while I was working extremely hard to get the thesis written and who helped me with proof-reading the thesis chapters. I wouldn't have been able to do this without you!

Lebenslauf

PERSÖNLICHE DATEN

Name: Birgit Haßler

Geburtsdatum: 11. November 1974

Geburtsort: Tübingen, Deutschland

AUSBILDUNG

- 09/1981 – 07/1985 Grundschule Neresheim
- 09/1985 – 07/1991 Progymnasium Neresheim
- 09/1991 – 06/1994 Max-Planck-Gymnasium Heidenheim a. Br.
Leistungskurse: Mathematik, Chemie
- 09/1996 – 06/1997 Studium an der Brock University, St. Catharines, Ontario/Kanada
- 10/1994 – 01/2001 Diplom in Hydrologie an der Albert-Ludwigs-Universität Freiburg
i. Br.
Diplomarbeit: *Untersuchung von Klimavariabilität und ihre
Auswirkung auf hydrologische Dürre in Europa*
- 07/2005 & 02/2006 Promotions-Zulassungsprüfungen in ‘Theoretische Mechanik’
und ‘Hydrodynamik’
- 05/2005 – 04/2007 Promotionsstudium der Meteorologie an der Ludwig-Maximilians-Universität München
- 03/2007 – 04/2009 Stipendiaufenthalt bei NIWA in Lauder/Neuseeland
(DAAD-Auslands-Promotions-Stipendium, NIWA Teilstipendien)

BERUFSTÄTIGKEIT

- 07/2001 – 06/2004 Wissenschaftliche Mitarbeiterin am Meteorologischen Observatorium Hohenpeißenberg (DWD)
AFO2000-Projekt ‘KODYACS’
- 09/2004 – 10/2006 Wissenschaftliche Mitarbeiterin am Meteorologischen Observatorium Hohenpeißenberg (DWD)
Aktionsprogramm 2003 des Deutschen Wetterdienstes
- 03/2006 – 04/2006 Consultant für den Finnischen Wetterdienst (FMI)
SAUNA Messkampagne in Sodankylä
- 11/2006 selbständig tätig als Wissenschaftlerin
Aerosoldaten-Aufbereitung für DWD
- 07/2008 – 08/2008 Gastwissenschaftlerin am Institut für Physik der Atmosphäre,
DLR Oberpfaffenhofen
- 05/2009 – 10/2009 Wissenschaftliche Angestellte am Institut für Physik der Atmosphäre,
DLR Oberpfaffenhofen

München, 29. Juli 2009